STRUCTURAL BOND BEHAVIOUR OF RIBBED GFRP REBARS IN CONCRETE BEAMS UNDER DYNAMIC LOADING

A dissertation submitted in the fulfilment of the requirements for the degree Magister Technologiae: Engineering: Civil

In the Faculty of Engineering and Technology

Mukalay, J.N.

213050463

Vaal University of Technology

Supervisor: Prof. R. W. Salim

Co- Supervisors: Prof. L. M. Masu

Dr. S. Rwanga

DECLARATION

I, Mukalay Joella Ngoie, hereby declare that this dissertation is my own work, except for what is clearly acknowledged in the form of references. This dissertation has never been submitted before for any degree or examination to any institution.

Signature: _____

_____ day of _____ 2019

ACKNOWLEDGEMENTS

I would like to express my sincere appreciation to my supervisor, Prof. Salim R. Wanjala and co-supervisors, Prof. L.M. Masu and Dr Sophia Rwanga for their guidance and support, without which this work would not have been possible.

I am truly grateful to the Civil Engineering Head of Department, staff and technicians.

I also would like to express my heartfelt gratitude to the Head of the Department of Civil Engineering, Tshwane University of Technology as well as to the laboratory technician, Ms Thembi Sibeko for allowing me to use their facilities for my experimental work.

My sincere gratitude goes to the Head of Department of the Motor Fleet Department of Vaal University of Technology, Mr Thabang, for always availing a vehicle for my trips to Tshwane University of Technology, in order to perform my experimental work.

DEDICATION

To my parents,

For teaching me to trust in God,

For supporting me and always encouraging me.

ABSTRACT

This research investigated the structural bond strength of GFRP rebars in concrete beams under dynamic loading with the aim to characterize the structural bond behaviour and evaluate the limitations of the GFRP rebars under dynamic loading.

The dynamic loading in this study was set at 500 repeating cycles to simulate a more realistic dynamic loading scenario such as earthquake since most dynamic loading studies are carried under ten repeating cycles.

The experimental work was divided into 2 main tests which were firstly, the tensile tests of the GFRP rebars in order to evaluate the tensile strength of the rebars and characterize their properties. Secondly, the flexural tests of GFRP and steel reinforced concrete beams in order to evaluate the bond strength of GFRP and steel rebars, to characterize the average bond strength of GFRP and steel reinforced concrete beams under dynamic loading and finally to compare the average bond strength of GFRP rebars to Steel rebars in both dynamic and static loadings.

The tensile tests were carried out using a Universal Testing Machine (UTM) and the results of the tensile tests of the GFRP rebars showed that the average experimental tensile strength of GFRP rebars was only 56.65% of the nominal tensile strength provided on the supplier data sheet. As for flexural tests, they were carried out through a four-point bending test using a UTM in conjunction with a universal dynamic shaker to create the dynamic loading set up. Steel reinforced concrete beams were used as control beams during the tests and factors such as the tensile strength of the GFRP rebars, the slip of the rebars, the load-deflection relationship and the stress-strain relationship were investigated. The results of the tests showed that the tensile strength of the GFRP rebar is strongly proportional to the maximum beam load bearing capacity and the maximum stresses of GFRP reinforced concrete beams. The results also showed that the average bond strength of GFRP rebars in static loading (8.44 MPa) was only 80% of the average bond strength in dynamic loading (10.95 MPa). Moreover, the experimental work showed that the failure of GFRP reinforced concrete beams depicted large deflections (19 mm) and slips (5 mm to 12.5 mm) when compared to steel reinforced concrete beams (for which the maximum deflection was 9.66 mm at failure and slippage values of 2 mm to 10 mm). Based on that it could be stipulated that the tensile strength of GFRP rebars is one determinant factor to the bond strength behaviour of GFRP rebars in concrete. Hence, the structural bond behaviour of GFRP rebars could be well-defined if more studies were done on

the bond behaviour of GFRP rebars in concrete beams under dynamic loading using another type of GFRP rebars that would consist of a relatively high tensile strength as compared to the ones used in this study and different surface texture.

Table of Contents

DECLARATION i
ACKNOWLEDGEMENTS ii
DEDICATION iii
ABSTRACT iv
Table of Contents vii
List of Figures ix
List of Tables xi
List of Symbols xii
List of Abbreviations xvi
1. INTRODUCTION 1
1.1 Background 1
1.2 Significance of the Study 2
1.3 Problem Statement 2
1.4 Aim and Objectives of the Study 3
1.5 Scope 3
1.6 Outline of the dissertation 3
2. LITERATURE REVIEW 4
2.1 Introduction 4
2.2 Factors Influencing the Bond Behaviour of Glass Fibre-Reinforced Polymer Rebars in Concrete Beam 5
2.2.1 The concrete compressive strength 5
2.2.2 The surface configuration of Glass FRP rebars 6
2.2.3 The mechanical properties of GFRP rebars 8
2.2.4 The concrete beam specifications 9
2.2.5 Concrete beam mode of failure 10
2.3 Types of Test Set-Up 11
2.3.1 Pull out test 12
2.3.2 Beam tests 12
2.3.3 Summary 13
2.4 Dynamic Testing of FRP Rebars 14
2.4.1 The dynamic testing approach 14
2.4.2 Dynamic signature test 14

2.4.3 The Miner's hypothesis 15
2.4.4 General bond behaviour of GFRP rebars in dynamic loading 15
2.5 Summary 16
3. RESEARCH METHODOLOGY 18
3.1 Introduction 18
3.2 Experimental Design 18
3.3 Research Materials 20
3.3.1 Ready mix concrete 20
3.3.2 Reinforcing bars 21
3.4 Equipment and Tools used in the Experimental Tests. 25
3.4.1 Equipment and tools for the tensile tests. 25
3.4.2 Equipment for concrete compressive tests 26
3.4.3 Equipment and tools for the flexural tests 26
3.4.3.1 Introduction 26
3.4.3.2 Measurement of slip 28
3.4.3.3 Measurement of strain 30
3.4.3.4 Dynamic loading set-up 35
3.4.3.5 Loading rate 38
3. 5 Model Design of the Concrete Beams 39
3.5.1 Experimental set-up and design of the beam 39
3.5.2 Design of GFRP reinforced concrete beam specimen 40
3.5.2.1 Dimensioning of the concrete beam 40
3.5.2.2 Modes of failure and minimum area of GFRP reinforcement 41
3.5.2.3 Determination of the maximum load 44
3.5.2.4 Determination of the beam deflection 45
3.5.2.5 Compression reinforcement 47
3.5.2.6 Evaluation of the shear reinforcement 47
3.5.2.7 Determination of the ultimate bending strength 48
3.5.2.8 Design of the proposed beam 49
3.5.2.9 Determination of the maximum predicted bond strength 49
3.5.3 Design of steel reinforced concrete beam according to SANS 10100-1: 2000 50
3.5.3.1 Dimensioning of the steel reinforced concrete beam and determination of the maximum load 50
3.5.3.2 Calculation of the shear reinforcement 51

3.5.3.3 Determination of the beam deflection 52
3.5.3.4 Determination of the ultimate bending strength 53
3.5.3.5 Design of the proposed beam 53
3.5.3.6 Determination of the maximum predicted bond strength 54
4. PRESENTATION AND ANALYSIS OF RESULTS 55
4.1 Introduction 55
4.2 Tensile Test Results 55
4.2.1 Introduction 55
4.2.2 Presentation of results 55
4.2.3 Load-Extension curves of ribbed GFRP rebars 56
4.2.4 Failure mode and analysis of results 59
4.3 Concrete Compressive Strength Results 61
4.3.1 Introduction 61
4.3.2 Presentation of the results 61
4.4 Flexural Test Results 62
4.4.1 Introduction 62
4.4.2 Presentation of results 62
4.4.3 Load-deflection curves for GFRP and Steel reinforced concrete beams 66
4.4.4 Stress-strain curves for GFRP and Steel reinforced concrete beams 68
4.4.5 Slips measurement results 70
4.4.6 Strain measurement results 72
4.4.7 Results of the beams failure modes 74
4.4.8 Analysis of Results for flexural tests 76
4.4.8.1 Effects of the concrete compressive strength on the bond strength and the resulting modes of failure 76
4.4.8.2 Effects of the surface configuration on the bond strength and the resulting modes of failure 79
4.4.8.3 Effects of the rebars mechanical properties on the bond strength and the resulting modes of failure 82
4.4.8.4 Effects of the loading mode on the bond strength and the resulting modes of failure 85
5. CONCLUSIONS AND RECOMMENDATIONS 87
5.1 Conclusions 87
5.2 Recommendations 89
REFERENCES 90
APPENDICES 96

List of Figures

Figure 2.1 Mass-spring representing dynamic loadings 14
Figure 3.1 Formwork and reinforcing bars preparation. 19
Figure 3.2 Casting of concrete beams. 19
Figure 3.3 Curing of concrete specimens. 20
Figure 3.4 Ribbed Glass Fibre – Reinforced Polymer rebars 21
Figure 3.5 Steel rebars 21
Figure 3.6 Ribbed GFRP Shear reinforcements 22
Figure 3.7 Fibrous thread wrapped along the rebar 23
Figure 3.8 Cross-sectional test of GFRP rebars 23
Figure 3.9 Tensile test: load frame configuration 25
Figure 3.10 Cube testing set-up 26
Figure 3.11 Explicit flexural test set-up 27
Figure 3.12 Cross-section A-A of the explicit test set-up 27
Figure 3.13Actual flexural test set-up 28
Figure 3.14 LVDT connections. 30
Figure 3.15 KFRP Foil strain gage. 30
Figure 3.16 (a) Strain gauge cement. 31
Figure 3.16 (b) and strain gauge placed on the rebars. 31
Figure 3.17 (a) Waterproof tape strips 32
Figure 3.17 (b) placing on the rebar. 32
Figure 3.18 (a) Bituminous substance 32
Figure 3.18 (b) placed on the rebar. 32
Figure 3.19 Strain gauges connection to the interface and logger. 33
Figure 3.20 (a) Prepared surface of the GFRP rebar 34
Figure 3.20 (b) sand paper. 34
Figure 3.21 Dynamic shaker MB dynamic 50A. 36
Figure 3.22 (a) BK Precision function generator 37
Figure 3.22 (b) MB SL 500 amplifier. 37
Figure 3.23 Steel plates used on the beams highlighted in red. 38
Figure 3.24 Loading and Bending moment diagram. 39

Figure 3.25 Concrete beam cross-section. 40
Figure 3.26 Stress-strain distribution diagram in flexure for failure by concrete crushing 48
Figure 3.27 Designed GFRP reinforced concrete beam 49
Figure 3.28 Cross Section A-A 49
Figure 3.29 Designed steel reinforced concrete beam 53
Figure 3.30 Cross section of designed steel reinforced concrete beam 54
Figure 4.1 A1 load-extension curve 56
Figure 4.2 A2 load-extension curve 56
Figure 4.3 A3 load-extension curve 57
Figure 4.4 A4 load-extension curve 57
Figure 4.5 A5 load-extension curve 58
Figure 4.6 (a) A1 specimen resin failing 60
Figure 4.6 (b) A3 specimen resin failing 60
Figure 4.7 Load-deflection curves for GFRP and Steel reinforced concrete beams 67
Figure 4.8 Stress-strain curves for GFRP and Steel reinforced concrete beams 69
Figure 4.9 Influence of the concrete compressive strength on the peak bond strength 78
Figure 4.10 Influence of the concrete compressive strength on the bond strength behaviour. 79
Figure 4.11 Influence of the surface treatment on the bond strength behaviour 80
Figure 4.12 Effects of the surface texture mechanisms on the bond behaviour 82

List of Tables

Table 3.1 Experimental test program 18
Table 3.2 Concrete proportion used. 20
Table 3.3 Specifications for 12 mm diameter ribbed GFRP rebars (Shanghai Xuyao Fibreglass Reinforcement Products Co., Ltd). 22
Table 3.4 Specifications for 6 mm diameter ribbed GFRP rebars (Shanghai Xuyao Fibreglass Reinforcement Products Co., Ltd). 22
Table 3.5 Calculated physical parameters of 12 mm ribbed GFRP rebars 24
Table 3.6 Calibrated specifications of LVDTs provided by the supplier. 29
Table 3.7 Specifications of KFRP (Kevlar Fibre Reinforced Polymer) foil strain gauges. 31
Table 3.8 Specifications of the BK Precision function generator. 36
Table 3.9 Specifications of the amplifier MB SL 500. 37
Table 4.1 Results of the tensile tests of ribbed GFRP rebars 55
Table 4.2 Average concrete compressive strengths obtained from cube tests. 61
Table 4.3 Results of the beams flexural tests at serviceability. 64
Table 4.4 Slip values recorded via LVDT 71
Table 4.5 Strain values recorded via strain gauges. 73
Table 4.6 Proposed mode of failure. 75
Table 4.7 Concrete compressive strength data 77
Table 4.8 Comparison of GFRP and steel rebars mechanical properties 84

List of Symbols

A	Rebar samples for tensile test
A_c	Cross-sectional area of the concrete cube
A_f	Cross-sectional area of the GFRP rebars
A_{fv}, A_{sv}	Amount of FRP and steel shear reinforcement respectively
$A_{fv,min}$	Minimum shear reinforcement
A_s	Area of steel reinforcement
b	Width of the concrete beam
b_w	Width of the web
C_0	Lesser of the cover to the centre of the bar or one-half of the centre-on-centre spacing of the bar being developed
C_E	Environment reduction factor for various fibre type and exposure conditions
C_f	Circumference of the rebar
c	Concrete cover
d	Distance from the extreme compression fibre to the centroid of tension reinforcement
d_b	Diameter of the rebar
E_c	Modulus of elasticity of the concrete
E_f	Modulus of elasticity of GFRP rebars
E_s	Voltage of the Wheatstone bridge interface, Elastic modulus of steel rebars
e_0	Increment output voltage
F_m	Apparent maximum yield load
F_P	Apparent yield load

f_c	The cylinder concrete compressive strength
f_{cu}	The cube concrete compressive strength
f_f	Stress in the GFRP rebar in tension
f_{fu}	Theoretical design tensile strength of FRP
f_{fu}^*	Guaranteed tensile strength of GFRP rebar
f_{fu-Ex}	Experimental tensile strength
f_{fu-s}	Supplier guaranteed tensile strength
f_{fu-th}	Theoretical tensile strength
f_{fv}	Tensile strength of FRP for shear design, design tensile strength of steel for shear design
f_r	Modulus of rupture of concrete
f_y	Tensile strength of steel rebar
h	Depth of the beam
I_{cr}	Moment of inertia of the transformed cracked concrete beam section
I_e	Effective moment of inertia
I_g	Gross moment of inertia of the concrete beam
K_s	Gauge factor of the strain gauge
k	Positive constant of the spring, Ratio of the depth of neutral axis to reinforcement depth
L_0	Span length of the beam.
L_f	Measured length of the rebar
L_{sh}	Shear length of the beam
l_e	Development length of the bar

M	Mass, Moment
M_n	Nominal moment capacity
M_{max}	Maximum moment
M_{cr}	Cracking moment
n_f	Equivalent ratio of elasticity of the reinforced concrete beam
P, P_{max}	Load, maximum load
R_A , R_B	Reactions at the supports
S_v	Spacing between the stirrups
V	Maximum shear force
V_1 , V_0	Volumes of water in the graduated cylinder glass, after and before immersing the rebar, respectively
$\ddot{x}$, $\dot{x}$	Second and first derivatives of the spring's position with respect of time
y	Distance from the extreme compression fibre to the Neutral axis N.A
Z	Lever arm from the centroid of the full compression area to the centroid of the tension reinforcement
α_1, β_1	Stress-block factors for concrete
$\delta_{allowable}$	Maximum allowable deflection in concrete beam
$\delta_{GFRP-th}$	Theoretical deflection in GFRP reinforced concrete beam
$\delta_{GFRP-Exs}$	Experimental deflection in GFRP reinforced concrete beam under static loading
$\delta_{GFRP-Exd}$	Experimental deflection in GFRP reinforced concrete beam under dynamic loading
δ_{max}	Maximum deflection in the reinforced concrete beam
$\delta_{Steel-th}$	Theoretical deflection in steel reinforced concrete beam

$\delta_{Steel-Exs}$	Experimental deflection in steel reinforced concrete beam under static loading
$\delta_{Steel-Exd}$	Experimental deflection in steel reinforced concrete beam under dynamic loading
ε_0	Strain quantity
ε_{cu}	Ultimate strain in concrete in compression
ε_{fu}	Ultimate strain in FRP in tension
θ_c	Concrete resistance factor
θ_f	GFRP rebar resistance factor
$\mu_{th-GFRP}$	Theoretical bond strength of GFRP is rebars in concrete beams
$\mu_{th-Steel}$	Theoretical bond strength of steel rebars
ρ_f	GFRP reinforcement ratio
ρ_{fb}	Balanced ratio reinforcement
τ_s	Shear stress
Δs	slippage of the rebar
μ_{max}	Maximum bond strength
$\Delta \mu V$	change in voltage
μV_1	Output voltage at the beginning of the test
μV_2	Output voltage at the end of the test
γ	Parameter that accounts for the variation in stiffness along the length of the concrete member
σ	Bending strength
σ_{max}	Maximum bending strength

List of Abbreviations

ASTM	American Society for Testing and Materials
GFRP	Glass-Fibre-Reinforced-Polymer
FRP	Fibre-Reinforced-Polymer
KFRP	Kevlar Fibre Reinforced Polymer
RCGFRP	GFRP Reinforced Concrete beam
RCS	Steel Reinforced Concrete beam
SANS	South African National Standard
UTM	Universal Testing Machine

1. INTRODUCTION

1.1 Background

The primary cause of deterioration of reinforced concrete is the corrosion of the steel reinforcement (Young-jun, et al., 2015). Though the steel reinforcement is physically protected by concrete, an aggressive environment can reduce the alkalinity of the concrete which results in the corrosion of the steel and spalling of concrete cover. Over the recent years, many researchers have investigated the possibility of replacing the conventional steel reinforcement by the Fibre-Reinforced Polymer (FRP) rebar which is a composite material made by combining fibres and a resin to give a new combination of properties (ACI 440 R1-03 , 2005). Three types of FRP rebars are more commonly used in the civil engineering industry: Glass FRP, Carbon FRP and Aramid FRP rebar. Each of them has their advantages and disadvantages (Meier, 2000). The Glass FRP rebar is the most commonly used in civil engineering applications owing to its high tensile strength, its low price and its availability (Meier, 2000). However, its performance (high tensile strength and modulus of elasticity) and durability resistance are not superior to those of Aramid and Carbon FRP rebar. Aramid FRP rebar has higher tensile strength and modulus of elasticity than Glass FRP rebar but the impediment with its utilization is that it's difficult to cut and machine, moreover its cost is slightly higher than that of Glass FRP rebar. The carbon FRP rebar has higher tensile strength and modulus of elasticity over the other two types. Further investigations have been done on the bond behaviour under static loading condition of different types of FRP rebars through different types of tests. The results of the static tests were in agreement with the prediction that carbon FRP rebars have high durability resistance in concrete (Meier, 2000). However, carbon FRP rebar's high price constitutes its drawback (Davalos, et al., 2008 and Oshan & Zhang, 2013). Furthermore, the bond behaviour of FRP rebars depends on a great number of parameters compared to the conventional steel rebar (Tamuzs, et al., 2001). Tighiouart , et al., (1999); Yoon-lee, et al., (2013); Taher & Burgoyne, (2011); Wan, et al., (2002) and Ametrone (2001) considered different parameters in their investigations of the bond behaviour but a lot still needs to be done to really understand and assess the bond behaviour of FRP rebars. The bonding between FRP reinforcing rebars and the surrounding concrete can be defined as the continuous interaction between the two materials and is known to play an essential role in transferring the stress from the concrete to the reinforcing bar. The average bond strength and the longitudinal modulus of elasticity of FRP rebars are lower than that of steel rebar (Vogel & Svecova, 2009).

1.2 Significance of the Study

Steel rebar has been considered as the only reliable reinforcement of concrete structures (Nutt, 2007) until the discovery of advanced composite material (FRP rebars). However, the corrosion of steel reinforcement leads to costly repairs and catastrophic failures every year. Many approaches have been undertaken to control the corrosion process, but they are not suitable as a long-term solution (Bru, et al., 2016). The advantages of FRP rebars over the conventional steel rebar are their properties such as the chemical resistance, ease of handling, high tensile strength to weight ratio, and the ability to be moulded into various shapes (Pleinmann, 1991). FRP rebars properties have made them alternative reinforcement for future construction as the use of FRP rebar for internal reinforcement constitutes an economical solution since the cost of repair of the damaged reinforced concrete structures is extremely low (about 1% - 2% of the original cost) (INC, 2011). One of the major disadvantages of FRP rebars is the understanding of the bond behaviour in concrete structures. The limited knowledge on their bond behaviour in concrete members constitutes a drawback to their use in construction applications. The understanding of its bond behaviour will considerably help to fully accept FRP rebars as internal reinforcement in civil engineering and will contribute to their safe use.

1.3 Problem Statement

One of the most challenging issues of FRP is their bond reliability and durability in concrete structures. FRP rebar bond has been investigated through different parameters but most of them have been carried out considering only a monotonic static loading (Issa, et al., 2011; Tighiouart et al., 1999 and Ehsani, et al., 1996). However, the monotonic static load is far from reflecting the reality of the loading regime on a structure because reinforced concrete structures are also subjected to different forms of dynamic loading throughout their lifespan. Little is known on FRP rebars bond behaviour under repeated loading. So far, cyclic loading studies that have been carried out on FRP rebars, did not exceed a cycle of loading of ten and was only carried out for Glass FRP rebar (Yoon-lee, et al., 2013). The reality is that concrete beams are subjected to more than ten cycles of repeated loading. This study focused on assessing the bond behaviour of ribbed Glass FRP rebar under a loading of more than ten cycles.

1.4 Aim and Objectives of the Study

The aim of the study was to experimentally determine the bond behaviour of ribbed GFRP rebars in concrete beams under dynamic load.

The specific objectives of the study were to:

(a) Evaluate the maximum tensile strength of ribbed GFRP rebars,

(b) Evaluate and characterize the average bond strengths of ribbed GFRP through the average maximum tensile strength of the GFRP rebars and steel rebars bond strengths in concrete beams,

(c) Compare GFRP rebars average bond strengths to steel rebars average bond strength in static loading and in dynamic loading.

1.5 Scope

This study aimed to investigate the structural bond behaviour of ribbed GFRP rebars in concrete beams under dynamic loading. The experimental work consisted of the investigation of the tensile strength of ribbed GFRP rebars and the flexural tests of ribbed GFRP reinforced concrete beams. The tensile tests of the ribbed GFRP rebars focused on characterizing the rebars behaviour and failure in tension prior to being used as internal reinforcement in concrete beams, while the flexural tests of ribbed GFRP reinforced concrete beams focused on characterizing the bond strength behaviour of ribbed GFRP rebars in concrete under a specific type of dynamic loading mode. The results of the flexural tests were analysed with regards to parameters such as the load-deflection relationships, the stress-strain relationships, the slip of the rebars in the concrete beams but also by using steel reinforced concrete beams as benchmarks.

1.6 Outline of the dissertation

The dissertation has five chapters, namely:

Chapter 1: Introduction;

Chapter 2: Literature Review;

Chapter 3: Research Methodology;

Chapter 4: Presentation and Analysis of Results; and

Chapter 5: Conclusions and Recommendations.

2. LITERATURE REVIEW

2.1 Introduction

Fibre-Reinforced Polymer (FRP) rebars have been used in the recent past, as internal reinforcement instead of steel reinforcement. Many successful applications worldwide have demonstrated their practical use in civil engineering (ACI 440 R1-06, 2006 and Tuakta, 2005). However, they haven't gained full acceptance in the civil engineering world, due to the fact that no general agreement has been achieved about the correct test set up to assess the bond behaviour for the distinct FRP systems. That means that up to date, experiments are undertaken with rough approximations of what could actually represent a FRP system in service life. The durability of various FRP system has hence been assessed taking into account a more known material which is steel reinforced concrete (Ceroni, et al., 2006 and Lin & Zhang, 2014). That assumption has been the basis of the controversy about the full acceptance of FRP materials in construction. The main reason being that the bond between FRP reinforcing rebars and the surrounding concrete is complicated and influenced by many more factors than in the case of steel reinforced concrete structures (Ceroni, et al., 2006 and Lin & Zhang, 2014). This reason on its own constitutes a big impediment to their implementation in the construction industry but it weighs even more when considering the fact that FRP properties vary according to the type of fibre manufactured source, the manufacturing process and the resin/matrix used (CNR-DT 203/2006, 2007). Moreover, when considering the concrete and FRP rebars materials behaviours on their own and subjected to various loads, concrete on one hand can present a complexity of behaviours which are characterized by strong non-linear response and the development and opening of cracks and fractures in tension. While in compression, concrete presents a plastic response characterized by the development of micro crushes and dislocations of aggregates. Whereas FRP rebars show a lack of ductility in tension (Billah & Alam, 2012) and their compressive strength is negligible (Marfia, et al., 2004). There is a complexity arising from the composite material itself and from the combination of FRP rebar and the concrete (Ceroni, et al., 2006). All these complexities make it even harder for a test set up of a FRP system (Marfia, et al., 2004).

2.2 Factors Influencing the Bond Behaviour of Glass Fibre-Reinforced Polymer Rebars in Concrete Beam

The bond strength between Glass Fibre-Reinforced Polymer (GFRP) rebars and concrete determines the strength and the long-term performance of the reinforced structure (Chin, 1996). The bond strength is strongly affected by the anisotropic nature of GFRP rebars, thus, it becomes very important to investigate the individual behaviour of each of the components of the reinforced structure such as the concrete matrix, the fibres constituting the rebar, the matrix of the rebars and the interface zone, but also the behaviour of the reinforced structure as a whole unit (Nanni, 2003; Egyptian Standing Committee, 2005 and Ray & Rathore, 2015). The influence of each of these factors on the bond strength behaviour has mostly been analysed with regard of the following parameters:

- The concrete compressive strength;
- The surface configuration of GFRP rebars;
- The mechanical properties of GFRP rebars;
- The concrete beam specifications; and
- Concrete beam mode of failure.

2.2.1 The concrete compressive strength

Researches have been performed either with normal strength concrete (Hao, et al., 2008 and Katz, 1999) or with high strength concrete (Akbarzadeh & Maghsoudi, 2009 and Katz, 1999) and the influence of concrete compressive strength could obviously be noticed on the average bond strength of FRP rebars (Baena, et al., 2009 and Cosenza, et al., 1997). It was found that the concrete compressive strength affects the bond mode of failure; moreover, it is correlated to the bearing resistance of the reinforced concrete element. Therefore, the bond strength significantly influences the behaviour of FRP rebars regardless of the surface treatment (Baena, et al., 2009).

It has been established that when concrete compressive strength is relatively low (below 20 MPa), the average bond strength is proportional to the concrete compressive strength and failure is due to cracking and tensile stresses as in the case of steel rebar. That can be explained by the fact that concrete becomes unable to attain its maximum strain and fails prematurely. In this case, the influence of surface treatment on the bond strength is less obvious (Baena, et al., 2009). For concrete with high compressive strength, beyond 30 MPa, this correlation is no longer apparent. The bond strength doesn't depend heavily on the value

of concrete strength but rather on the rebar properties and their ability to bond to concrete (Baena, et al., 2009). Thus, the interface mode of failure is due to a combined effect of concrete and FRP rebar's surface degradation with failure being increasingly dominated by FRP rebar surface damage (Davalos, et al., 2008). This means that the failure is due to the degradation of the bond between the rebar and the surrounding concrete. The use of high-strength concrete allows better use of the rebars strength properties as compared with normal strength-concrete since the stiffness is increased (ACI 440 R1-06, 2006). Generally low stiffness increases the overall deformability of a flexural member (ACI 440 R1-06, 2006) or causes large deflections and cracks width which can affect the bond and thus the serviceability of the flexural member (Fico, 2007). The above research findings were mostly based on either low strength or high strength concrete (Baena, et al., 2009), omitting normal strength concrete which is more commonly used in civil engineering construction. As for the test results performed on normal strength concrete that were published (Hao, et al., 2008), they did not establish any relationship between the strength of the concrete and the bond strength behaviour (Hao, et al., 2008). Therefore, this study tried to fill this gap by investigating the bond behaviour of GFRP rebars and its governing factors in normal concrete compressive strength under dynamic loading.

2.2.2 The surface configuration of Glass FRP rebars

The surface texture of the rebar is important for its role in developing the bond strength between the rebar and concrete (Ceroni, et al., 2006 and CNR-DT 203/2006, 2007). The bond strength between FRP rebar and the surrounding concrete depends on three things, namely:

- The adhesion resistance (ACI 440 R1-06, 2006 and Wang & Belarbi, 2009);
- The friction resistance (ACI 440 R1-06, 2006 and Cosenza, et al., 1997); and
- The mechanical interaction or interlocking (ACI 440 R1-06, 2006 and Cosenza, et al., 1997).

a. The adhesion resistance

The adhesion resistance also known as the chemical bond is ensured at low values of stresses (Marfia, et al., 2004; ACI 440 R1-06, 2006 and Belarbi & Wang, 2004). For higher values of stresses, the chemical bond breaks down. As tensile stresses increase, deformations on the surface of the rebar cause inclined contact forces at the rebar-concrete interface giving rise to micro cracks (ACI 440 R1-06, 2006).

There are currently many types of FRP rebars with different surface treatment available on the market (sand coated, helically wrapped, helically wrapped and sand coated, grooved surface, ribbed rebars, etc.). They all seem to behave similarly when the adhesion resistance exists, but once this bond fails different behaviours are obtained for the different surface-treatments, depending either on the friction resistance or the mechanical interlocking (Baena, et al., 2009 and Lin & Zhang, 2013).

b. The friction resistance

The friction resistance develops bond strengths at the rebar-concrete interface preventing any significant slippage (Oshan & Zhang, 2013). As the tensile stress increases, the mechanical interlock breaks down and the bond behaviour tends to become dry-friction since the concrete between the indentations/ribs is crushed as in the case of steel rebars (Marfia, et al., 2004). Moreover, the FRP rebar's surface is stripped off increasing the slip value (Lee, et al., 2013 and Marfia, et al., 2004). Indeed, only when rebars possess adequate characteristics to provide enough lateral confinement through the ribs or indentations that the dependence of bond strength on concrete compressive strength is observed (Cosenza, et al., 1997 and ACI 440 R1-06, 2006). This leads to the consideration of the physical characteristics of the FRP rebar's surface which are the shape, the height and/or size of the ribs or sand coated layer of the FRP rebar's surface. For ribbed GFRP, the shape and the height of the ribs constitute the main factors that affect the bond strength.

c. The mechanical interaction or interlocking

The mechanical interaction or interlocking between the deformed surface of the rebar and the surrounding concrete are governed by the outer surface of the rebar (Cosenza, et al., 1997; Hao, et al., 2008 and Belarbi & Wang, 2004) and is said to be the dominant mechanism over the two other bond mechanisms (adhesion and friction resistance mechanisms) (Jalili, et al., 2009). That being said, further comparisons were made between smooth rebars and deformed surface rebars. It was found that the bond strength of smooth rebars is primarily governed by the adhesion resistance and friction forces which depend on the transverse pressure. Low mechanical interaction forces are expected and the failure occurs as the friction diminishes when the contact surface is damaged. At this point, the main factors governing the bond behaviour are the type of fibers and the matrix (Baena, et al., 2009). FRP reinforced concrete beams (reinforced with smooth rebars) exhibit large increases in

deflection with small increases in load due to their low load bearing capacities (Lin & Zhang, 2013).

For deformed surface of the FRP rebars, the bond strength is governed by all the three mechanisms, moreover the mechanical interaction lasts up to failure and less slips are recorded (Baena, et al., 2009). On this regard, the bond behaviour of different surface textures was compared as well (Lin & Zhang, 2013). It appeared that ribbed rebars and helically wrapped rebars seem to have a similar flexural behaviour (Lin & Zhang, 2013). Surprisingly, grooved surface rebars behave similarly to sand coated rebars, although they possess indentations as ribbed and wrapped rebars. This phenomenon can be explained by the fact that the wedging action resulting from the crushed concrete sticking to the ribs is less pronounced for grooved surface rebars (Baena, et al., 2009). Finally, sand coated rebars showed much better bonding with concrete than the other ones. An initial good bond performance was recorded until the maximum bond strength is reached, afterwards an abrupt decay occurs. However, a low slip value is recorded (Baena, et al., 2009 and Lin & Zhang, 2013).

It is important to specify that those findings are still not conclusive but specific to a certain domain, since they were either based on one specific test (pull-out test) (Baena, et al., 2009) or a specific concrete age (concrete compressive strength) (Lin & Zhang, 2013). This study also sought to understand the bond behaviour of ribbed GFRP rebars, by investigating the bond strength and the mechanisms governing the bond strength in normal strength concrete. This was done through a four-point bending test, from the moment the concrete has reached its maturity.

2.2.3 The mechanical properties of GFRP rebars

GFRP rebars are characterized by high tensile strength only in the direction of the reinforcing fibres (ACI 440 R1-06, 2006) and lower transverse modulus of elasticity than their counterparts (ACI 440 R1-03, 2005). Therefore, they are stiff in the longitudinal direction and very susceptible to bending forces in the transverse direction (Ochola, 2004), that implies larger strain, curvatures, midspan deflection and wider cracks than in steel reinforced concrete (ACI 440 R1-03, 2005 and Ding, et al., 2014). That induces significant prying forces on the reinforcing rebar and the spalling of the concrete could be accelerated (ACI 440 R1-03, 2005). Their bond stress-slip response is characterized by an initial increase in the bond stress with little slippage, followed by a softening once the maximum

bond stress is reached (Baena, et al., 2009). Yet, GFRP rebars are characterized by viscoelastic behaviour when dynamically loaded. The dissipation of strain energy leads to the degradation of the rebar itself, the microscopic failure of the interface zone, the degradation of the toughness and the rebars mechanical properties such as the ultimate tensile strength and shear strength (Bank, 2013 and Ray & Rathore, 2015).

Similar to steel rebars, FRP rebars play an important role in sustaining the tremendous tensile stresses applied to concrete structures. Therefore, characterizing the tensile strength of a specific type of FRP rebars is necessary for quality control, design purposes and standardization of specific types (Kocaoz, et al., 2005). This study sought to correlate the mechanical properties of GFRP rebars to their bond behaviour in normal concrete under dynamic loading.

2.2.4 The concrete beam specifications

FRP reinforced concrete beams exhibit no ductility due to the linear elastic brittle behaviour of the reinforcement (Issa, et al., 2011). Concrete sections are commonly under reinforced to allow the yielding of steel rebars before the crushing of the concrete which leads to debonding (ACI 440 R1-06, 2006). In the case of flexural members reinforced with FRP rebars, a lot of consideration needs to be given to the flexural design philosophy. Concrete structures cannot depend on the strength and stiffness contributions provided by the compressed FRP rebars, because FRP rebars are assumed to resist only tensile forces (CNR-DT 203/2006, 2007). Thus, to compensate for the lack of ductility, the reinforced concrete must possess a higher reserve of strength. That means the member should be made of high-strength concrete and over-reinforced (ACI 440 R1-06, 2006 and Fico, 2007).

The brittle behaviour of both FRP reinforcement and concrete allows considerations to be given to three main types of failures that govern the modes of failure of FRP-concrete specimens namely, the FRP rupture, the bar pull out and the concrete crushing (ACI 440 R1-06, 2006 and Fico, 2007). The bar pull out and concrete crushing modes of failure are marginally more desirable than tension failure of the rebar in investigating the bond strength. This is because the tension failure is sudden and catastrophic and would indicate that the maximum concrete strain (0.0035) may not be attained (ACI 440 R1-06, 2006 and Egyptian Standing Committee, 2005). To ensure that rupture of FRP rebars will not govern the mode of failure of a FRP-concrete specimen, the FRP reinforcement ratio should be greater than

1.4 ρ_{fb}(ρ_{fb} denotes the balanced reinforcement ratio) (Egyptian Standing Committee, 2005).

In the bar pull out mode of failure, FRP reinforced concrete beams behave linearly up to the first flexural crack. Afterwards, several behaviours are observed accordingly to the surface texture of the FRP rebars (Lin & Zhang, 2013). In this case, the bond slip value that will be recorded, is a function of the considered embedment length (Oshan & Zhang, 2013) and as for steel reinforcement, when the development length increases the effectiveness of the bond strength decreases owing to the non-uniform bond distribution along the rebars (Fico, 2007). Investigation of the embedment length of FRP rebars in concrete, and of different ranges of diameter demonstrated that the rebar size has a direct influence on the average bond strength (Makitani, et al., 1993). The average bond strength decreases as the diameter of the rebar increases (Makitani, et al., 1993). Another investigation of geometrically similar specimens reinforced with different sizes of diameter showed that the larger the diameter, the lower the bond strength (Baena, et al., 2009). This can be attributed to the Poisson effect which is more pronounced for larger diameter under tension. Therefore, there is a reduction in the frictional and mechanical bond mechanisms (Baena, et al., 2009).

In regard to what has been stipulated above, this study investigated the bond behaviour of GFRP rebars in normal concrete and under dynamic loading by ensuring that the rupture of FRP rebars will not govern the mode of failure of a FRP-concrete specimen. Therefore, in this study, a balanced reinforcement ratio of 1.4 ρ_{fb} or more will be ensured for all samples.

2.2.5 Concrete beam mode of failure

The mode of failure of reinforced concrete structures is known to be complex due to the heterogeneous property of the concrete microstructure, and varies according to the type of stress and the internal structure of the specimen (Owens, et al., 2009). Moreover, concrete structures are considered to have stable existing systems of cracks in the vicinity of coarse aggregates that start developing at load higher or equal to 30% of the structure's ultimate load (Owens, et al., 2009). Therefore, the formation of cracks in reinforced concrete members is inevitable in flexure. This is due to the brittle behaviour of concrete in tension, when the extreme bottom fibre sags in tension (Owens, et al., 2009).

However, there are various types of cracks formation that can happen in concrete beams in flexure, which are mostly bending and shear cracks (for short beams) (Obrien, et al., 2012).

They can be differentiated throughout their arrangement in the concrete beam structure. Bending cracks tend to form more vertically as compared to shear cracks that tend to curve out or form angles close to 45° (Obrien, et al., 2012). Hence, each type of crack or their combination will characterize a mode of failure which is related to the shear length and the depth of the beam (Obrien, et al., 2012). Thus, when the ratio of the shear length to the depth of the beam is ranging between 1 and 2.5 the following crack arrangement can be observed (Obrien, et al., 2012):

For

$$1 < \frac{L_{sh}}{h} < 2.5 \quad (1)$$

Where L_{sh} is the shear length of the beam and h, the depth of the beam.

a. The shear bond failure, where the cracks propagate in direct line from the loading point to the support, and then towards the tension zone. This mode of failure is very destructive of the bond strength, as it destroys the interface zone between the reinforcement and the concrete (Obrien, et al., 2012).
b. The dowel failure, which is characterized by deep cracks crossing the tension reinforcement bar (Obrien, et al., 2012).
c. The shear compression failure which is characterized by the crushing of the concrete at the loading point and develops into shear cracks into the tension zone (Obrien, et al., 2012).

2.3 Types of Test Set-Up

Current design guidelines for FRP reinforced structures haven't reached an agreement on the correct set-up to test the average bond strength of FRP reinforced concrete structures (Ceroni, et al., 2006). However, investigations have demonstrated the relevance of each particular parameter influencing the bond strength behaviour in concrete structure, such as the evolution of the slip value, the study of the stress-strain relationship, the analysis of the shear span, etc (ASTM A944-10, 2010; ASTM D7616/D7616M-11, 2011; ASTM D7264/D7264M-15, 2015 and ASTM D5379/D5379M-05, 2005). Hence, the average bond strength can be evaluated through one of the following tests: The pull out test or the beam tests.

2.3.1 Pull out test

This test gives unconservative results while compared to the beam tests. This is due to the embedment length considered in the set-up and the absence of flexural cracks in the concrete, considering the thickness of the concrete cover (Cosenza, et al., 1997 and Foccaci, et al., 2000). It is therefore useful in evaluating the load-slip response of reinforcing bars (ACI 440 R1-06, 2006).

2.3.2 Beam tests

Beam tests are costly compared to the pull out test owing to the equipment required, but more realistic. They reflect the actual beam behaviour because they allow random distribution of flexural cracks since the concrete surrounding the rebar is under tension and the flexural stresses are not affected by the loading configuration. The average bond strength development and splice length are represented in full size flexural members (ACI 440 R1-06, 2006; Lin & Zhang, 2013 and Orozco & Maji, 2003). Beam tests can be performed through one of the following methods:

- The notched test;
- The splice test;
- The three point bending test;
- The beam end test; and
- The four point bending test.

a) The notched test

This method is used to characterize the shear properties of a reinforced structure such as the shear strain, shear stress and shear modulus. In this test, a load is applied at a specified rate until the specimen failure occurs by shear and not twisting. The samples are notched at the midspan (ASTM D5379/D5379M-05, 2005 and Bru, et al., 2016).

b) The splice test

Overlap splices are inevitable in the field due to the length limitations of the rebars or construction requirements. The splice test determines the shear strength of an overlap splice of a reinforced structure. It serves as a quality control mechanism of overlap splices constructed under field conditions (ASTM D7616/D7616M-11, 2011 and Seffo & Hamcho, 2016).

c) The three point bending test

In the three point bending test, the specimens are simply supported and loaded at their center. The samples attain the peak stress at the specimen mid-point and reduced stresses are localized elsewhere. This method is ideal in the investigation of specific isolation of stress on a material (ASTM D7264/D7264M-15, 2015 and Shillings, 2015).

d) The beam end test

This method determines the bond strength of reinforcing bars in concrete, by investigating the effects of the rebars surface preparation. The bond strength obtained in this method is generally high as the concrete is subjected to compressive load. The results obtained from this test are only used for comparison purposes (ASTM A944-10, 2010 and Farshadfar, et al., 2008).

e) The four point bending test

This test is used to characterize the flexural behaviour of specimens. This test set-up utilizes two load points equally spaced from the supports points (ASTM D7264/D7264M-15, 2015 and Shillings, 2015). It has its own advantages of characterizing the mechanical properties of materials as it produces a uniform moment between the two inner loading rollers (Zhai, et al., 1999). This results in a uniform maximum tensile stress in the specimen, thus, less complicated to be evaluated. This test is usually performed with a uniform rectangular cross section, making the set up fairly straight-forward which allows the testing of brittle materials in tension or axial fatigue tests (Zhai, et al., 1999). The lack of sufficient data on this test implies that the samples geometries are arbitrarily set. The inner span between the rollers is usually set to be L/2 or L/3 (L denotes the span of the FRP reinforced concrete structure) as it is simple to handle and mitigates errors (Zhai, et al., 1999). This test set-up was adopted in this study as it has the advantages of providing uniform moments distributions between the supports and more realistic test values.

2.3.3 Summary

The average bond strength obtained from pull out test is relatively higher than that in the beam tests (ACI 318-05, 2005 and Quayyum, 2010). Therefore, this value cannot directly be applied to the design of a FRP reinforced structure (ASTM A944-10, 2010; ASTM D7616/D7616M-11, 2011 and ACI 440 R1-06, 2006). The results must be supported by beam test values. Moreover, it was also found that not all beam tests are suitable in the

determination of the average bond strength of GFRP rebars in concrete beams. Some, such as the beam end test and the splice test, are mostly used for quality control (ASTM A944-10, 2010 and ASTM D7616/D7616M-11, 2011). However, the four point bending test has the advantage of providing a better understanding of the bond behaviour and more realistic values of bond strength (Zhai, et al., 1999). This study sought to understand the bond behaviour of GFRP rebars in normal strength concrete under dynamic loading using the four-point bending test which can provide more realistic values.

2.4 Dynamic Testing of FRP Rebars

2.4.1 The dynamic testing approach

A dynamic loading is a loading mode where the load, P, is applied to a structure in a pulsating manner. From a mechanical point of view, the dynamic loading concept of a concrete beam structure can be simplified to the mechanism of a classical mechanical harmonic oscillator of a single-degree-of freedom system consisting of a mass, M, connected to a fixed point by means of an elastic spring of stiffness K (Groblacher, 2010 and Hao, et al., 2008) as shown in Figure 2.1.

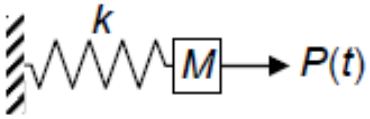

Figure 2.1 Mass-spring representing dynamic loadings

Thus,

$$P(t) = M\ddot{x} + k\dot{x} \quad (2)$$

Where the load P is a function of the time, M is the mass, $\ddot{x}$ and $\dot{x}$ are respectively the second and first derivatives of the spring's position with respect of time, and k is the positive constant of the spring.

2.4.2 Dynamic signature test

In a dynamic signature test (DST), the load induced on to the reinforced structure generates harmonic forces or vibration throughout the beam. The vibration and the degradation in the reinforced structure are thus calibrated in an interval of time. This set up involves the use of an oscillator and steel plates in a flexural set up (Cheng, et al., 1999).

a) Harmonic oscillator

The harmonic oscillator is fixed to the top surface of the beam, at the point of loading to generate harmonic forces with a constant frequency. The frequency induced throughout the concrete beam will vary with the degree of damage or cracks propagation that occurs in the reinforced structure (Cheng, et al., 1999).

b) Steel plates

Steel plates are used as preload. They are attached on top of the beam and must weigh about 50% of the reinforced structure weight. They are used to reduce the effort for frequency identification, to improve the quality of test data and to accelerate the degradation of the loaded structure (Cheng, et al., 1999). However, they are not used to generate cracks but to keep them open from the moment cracks start propagating in the structure. The propagation of cracks induces a variation in frequency in the beam that is easy to monitor as the dynamic loading is in progress. In DST, Steel plates also represent the realistic service load to which a concrete structure is subjected to before undergoing any kind of dynamic loading (Cheng, et al., 1999).

This study used a similar approach to the DST to set a dynamic loading set-up. However, a different frequency inducer was used instead of a harmonic oscillator. The frequency inducer that generated harmonic forces with a constant frequency was a dynamic shaker.

2.4.3 The Miner's hypothesis

The commonly accepted Miner's hypothesis states that the residual slip under fatigue loading accumulates over time (Wang & Belarbi, 2009). It is also interpreted as follows: At the time of fabrication, the reinforcing bar is not in full contact with the surrounding concrete, since there exists micro-voids (Wang & Belarbi, 2009). As the reinforced concrete specimen is subjected to a sustained load or cyclic loads, some micro-voids should be gradually filled, reducing the chances of slippage of the reinforcement. The system should become over time stabilized and the accumulation rate should slow down (Wang & Belarbi, 2009). This research investigated the bond strength behaviour of GFRP rebars in dynamic loading by the analysis of the slip, bond strength, as well as stress and strain values in order to verify this hypothesis.

2.4.4 General bond behaviour of GFRP rebars in dynamic loading

In FRP reinforced concrete structure, the interface zone between the rebar and the concrete is the most highly stressed region of the composite material. It plays an important role in

transferring the stress and dissipating the strain (Ray & Rathore, 2015). The degradation of the interface zone is detrimental for the properties and performance of FRP rebars, the reason being that the microscopic materials' failure leads to the macroscopic failure which happens later on and suddenly (Ray & Rathore, 2015).

Dynamic loading induces significant bond reduction even at low tensile loads because of the particles that are stripped off from the rebars (indentation or coating) and remain wedged at the interface region. This prevents the bonding between the rebar and the surrounding concrete during the different rate of loading-reloading tensile cycle (Lee, et al., 2013). FRP systems subjected to uniaxial bending moment (when the loading axis coincides with a symmetric axis of the reinforced element's cross section) are characterized by a flexural behaviour that exhibits no ductility, hence no yielding before rupture (ACI 440 R1-06, 2006; Fico, 2007 and Egyptian Standing Committee, 2005). The global behaviour of GFRP rebars bond strength in dynamic loading is characterized by an increase in bond stress and stiffness with little slippage and propagation of cracks (Baena, et al., 2009; Ochola, 2004 and Adhikary, et al., 2012). The reason being that GFRP rebars hardly dissipate strain energy without the presence of cracks inside the concrete matrix (Bank, 2013 and Yan, et al., 2000).

The above bond behaviour of FRP rebar has mostly been investigated under monotonic loads. The reality is that concrete beams are subjected to various types of dynamic loading in the form of earthquakes, blasts or simply repeated loading-unloading during their service life (Adhikary, et al., 2012 and Lee, et al., 2013).

2.5 Summary

Numerous studies investigated the bond strength behaviour of GFRP rebars using various set-ups of GFRP's surface configuration in monotonic loading mode. It was found that the average bond strength is greatly dependent on the properties of the composite materials made of FRP rebars and concrete and the test set-up (ASTM A944-10, 2010; ASTM D7616/D7616M-11, 2011and ACI 440 R1-06, 2006).

The investigations of the bond strength of GFRP rebars throughout different types of test set-up revealed that the bond behaviour of GFRP rebars, the strain, stress and slip response are related to the rebar's surface treatment in monotonic and fatigue loading modes (Chin, 1996). However, dynamic loads are known to generate higher local stresses and strains in the rebars leading to complex damage modes or failures and behaviour due to the

heterogeneous nature of the reinforcing bar (Ullah, et al., 2014). The Miner's hypothesis assumes that in dynamic or fatigue loading mode, the degradation of the bond strength is attenuated for a certain period of time of loading and the system should not fail suddenly but slowly due to fatigue (Wang & Belarbi, 2009). However, this is just an assumption that needs to be verified. Thus, this study investigated the bond strength behaviour of ribbed GFRP rebars by analysing the stress, strain and slip response during a test.

3. RESEARCH METHODOLOGY

3.1 Introduction

The experimental work consisted of three main tests which are the tensile test of the reinforcements, the compressive test of the concrete cubes and the flexural test of concrete beams. Two types of reinforced concrete beams were investigated in the flexural tests, which are Steel reinforced concrete beams and GFRP reinforced concrete beams. Steel reinforced concrete beams were used as control samples.

3.2 Experimental Design

The experimental work consisted of three main tests as mentioned previously. Table 3.1 presents the experimental tests programme of this study:

Table 3.1 Experimental test programme

Types of Test	Specimens Tested	Number of Specimens	Objectives of the Test
1. Tensile Test according to ASTM A370 and ASTM D3916	Ribbed GFRP Rebars	5	To evaluate the maximum tensile strength of ribbed GFRP reinforcement prior to utilizing them as reinforcing bars in concrete beams for the subsequent flexural tests.
2. Compressive Test according to SANS 5863:2006	Concrete Cubes	9	To Determine the average compressive strength of concrete used for the flexural tests.
3. Flexural Test according to ASTM D7264/D7264M	Ribbed GFRP Reinforced Concrete Beams	36	• To evaluate and characterize the average bond strength of ribbed GFRP rebars through average maximum tensile strength of GFRP rebars. • To compare the GFRP rebars average bond strength to steel rebar average bond strength in static and dynamic.
	Steel Reinforced Concrete Beams	12	

A total number of 48 beams were tested in flexural tests in order to have a representative sample size which helped in characterizing the material behaviour. The concrete cubes were cured for 14, 21 and 28 days, and then tested at these ages respectively. All the beams (GFRP

and steel reinforced concrete beams) were also cured for 28 days and tested at 28 days. Parameters such as the maximum load, the slip at the end of the rebars, the strains and stresses in the concrete matrix and rebars were constantly monitored during the tests.

Figures 3.1, 3.2 and 3.3 below show the preparation, casting and curing of the beam samples respectively.

Figure 3.1 Formwork and reinforcing bars preparation.

Figure 3.2 Casting of concrete beams.

Figure 3.3 Curing of concrete specimens.

3.3 Research Materials

3.3.1 Ready mix concrete

The ready mix concrete used in the preparation of the cubes and beams was of strength class 20 MPa tested through cube testing in a laboratory environment. Ready mix concrete was supplied by a local company named Wearne Readymix (Pty) Ltd. The concrete had a ratio of 70/30 OPC (ordinary Portland cement)/Fly Ash mix. Table 3.2 summarizes the specifications and ratios of the constituents used to prepare the concrete beams.

Table 3.2 Concrete proportion used

Material	Description and source	Relative density	Unit	Quantity
Water	Potable water from municipality (vanderbijlpark)	1	L	190
Cement 1	Afrisam High Strength Concrete cem II/AM(V-L) 42.5R Afrisam	2.6	kg/m^3	239
Cement 2	Classified Ash-Ash resource Lethabo	2.2	kg/m^3	103
Stone	19 mm WG Wearne	2.7	kg/m^3	1000
Sand 1	Crush dust Wearne/ Agent-Based-Model Carletonville	2.7	kg/m^3	506
Sand 2	Washed plaster-sky sand Group five-Vereeniging	2.6	kg/m^3	325

3.2.2 Reinforcing bars

Figures 3.4 and 3.5 show the two types of longitudinal reinforcing bars that were used in the study, namely: Ribbed Glass Fibre-Reinforced Polymer (GFRP) rebars and Steel rebars. Figure 3.6 shows the ribbed GFRP shear reinforcements used on GFRP longitudinal rebars.

Figure 3.4 Ribbed Glass Fibre – Reinforced Polymer rebars

Figure 3.5 Steel rebars

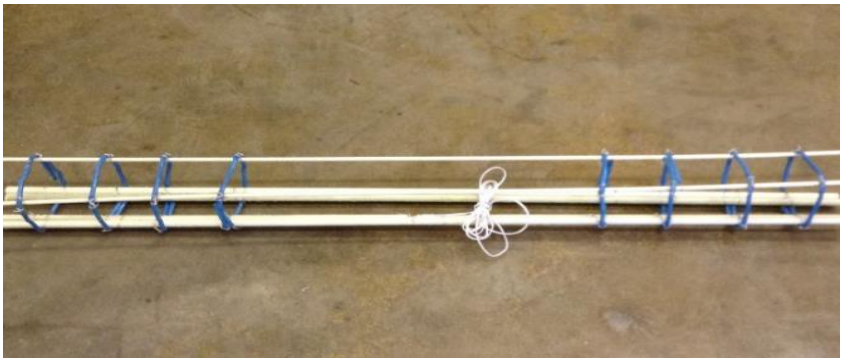

Figure 3.6 Ribbed GFRP Shear reinforcements

a) Glass Fibre-Reinforced Polymer (GFRP) rebars

A total number of 36 reinforced concrete beam specimens were reinforced with ribbed GFRP rebars. Tables 3.3 and 3.4 summarize the supplier's specifications of the rebars (Appendix B).

Table 3.3 Specifications for 12 mm diameter ribbed GFRP rebars (Shanghai Xuyao Fibreglass Reinforcement Products Co., Ltd)

SPECIFICATION	UNIT	VALUE
Effective cross section	mm^2	113
Tensile strength in core	N/mm^2	850
E_f-modulus	N/mm^2	40 000
Weight	g/m	240-270
Diameter	mm	12.0 ± 0.3

Table 3.4 Specifications for 6 mm diameter ribbed GFRP rebars (Shanghai Xuyao Fibreglass Reinforcement Products Co., Ltd)

SPECIFICATION	UNIT	VALUE
Effective cross section	mm^2	28.3
Tensile strength in core	N/mm^2	900
E_f-modulus	N/mm^2	40 000
Weight	g/m	55-65
Diameter	mm	6.0 ± 0.5

The rebars were characterized by a fibrous thread wrapped at constant rib spacing around the rebars, as shown in Figure 3.7:

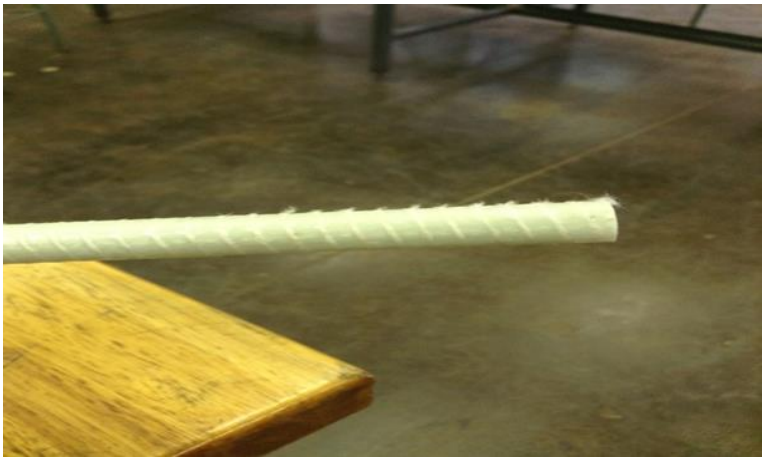

Figure 3.7 Fibrous thread wrapped along the rebar

However, the actual physical parameters of the rebars such as the diameter, the cross sectional area of the rebar and the circumference of the rebar were difficult to determine because of the surface deformation of the rebar. To determine those parameters, the method described in ASTM D618 was used. This method consisted of plunging 5 rebars of 265 mm in length in graduated measuring cylinders filled with water as shown in Figure 3.8.

Figure 3.8 Cross-sectional test of GFRP rebars

The specimens were kept for 24 hours in laboratory environment where the average temperature was 24.6 ℃ and a relative humidity of 38 %. The lengths of the specimens were

measured and the volumes of water in the graduated cylinders were recorded before and after immersing the rebars. The cross-sectional areas of the rebars were then calculated as follows:

$$A_f = \frac{V_1 - V_0}{L_f} \times 1000 \quad (3)$$

Where, A_f is the cross-sectional area of the GFRP rebar;

V_1 and V_0 are the volumes of water in the graduated cylinder glass, after and before immersing the rebar, respectively and L_f is the measured length of one rebar.

The average diameter and the circumference of the rebars could then be determined using the formulae:

$$d_b = 2\sqrt{\frac{A_f}{\pi}} \text{ and} \quad (4)$$

$$C_f = 2\sqrt{\pi . A_f} \quad (5)$$

Where d_b is the diameter of the rebar and C_f is the circumference of the rebar. Table 3.5 presents the physical parameters of the 12 mm ribbed GFRP rebars.

Table 3.5 Calculated physical parameters of 12 mm ribbed GFRP rebars

SPECIFICATION	UNIT	VALUE
Effective cross section A_f	mm^2	106.06
Circumference C_f	mm	36.51
Diameter d_b	mm	11.62

b) Steel rebars

Steel reinforcing rebars used in this experiment were ribbed as seen in Figure 3.5 on page 21. They were supplied by a local company, Cashbuild. The rebars had the following specifications (supplier data):

- Ultimate tensile strength of 450 MPa;
- Young modulus, E_s= 200 000 MPa; and
- Diameter of 10 mm.

3.4 Equipment and Tools used in the Experimental Tests

3.4.1 Equipment and tools for the tensile tests

Ribbed GFRP rebar samples were tested to failure, to investigate their tensile strength and the variables affecting it, using the Computer Control Electro-hydraulic Servo-Universal testing Machine as shown in Figure 3.9. The technical specifications of the machine used are:

- Max load: 2000 kN
- Load accuracy: ≤ ±1%
- Deformation accuracy: ≤ ±1 %
- Load Resolution: 1/10000

The tests were performed according to ASTM A370 and ASTM D3916. The tensile load was applied to rebars at a minimum constant loading rate of 70 MPa/minute as recommended by the ASTM A370. This test also served as a pilot test to spot the signs and mode of possible failure of the rebars in tension for further experiments in this study; hence a representative specimen size of 5 rebars of 12 mm of diameter were tested as recommended by the ASTM D3916.

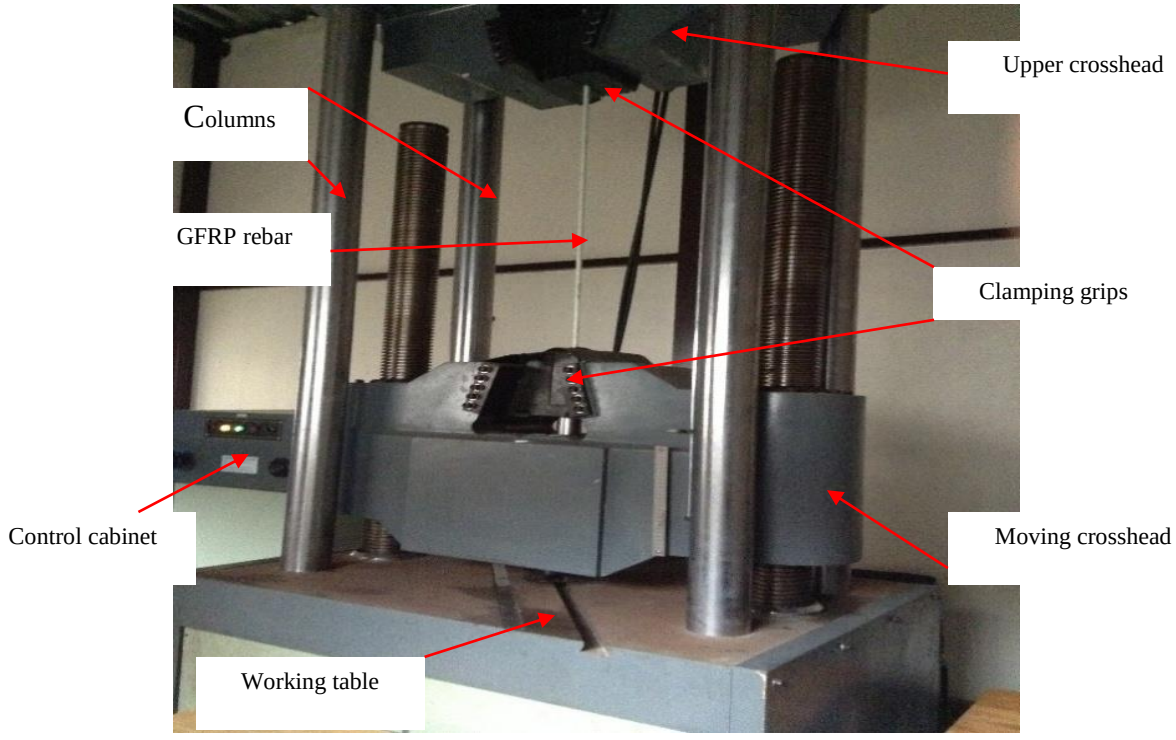

Figure 3.9 Tensile test: load frame configuration

3.4.2 Equipment for concrete compressive tests

Concrete cubes were tested in compression in order to characterize the average compressive strength of the concrete used for the flexural tests. The tests were performed using a concrete cube machine (Figure 3.10), following SANS 5863:2006 requirements. The specimens had a volume of 150 x 150 x 150 mm. A minimum of three concrete cubes were tested per batch as required by SANS 5863:2006, meaning 3 specimens at 14, 21 and 28 days, thus a total of 9 concrete cubes.

Figure 3.10 Cube testing set-up

3.4.3 Equipment and tools for the flexural tests

3.4.3.1 Introduction

The flexural tests were conducted in order to evaluate and characterize the average bond strength of ribbed GFRP rebars and steel rebars through the average maximum tensile strength of the rebars; and in order to compare the GFRP rebars average bond strength to steel rebar average bond strength in static and dynamic modes. The tests were performed according to ASTM D7264/7264M. The flexural tests set-up required the use of several instruments and tools in order to create the desired type of load and also in order to collect the required data such as the slip values, the strain values, the stresses and the loads. The test set-ups shown in Figures 3.11, 3.12 and 3.13 display how the various instruments and tools were connected to one another and to the concrete beam to be tested. The use of each instrument and tool used are explained further in the subsequent sections.

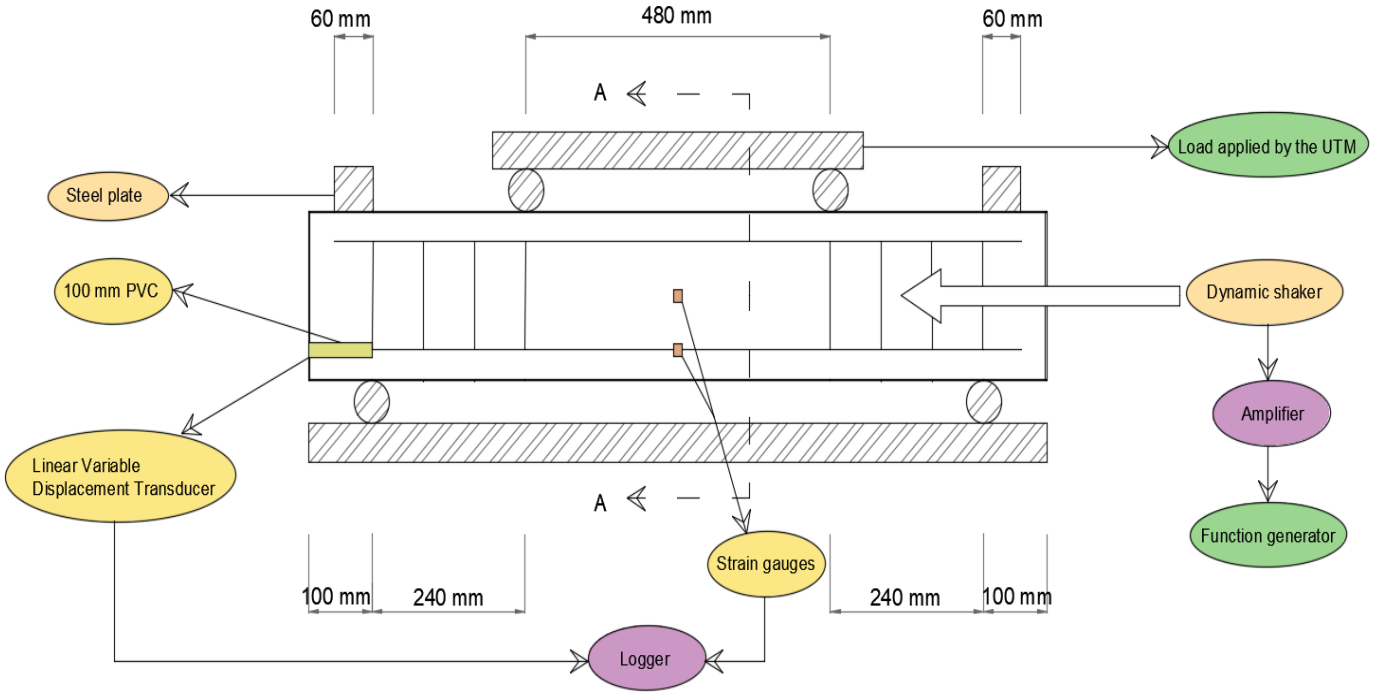

Figure 3.11 Explicit flexural test set-up

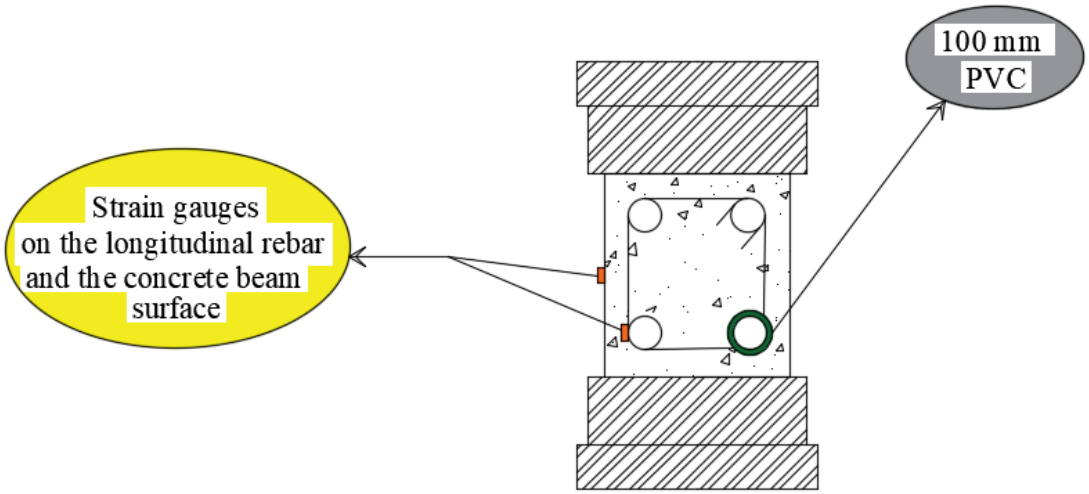

Figure 3.12 Cross-section A-A of the explicit test set-up

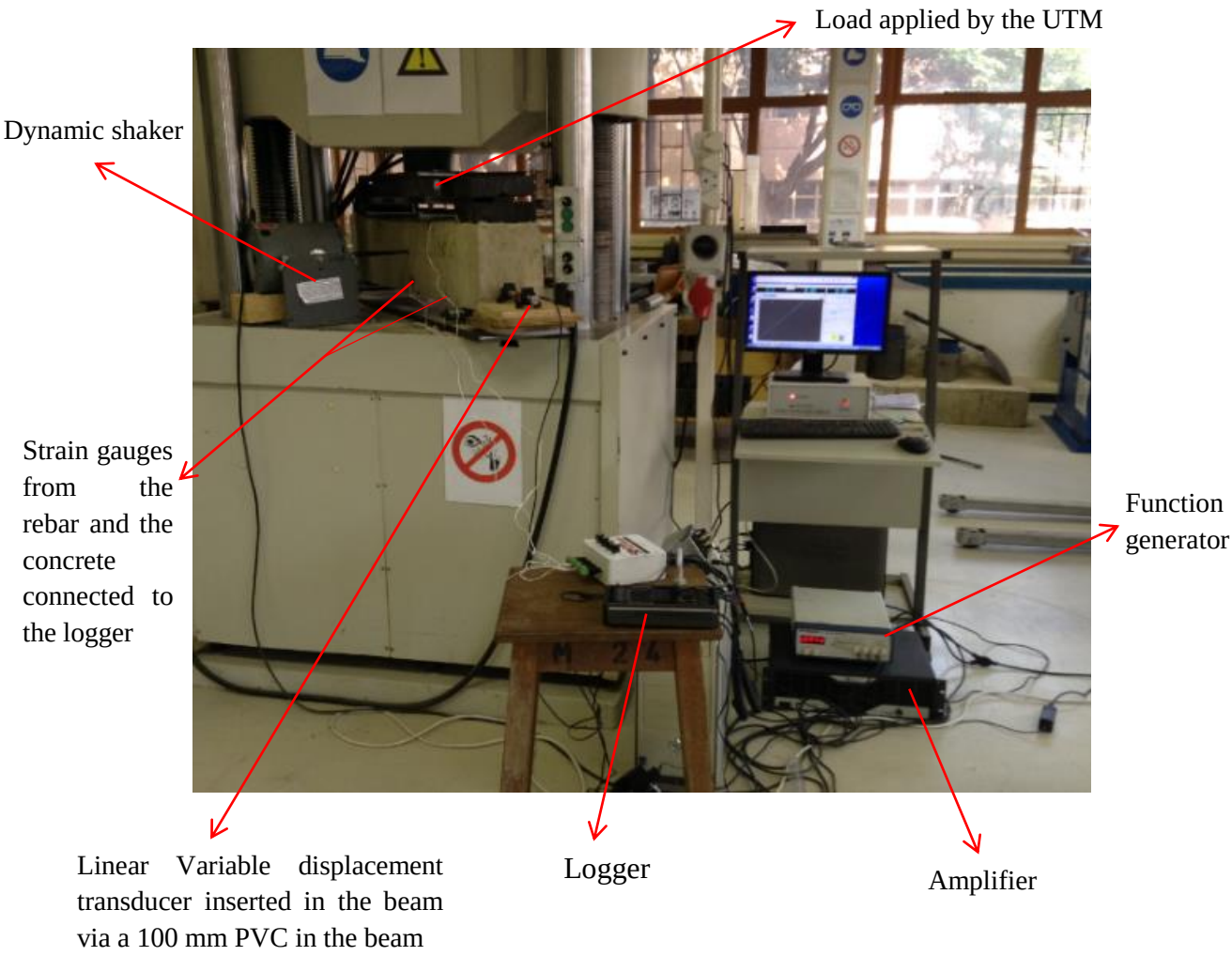

Figure 3.13 Actual flexural test set-up

3.4.3.2 Measurement of slip

The main objective of the study was to investigate the bond behaviour of GFRP rebars in concrete beams under dynamic loading. The bond can be defined as the continuous interaction between the reinforcement and the surrounding concrete which means that it is out of reach and cannot be easily observed and investigated. However, the result of the bond failure, which is the slippage of the rebar, can be measured. To this regard, the resulting slippage of the GFRP rebars under dynamic loading was investigated in order to understand the bond behaviour of the rebars. To accurately achieve the main objective of this study, Linear Variable Displacement Transducers (LVDTs) also known as displacement transducers (DTs) were used.

LVDTs are devices that accurately measure positions and displacements, by the fact that there is no physical contact across the sensing element. They can detect the smallest fraction of movement by suitable signal conditioning electronics. Table 3.6 summarizes the calibrated specifications of the LVDTs used to measure the slip:

Table 3.6 Calibrated specifications of LVDTs provided by the supplier

Type	DCTH500C
Linear range	±12.5 mm
Sensitivity	390.44 mV/mm
Linearity	0.12%
Calibration temperature	20° C
Calibration load impedance	10k (min) ohms

a) LVDTs working principles

The LVDTs sensors used in this study were made of a cylindrical array of primary and secondary windings which were separated by a core passing through the center. The primary windings were energized with a constant amplitude supply at a frequency of 1 to 10 KHz. This produced an alternating magnetic field in the center of the transducer, which induced a signal into the secondary windings depending on the position of the core. Thus, the movement of the core within this area caused the secondary signal to change. The secondary windings were then positioned and connected in a set arrangement (push-pull mode). The slip could then be read from the core movement. When the core was positioned at the center, a zero signal was derived. Any movement of the core from this point in either direction caused the signal to increase. The signal output has a linear relationship with the actual mechanical movement of the core, and was subsequently rectified and filtered. Finally, the output signal which is proportional to the core movement could indicate its direction (positive or negative position) from the central zone point.

b) LVDTs parts and connection

The LVDTs were of the type DCTH series and supplied by a company named Transducers Technology Ltd. They consisted of electronic sensors of 25 mm (stroke diameter), the mounting blocks for the sensors and the logger which is the indicator and signal conditioning instrumentation for the monitoring, measurement and control. The connection of the LVDT

to the logger can be seen in Figure 3.14 and the connection to the concrete beam can been seen in Figures 3.11, 3.12 and 3.13.

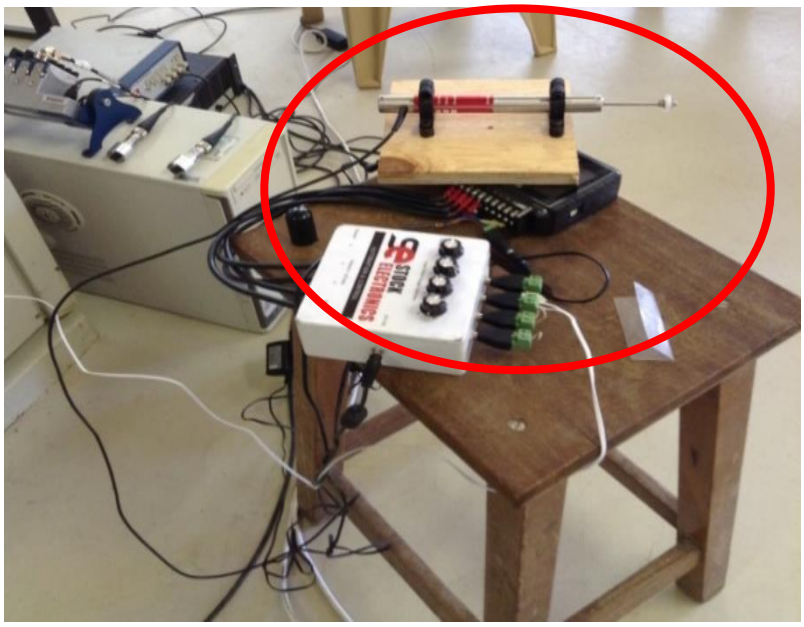

Figure 3.14 LVDT connections

3.4.3.3 Measurement of strain

Strain gauges, as shown in Figure 3.15, were used in order to measure the strain in the reinforcing rebars and the concrete matrix during the flexural tests. They were supplied by a company named Kyowa Electronic Instruments Co. Ltd.

Figure 3.15 KFRP Foil strain gage

The specifications of the strain gauges used in this study are reported in Table 3.7.

Table 3.7 Specifications of Kevlar Fibre Reinforced Polymer (KFRP) foil strain gauges

Type	KFRP Foil strain gage
Resistor	Special alloy
Operating temperature range	-196 to 200℃
Temperature compensating range	0 to 150 ℃
Applicable adhesive	CC-33A (-196 to 120 ℃) EP-34B (-55 to 200℃)
Gage length	2 mm
Temperature coefficient of gage factor	-0.015 %/℃
Adoptable thermal expansion	1.0 PPM/℃
Gage resistance	120.2 ±0.2 Ω
Gage base	Polyimide

a) Strain gauges connection to the rebars and the logger

The gauges were bonded to the materials (the rebar or/and the concrete matrix) and then connected to a logger to facilitate the reading of data during the tests. However, challenges arose from this set-up, which were:

i. The strain gauges connected on the rebars had to come in contact with fresh concrete during the casting. However, the strain gauges were not of the waterproof type and that means that the strain gauges were going to be damaged during the casting. To overcome this challenge, a waterproof resin was used to coat the connected base of the strain gauge and then a self-adhesive aluminum waterproof tape and a bituminous substance were wrapped around the gauge to provide more protection as shown in Figures 3.16, 3.17 and 3.18;

(a) (b)

Figure 3.16 (a) Strain gauge cement, (b) and strain gauge placed on the rebars

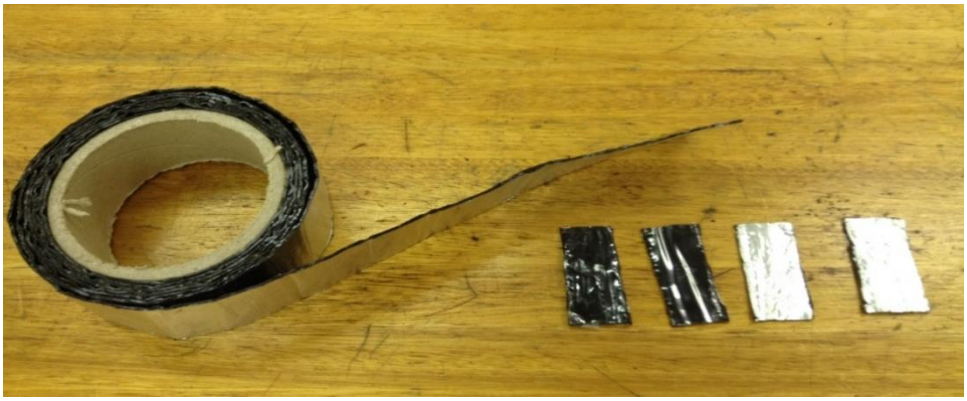

(a)

(b)

Figure 3.17 (a) Waterproof tape strips (b) placing on the rebar

(a)

(b)

Figure 3.18 (a) Bituminous substance (b) placed on the rebar

ii. The change in strain initiated resistance was extremely small, thus it was very difficult to be detected and be read on the logger if the strain gauges had to be directly connected to the logger. To overcome this challenge, a Wheatstone bridge interface amplifier was designed to magnify the change in resistance to a value readable on the logger as shown in Figure 3.19:

Figure 3.19 Strain gauges connection to the interface and logger

A Wheatstone bridge can be configured with 1 gauge (1/4 bridge), 2 gauges (1/2 bridge) or with 4 gauges (full bridge).

In the 1/4 bridge system, a strain gauge is connected to the interface and a fixed resistor or dummy resistor is connected to each of the other three sides of the bridge interface. In the 1/2 bridge system, two gauges are connected to the interface with fixed resistors connected to the two other sides. Either the two strain gauges can be active or one of them can be configured to play the dummy gauge to eliminate strain components other than the target strain. In the full bridge system, four strain gauges are connected on each of the four sides of the interface. This set-up ensures large output of strain gauge, improves temperature compensation in cases where wide temperature changes are expected, and it eliminates strains components other than the target strain.

iii. The design and the connection to the interface also depended on the output of strains expected and the number of gauges to be connected and used at the same time. In

this study, the full bridge system was used in the monitoring of both the concrete matrix and the reinforcing bars, as shown in Figures 3.11 and 3.12. The interface amplifier had 4 channels (input/output) to allow for the connection of more than one strain gauge and the monitoring of more than one material at the same time.

b) Placing of strain gauges

The strain gauges were placed at the midpoint of the longitudinal rebars inside of the concrete and on the surface of the concrete matrix at the same location. The assumption was that the beam would supposedly undergo the maximum deflection at the midpoint, hence maximum strains at the midpoint. The placing of strain gauges involved several steps which were:

i. The surface preparation as shown in Figure 3.20. During this process, the surface of the rebars was cleaned with sand paper to removed dirt from the rebar by lightly polishing.

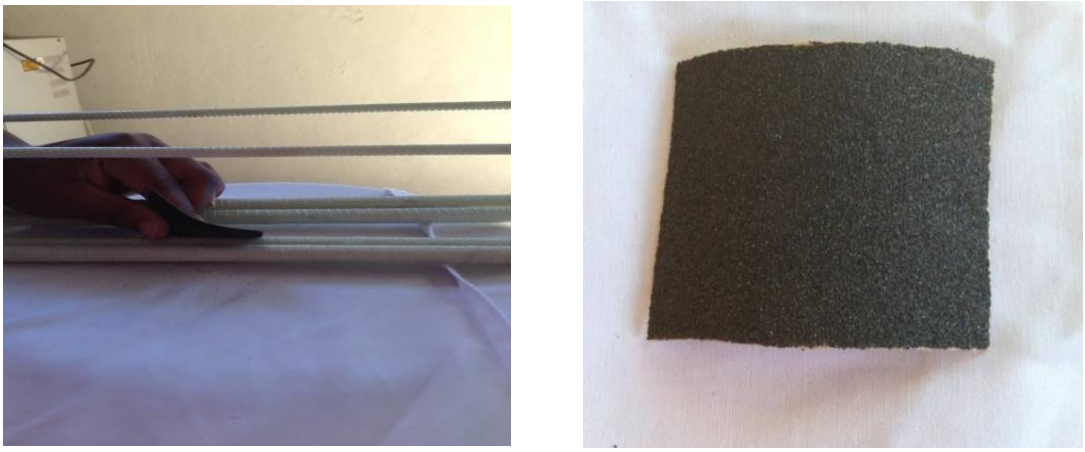

(a) (b)

Figure 3.20 (a) Prepared surface of the GFRP rebar (b) sand paper

ii. The bonding of the gauge to the material to be monitored is shown in Figures 3.16, 3.17 and 3.18. The gauge perimeter was then scribed on to the rebar's surface using a pencil. Afterwards, the adhesive which in this case was the CC-33A was applied on the bonding surface of the gauge. The gauge was then aligned with the scribed lines and fingertip pressed for 15 to 60 seconds to firmly bind the gauge to the surface of the material to monitor.

iii. The curing: The adhesive was then left to cure for at least 24 hours, at room temperature before proceeding with the casting.

3.4.3.4 Dynamic loading set-up

Several types of tests are differentiated in beam testing in terms of loading schemes, ranging from static to dynamic tests or from monotonic to cyclic tests. The former are concerned with the motion of the center of mass of the body which can be at rest or move over a period of time. The latter are a function of the variation of the load applied during a period of time. That has led to different loading schemes which are:

i. Monotonic static test where the position of center of mass does not change within a period of time and the load applied is constant;
ii. Cyclic static test where the position of the center of mass of the body moves within a certain period of time and the load applied still constant;
iii. Monotonic dynamic test where the position of the center of mass of the body does not change over time but the intensity of the load applied varies within a certain period of time; and
iv. Dynamic cyclic test where both the center of mass of the body and the intensity of the load applied vary within a certain period of time.

This study investigated the bond behaviour of GFRP rebars under a monotonic dynamic test, whereby the monotonic dynamic load is continuously applied during the test. In other words, the beam was continuously in contact with the source of vibration throughout the experiment. This loading mode was purposely selected because a monotonic loading mode alone does not reflect a real loading condition of concrete structures. Concrete structures are also subjected to some level of dynamic loading during their lifespan.

To create a monotonic dynamic loading scheme, a combination of different instruments were used as shown in Figure 3.13:

- The Universal Testing Machine which was used to apply a monotonic increasing load; and
- A dynamic system composed of a dynamic shaker, an amplifier and a function generator.

a) Universal dynamic shaker

The universal dynamic shaker shown in Figure 3.21 is of the type MB dynamic 50A. It is composed of a stroke or exciter delivering approximately a 22.7 kg force at selected frequency. It was positioned to perpendicularly strike one of the vertical faces of the beam as the UTM load was applied at the top of the beam.

Figure 3.21 Dynamic shaker MB dynamic 50A

b) The function generator

A function generator BK precision, model 4011A (Figure 3.22) was conjointly used with the dynamic shaker to create a built-in frequency. It means that it provides the possibility to create and induce a desired frequency at a specific frequency range (or cycle). It has the advantages of providing versatile signal sources, a wide frequency range and a waveform function, just to mention a few. Table 3.8 summarizes the specifications of the function generator.

Table 3.8 Specifications of the BK Precision function generator

Model	4011A
Waveforms	Sine, square, triangle, ± pulse, + ramp
Range	0.5 Hz to 5 MHz in 7 ranges
Dial accuracy	± 5%
Tuning range	Coarse 10:1; fine ± 5%
Temperature stability	0.6%/℃
Impedance	50 Ω ± 10%
Amplitude	Variable 20 db range type
Alternation	-20 db ±1 db

c) Amplifier

Figure 3.22 shows an amplifier MB SL 500 used to amplify the signal emitted by the function generator to the dynamic shaker and thus creating the desired frequency range. Table 3.9 presents the specifications of the amplifier used in the tests.

Table 3.9 Specifications of the amplifier MB SL 500

Frequency range	1 Hz to 20 000 Hz
Input power required	1200 VA (max)
Max. output volts	49 V RMS∗
Max. output Amps	4.0 A RMS∗
Total harmonic distortion	Coarse 10:1; fine ± 5%

RMS∗ stands for Root Mean Square, and refers to the best value.

Figure 3.22 (a) BK Precision function generator and (b) MB SL 500 amplifier

d) Steel plates set-up

A structure such as a beam in service life is not only subjected to its self-weight but also to some dead loads (concentrated and/or uniformly distributed load) and imposed loads. Therefore, to create a more or less realistic situation, steel plates were placed on the beam

to simulate the amount of imposed load a beam can be subjected to, during its service life, as shown in Figure 3.23. The steel plates represented approximately 40% of the beam's self-weight (the average beam weight was 0.979 kN), meaning they were about 0.746 kN. The steel plates were symmetrically placed on top of the surface in such a way that they would not obstruct with the UTM loading.

Figure 3.23 Steel plates used on the beams highlighted in red

e) Frequency of vibrations

The samples were subjected to a built-in frequency of 41 kHz of sinusoidal waveforms and at a frequency range of 500 cycles to investigate the bond behavior of GFRP rebars in concrete.

3.4.3.5 Loading rate

The test specimens in this study did not have the standard dimensions specified by SANS 5864 for four-point bending test. Therefore, the rate of force recommended by the code for specific cross-sectional dimensions and span length of the specimens, which varies from 0.07 kN/s to 0.30 kN/s, could not be applied. The loading rate which was also a function of the equipment used (UTM) was therefore set to a minimum of 0.10 kN/s to ensure a continuous application of the force and uniform nominal increase in stress.

The displacement rate was set to a minimum of 0.083mm/s so that the deflection could be constantly monitored.

3. 5 Model Design of the Concrete Beams

The beams of the study were reinforced with ribbed GFRP rebars and steel rebars. The depth and the width of the beams were deduced through calculations according to ACI 440.R1-06 and ACI 440. R1-03. The beams had the same length of 1160 mm and they were identical in size but not reinforcement for the two categories of beam series since steel reinforced concrete beam specimens will serve as control beams through the experiments. The design was based on serviceability limit state.

3.5.1 Experimental set-up and design of the beam

The investigation of the bond between GFRP rebars and concrete was carried out using the four-point bending test. The set-up of this test implied two loading points on top of a simply supported beam (ASTM D7264/D7264M-15, 2015). In other words, the total load P was equally divided into P_1 and P_2. The beam was also subjected to the total weight of the steel plates (0.746 kN) as well as the self-weight of the beam in a form of a uniformly distributed load that was weighted, calculated and taken equal to 0.979 kN/1.160 m or 0.844 kN/m. This can be seen in Figure 3.24 (a). The distance between the two loading points was a half of the span (ASTM D7264/D7264M-15, 2015).

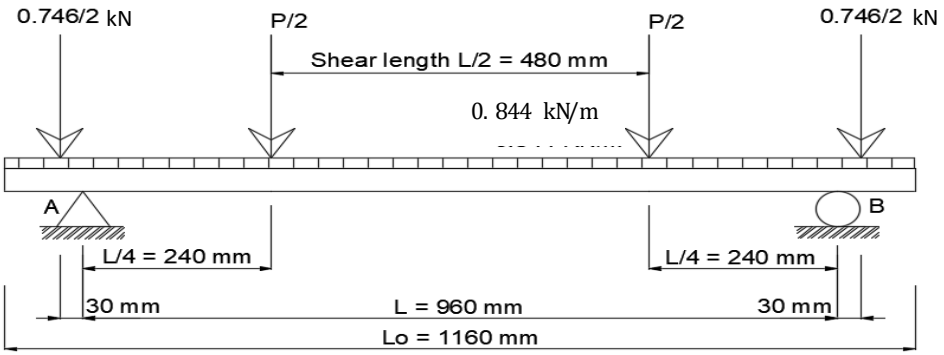

(a)

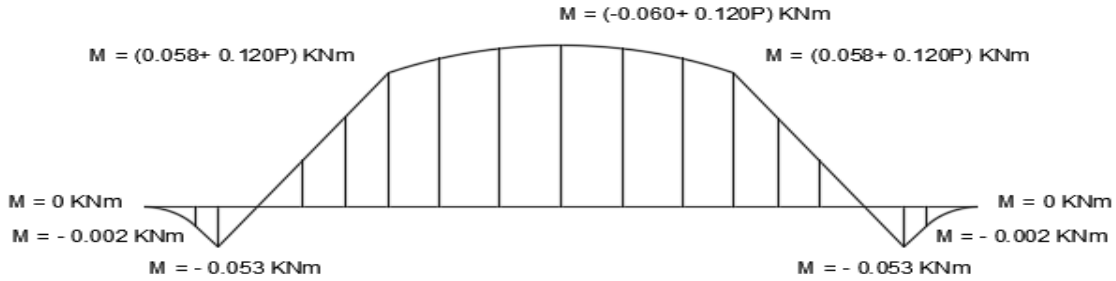

(b)

Figure 3.24 (a) Loading (b) Bending moment diagram

The reactions at the supports R_A and R_B can be computed as follows:

$$R_A = R_B = \frac{P}{2} + 0.863 \text{ (in kN)} \quad (6)$$

The maximum moment occurs without the shear length as seen in Figure 3.24 (b) and is given by:

$$M_{max} = -0.060 + 0.120P \text{ (in kNm)} \quad (7)$$

3.5.2 Design of GFRP reinforced concrete beam specimen

3.5.2.1 Dimensioning of the concrete beam

Figure 3.25 shows the cross-section of a proposed concrete beam used in this study. Referring to Figures 3.24 and 3.25, the following parameters can be deduced according to ACI 440. 1R-06 (2006):

The beam depth h can be calculated as:

$$h \geq \frac{L_o}{10} \quad (8)$$

$$h \geq \frac{1160}{10}$$

$h \geq 116$ mm. For practicability's sake in the construction of the reinforcement cage and also to accommodate a sufficient concrete cover as recommended by the Standard ACI 440. 1R-06 (2006), a beam depth h of 220 mm which is bigger than 116 mm was used.

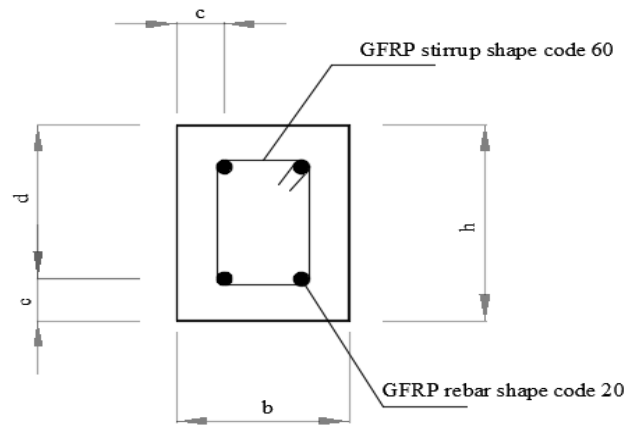

Figure 3.25 Concrete beam cross-section

The beam was reinforced with GFRP rebars of diameter d_b equal to 11.62 mm which has a cross-sectional area of the rebar A_f equal to 106.06 mm^2 (Table 3.5), the modulus of elasticity of the rebar E_f equal to 40000 MPa and the guaranteed tensile strength of the rebar f_{fu}^* equal to 850 MPa (Table 3.3). The maximum concrete cover, c can be taken equal to the greatest value between $2.5d_b$ and 40 mm where d_b is the diameter of the rebar (ACI 440 R1-06, 2006).

The concrete cover is calculated as follows:

Cover c = maximum {2.5×d_b or 40} (9)

c = maximum {2.5×11.62 or 40} = maximum {29.050; 40}

Thus, c = 40 mm

Determination of d, the distance from the extreme compression fibre to the centroid of tension reinforcement or the effective depth of the beam.

$$d = h - \frac{d_b}{2} - c \quad (10)$$

$$d = 220 - \frac{11.62}{2} - 40 = 174.190 \text{ mm}$$

For the width b: From Table 3.2, it could be seen that the maximum aggregates size was 19 mm, and the stirrup should be able to accommodate that size of aggregates. Moreover, the diameter of the main longitudinal and shear rebars should also accommodate the concrete cover.

Therefore,

$$b \geq \text{Maximum aggregate size} + (2\ d_b) + (2\ \text{stirrup size}) + (2c) \quad (11)$$

$$b \geq 19 + (2 \times 11.620) + (2 \times 6) + (2 \times 40)$$

$$b \geq 134.240 \text{ mm}$$

b could then be taken equal to 170 mm to ease the construction process.

3.5.2.2 Modes of failure and minimum area of GFRP reinforcement

GFRP reinforced concrete elements are governed by two main modes of failure namely, GFRP reinforcement rupture and concrete crushing modes of failure (ACI 440 R1-06, 2006). When GFRP reinforced concrete structures fail by reinforcement rupture, the failure is sudden and catastrophic with limited warnings (in terms of cracks and deflection) (ACI 440 R1-06, 2006). Concrete crushing mode of failure however allows some plastic behaviour

before failure, therefore it is more desirable in flexural members reinforced with GFRP rebars.

In order to prescribe a concrete crushing mode of failure in the concrete beam, it has to be ensured that the GFRP reinforcement ratio ρ_f is 1,4 times bigger than the GFRP reinforcement ratio ρ_{fb} producing balanced strain conditions (ACI 440 R1-06, 2006).

$$\rho_f > 1.4\,\rho_{fb} \quad (12)$$

ρ_f and ρ_{fb} can be computed as follows (ACI 440 R1-06, 2006):

$$\rho_f = A_f/(b \times d), \text{ and} \quad (13)$$

$$\rho_{fb} = \alpha_1 \times \beta_1 \times \left(\frac{\theta_c}{\theta_f}\right) \times \left[\left(\frac{f_c}{f_{fu}}\right)\right] \times \left[\left(\frac{\varepsilon_{cu}}{(\varepsilon_{cu}+\varepsilon_{fu})}\right)\right] \quad (14)$$

Where, b and d are the characteristics of the beam cross-section as seen in Figure 3.25, α_1 and β_1 are the stress-block factors for concrete and are equal to 0.8125 and 0.9075 respectively. They are computed using the formula stipulated in the standard ACI 440 R1-06 (2006):

Where f_c is the cylinder concrete compressive strength which is calculated using the cube compressive strength, f_{cu} and formula:

$$0.85\,f_c = 0.67\,f_{cu} \quad \text{(Alexander \& Beushaunsen, 2010)} \quad (15)$$

f_{cu} is assumed to be 20 MPa (as that's the concrete compressive strength of the concrete used in the casting), therefore: $f_c = \frac{0.67}{0.85} \cdot f_{cu} = 15.765$ MPa

$$\alpha_1 = 0.850 - 0.0015.f_c \geq 0.670 \quad (16)$$

$$\beta_1 = 0.970 - 0.0025.f_c \geq 0.670 \quad (17)$$

θ_c : Concrete resistance factor which is equal to 0.750 (ACI 440 R1-06, 2006).

θ_f : GFRP rebar resistance factor which is equal to 0.500 (ACI 440 R1-06, 2006).

ε_{cu}: Ultimate strain in concrete in compression which is equal to 0.0035 (ACI 440 R1-06, 2006).

ε_{fu}: Ultimate strain in FRP in tension which is equal to 0.01575 (ACI 440 R1-06, 2006).

f_{fu}: The theoretical design tensile strength of FRP, considering reductions for service environment which is equal to $C_E \times f_{fu}^*$ (ACI 440 R1-06, 2006 and Appendix A). C_E

is the environment reduction factor for various fibre type and exposure conditions which is equal to 0.800 for glass FRP-concrete specimen not exposed to earth and weather (ACI 440 R1-06, 2006); Then,

$f_{fu} = C_E \times f^*_{fu} = 0.800 \times 850 = 680$ MPa (18)

The area of GFRP reinforcement required is then determined by substituting Equations 13 and 14 in Equation 12:

$$\frac{A_f}{(b \times d)} > 1.4 \times \left\{ \alpha_1 \times \beta_1 \times \left(\frac{\theta_c}{\theta_f}\right) \times \left[\left(\frac{f_c}{f_{fu}}\right)\right] \times \left[\left(\frac{\varepsilon_{cu}}{(\varepsilon_{cu}+\varepsilon_{fu})}\right)\right] \right\} \quad (19)$$

$$\frac{A_f}{(170 \times 174.190)} > 1.4 \times 0.826 \times 0.931 \times \left(\frac{0.750}{0.500}\right) \times \left[\left(\frac{15.765}{680}\right)\right] \times \left[\left(\frac{0.0035}{(0.0035+0.01575)}\right)\right]$$

And $A_f > 201.578\ mm^2$

For the 4 GFRP rebars of diameter 11.620 mm (cross-sectional equal to 106.060 mm^2 from Table 3.5) used in the tension zone, the actual area of reinforcement is:

A_f = 4× cross-sectional area of the rebar (20)

A_f = 4× 106.060 = 424.240 mm^2 > 201.578 mm^2

Substituting Equation 20 in Equation 13, the actual FRP reinforcement ratio ρ_f is then:

$\rho_f = A_f/(b \times d) = 424.24/(170 \times 174.19) = 0.0143$ (21)

And from Equation 14 the actual balanced ratio ρ_{fb} is:

$$\rho_{fb} = \alpha_1 \times \beta_1 \times \frac{\theta_c}{\theta_f} \times \frac{f_{cu}}{f_{fu}} \times \frac{\varepsilon_{cu}}{\varepsilon_{cu} + \varepsilon_{fu}}$$

$$\rho_{fb} = 0.826 \times 0.931 \times \frac{0.750}{0.500} \times \frac{15.765}{680} \times \frac{0.0035}{0.0035 + 0.01575}$$

$\rho_{fb} = 0.005$

Thus, $\rho_f > 1.4\rho_{fb}$, this condition ensures that rupture of GFRP rebars will not govern the mode of failure of the reinforced beams. This means that the GFRP reinforced concrete beams shall either fail due to concrete crushing or GFRP rebar pull out.

3.5.2.3 Determination of the maximum load

In order to determine the maximum load P_{max} on the beam, the nominal moment capacity M_n was calculated first then equated to Equation 7 which gave the expression of the maximum moment of the beam M_{max}.

The expression of the nominal moment capacity is given by:

$$M_n = \rho_f \times f_f \times [\ 1 - 0.59 \times \frac{\rho_f \times f_f}{f_c}] \times b \times d^2 \quad (22)$$

In this equation, f_f denotes the stress in the GFRP rebar in tension, which was determined using the following formula (ACI 440.1R-15, 2015):

$$f_f = \left(\sqrt{\frac{(E_f \times \varepsilon_{cu})^2}{4} + \frac{0.85 \times \beta_1 \times f_c}{\rho_f}} \times E_f \times \varepsilon_{cu} - 0.5 \times E_f \times \varepsilon_{cu} \right) \leq f_{fu} \quad (23)$$

E_f was taken equal to 40000 MPa (Table 3.3) and f_{fu} was taken equal to 680 MPa from Equation 18. Thus,

$$f_f = \left(\sqrt{\frac{(40000 \times 0.0035)^2}{4} + \frac{0.85 \times 0.931 \times 15.765}{0.0143}} \times 40000 \times 0.0035 - 0.5 \times 40000 \times 0.0035 \right) \leq f_{fu}$$

$$f_f = 356.273 \text{ MPa} \leq f_{fu}$$

The nominal moment capacity was then calculated as:

$$M_n = 0.0143 \times 356.273 \times \left[1 - 0.59 \times \frac{0.0143 \times 356.273}{15.765}\right] \times 170 \times 174.190^2$$

$$M_n = 21268713.19 \text{ Nmm or } 21.269 \text{ kNm}$$

The nominal moment capacity was then equated to Equation 7:

$$M_{max} = (-0.060 + 0.120P) \text{ (in kNm)}$$

$$21.269 = (-0.060 + 0.120P) \text{ (in kNm)}$$

$$P_{max} = 177.743 \text{ kN}$$

3.5.2.4 Determination of the beam deflection

The maximum allowable deflection of the beam can be calculated according to SANS 10100-1: 2000 for simply supported beams which states that the maximum allowable deflection should be:

$$\delta_{allowable} \leq \frac{L}{250} \quad (24)$$

Where L is the span length of the beam. Referring to Figure 3.24 (a), the maximum allowable deflection is:

$\delta_{allowable} \leq \frac{960}{250}$ = 3.840 mm

To calculate the maximum deflection the beam would be subjected to, the following formulae and steps were used:

$$\delta_{max} = \frac{P_{max} \times \left(\frac{L}{4}\right) \times \left(3 \times L^2 - 4 \times \left(\frac{L}{4}\right)^2\right)}{48 \times E_c \times I_e} \quad \text{(ACI 440.1R-15, 2015) (25)}$$

- P_{max} was taken equal to 177.743 kN from Section 3.5.2.3 and L was taken as 960 mm from Figure 3.24 (a).
- The first step was to calculate the modulus of elasticity of the concrete beam E_c, using the formula:

$$E_c = 4750 \times \sqrt{f_{cu}} \quad \text{(ACI 440.1R-15, 2015) (26)}$$

$E_c = 4750 \times \sqrt{20} = 21242.646$ MPa

- The next step was to determine the effective moment of inertia of the reinforced concrete beam I_e, using the formula (ACI 440.1R-15, 2015):

$$I_e = \frac{I_{cr}}{1 - \gamma\left[\frac{M_{cr}}{M_{max}}\right]^2 \times \left[1 - \frac{I_{cr}}{I_g}\right]} \leq I_g \quad (27)$$

I_g is the gross moment of inertia of the concrete beam, calculated as:

$$I_g = \frac{b \times h^3}{12} \quad (28)$$

b and h are taken from Figure 3.25. Therefore, $I_g = \frac{170 \times 220^3}{12} = 1.508 \text{ x } 10^8$ mm^4

I_{cr} is the moment of inertia of the transformed cracked concrete beam section calculated as:

$$I_{cr} = \frac{b \times d^3}{3} \times k^3 + n_f \times A_f \times d^2 - (1 - k)^2 \quad \text{(ACI 440.1R-15, 2015) (29)}$$

In Equation 29, k is the ratio of the depth of neutral axis to reinforcement depth, calculated as (ACI 440.1R-15, 2015):

$$k = \left(\sqrt{(\rho_f \times n_f)^2 + 2 \times (\rho_f \times n_f)}\right) - \rho_f \times n_f \quad (30)$$

n_f is the equivalent ratio of elasticity of the reinforced concrete beam, computed using the formula:

$$n_f = \frac{E_f}{E_c} \quad (31)$$

In this formula E_f is taken from Table 3.3. and E_c is the modulus of elasticity of the concrete from Equation 26.

Thus, $n_f = \frac{40000}{21242.646} = 1.883$

Therefore, $k = \left(\sqrt{(0.0143 \times 1.883)^2 + 2 \times (0.0143 \times 1.883)}\right) - 0.0143 \times 1.883$

$$k = 0.207$$

The following step was to use the results of Equations 20, 30 and 31 to solve Equation 29:

$$I_{cr} = \frac{170 \times 174.190^3}{3} \times 0.207^3 + 1.883 \times 424.240 \times 174.190^2 - (1 - 0.207)^2$$

$I_{cr} = 0.269 \text{ x } 10^8 \text{ mm}^4$

M_{max} was taken equal to $M_n = 21.269$ kNm

To determine the cracking moment:

$$M_{cr} = \frac{2 \times f_r \times I_g}{h} \quad (32)$$

The modulus of rupture f_r of concrete was computed as:

$$f_r = 0.62\sqrt{f_c} \quad (33)$$

$f_r = 0.62\sqrt{15.76} = 2.461$ MPa,

Thus, $M_{cr} = \frac{2 \times 2.461 \times 150846666.667}{220} = 3374851.333$ Nmm or 3.375 kNm

Then, the parameter to account for the variation in stiffness along the length of the member γ was computed as (ACI 440.1R-15):

$$\gamma = 1.72 - 0.72\left[\frac{M_{cr}}{M_{max}}\right] \quad (34)$$

Substituting Equation 32 in Equation 34:

$$\gamma = 1.72 - 0.72\left[\frac{3.375}{21.269}\right] = 1.606$$

The effective moment of inertia of the reinforced concrete beam I_e was hence computed by substituting Equations 22, 29, 32 and 34 in Equation 27:

$$I_e = \frac{26895137.360}{1 - 1.606 \times \left[\frac{3.375}{21.269}\right]^2 \times \left[1 - \frac{26895137.360}{150846666.667}\right]} = 0.278 \text{ x } 10^8 \text{ mm}^4$$

- Finally, to calculate the deflection, Equations 26 and 27 were substituted in Equation 25:

$$\delta_{max} = \frac{177.743\times1000\times\left(\frac{960}{4}\right)\times\left(3\times960^2-4\times\left(\frac{960}{4}\right)^2\right)}{48\times21242.646\times27819548.570}$$

$$= 3.811 \text{ mm} < 3.840 \text{ mm } (\delta_{allowable})$$

3.5.2.5 Compression reinforcement

Compression reinforcements are required for only constructing the reinforcement cage as the stress in the compression zone was too small. Hence 2 GFRP rebars of diameter 6 mm were used.

3.5.2.6 Evaluation of the shear reinforcement

The minimum amount of shear reinforcement was computed as follows (ACI 440 R1-06, 2006) :

$$A_{fv,min} = \frac{(0.35\times b_w\times s)}{f_{fv}} \quad (35)$$

Where, A_{fv} is the amount of FRP shear reinforcement within spacing s.

f_{fv} is the tensile strength of FRP for shear design, that was computed as follows (ACI 440 R1-06, 2006):

f_{fv} =0.004× E_f = 0.004×40000=160 MPa (36)

b_w is the width of the web, that is computed as follows:

b_w= b-2c =170- 2×40= 90 mm (ACI 440 R1-06, 2006) (37)

And s is the minimum stirrup spacing that can be taken as less or equal to the smallest of either $\left\{d/2 ; 600 \text{ mm}\right\}$ (ACI 440 R1-06, 2006).

The minimum stirrup spacing, s was computed as follows:

s ≤ {d⁄2; 600 mm} = {174.190⁄2;600} = {87.1;600} (38)

Thus, s can be taken equal to 80 mm

Substituting Equations 36, 37 and 38 into Equation 39:

$$A_{fv,min} = \frac{0.35 \times b_w \times s}{f_{fv}} = \frac{0.35 \times 90 \times 80}{160} = 15.750 \text{ mm}^2$$

Since the smallest diameter of GFRP rebar is 6 mm with an area of 31 mm^2, the stirrups used in this study had a diameter of 6 mm and $A_{fv,min}$ was taken equal to 31mm^2, spaced at 80 mm.

3.5.2.7 Determination of the ultimate bending strength

Figure 3.26 shows the stress-strain distribution diagram in flexure when concrete crushing mode of failure governs the failure of the reinforced concrete beams. To calculate the ultimate bending strength, the formula:

$$\frac{M}{I_g} = \frac{\sigma}{y} \quad (39)$$

Where M is the maximum bending moment of the beam equals to 0.213×10^8 N-mm, I_g is the gross moment of inertia equals to 1.508×10^8 mm^4, σ is the bending strength and y is the distance from the extreme compression fibre to the Neutral Axis N.A and was computed as followed:

$$y = \beta_1 \times d \quad \text{(ACI 440 R1-06, 2006) (40)}$$

But $d = 174.190$ mm and $\beta_1 = 0.931$, thus, $y = 0.931 \times 174.190 = 162.171$ mm

Substituting Equation 40 in 39 to calculate σ:

$$\sigma = \frac{21268713.19 \times 162.171}{150846666.667} = 22.865 \text{ MPa}$$

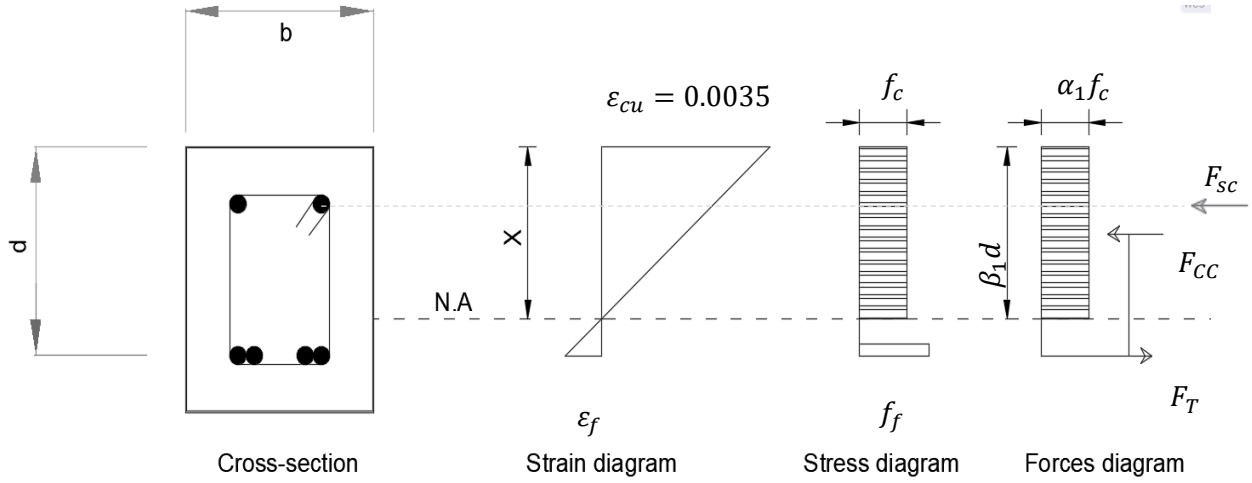

Figure 3.26 Stress-strain distribution diagram in flexure for failure by concrete crushing (Newhook, et al., 2002)

3.5.2.8 Physical properties of the proposed beam

Figures 3.27 and 3.28 shows the resulting designed beam used in this study.

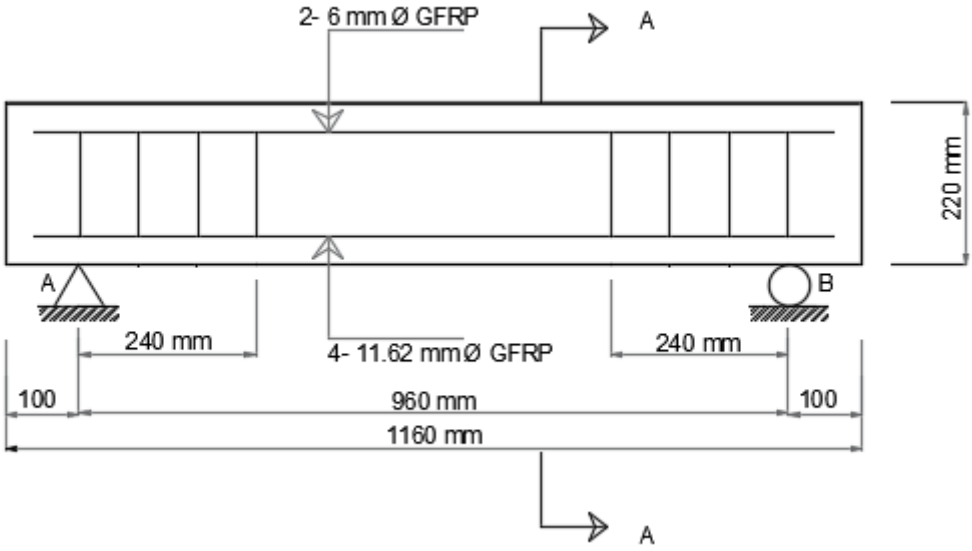

Figure 3.27 Designed GFRP reinforced concrete beam

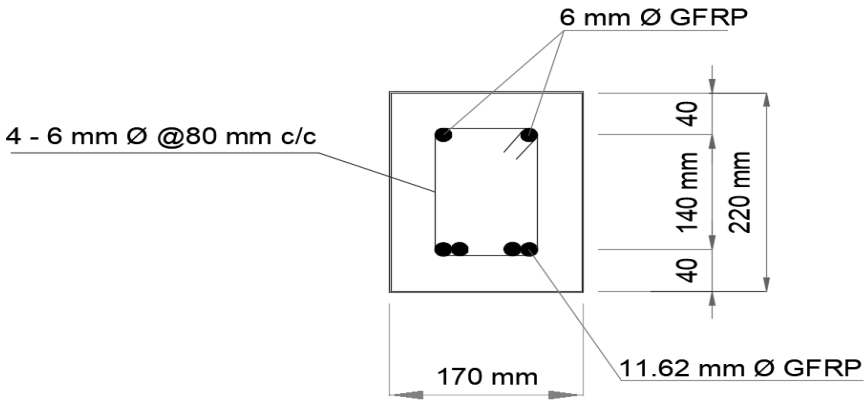

Figure 3.28 Cross Section A-A.

3.5.2.9 Determination of the maximum theoretical bond strength

Splice bars were used in the design of the reinforced beam. It was important to make provision for the splice lengths when determining the bond strength of the GFRP rebars in concrete beam. ACI 440.1R-15 (2015) gives a formula derived from previous works written as:

$$\frac{\mu_{th-GFRP}}{0.083\times\sqrt{f_c}} = 4 + 0.3\ \frac{C_0}{d_b} + 100 \times \frac{d_b}{l_e} \quad (41)$$

Where $\mu_{th-GFRP}$ is the predicted bond strength of GFRP is rebars in concrete beams, f_c is the compressive strength of the concrete cylinder equal to 15.765 MPa, d_b is the rebar diameter, l_e is the development length of the bar equal to:

The length of the beam $-$ 2 $\times$ concrete cover c ($1160 - 2 \times 40 = 1080$ mm) and C_0 is the lesser of the cover to the centre of the bar or one-half of the centre-on-centre (c/c) spacing of the bar being developed.

Thus, $C_0 = \min\left\{\frac{d_b}{2} + 40;\ \frac{^{c}/_{c}\ \text{Spacing}}{2}\right\} \leq 3.5d_b$

$C_0 = \min\{45.810;\ 27.570\} \leq 40.670$

$C_0 = 27.570$ mm

The predicted bond strength was then equal to:

$\frac{\mu_{th-GFRP}}{0.083\times\sqrt{15.765}} = 4 + 0.3\ \frac{27.570}{11.62} + 100 \times \frac{11.62}{1080}$

$\mu_{th-GFRP} = 1.907$ MPa

3.5.3 Design of steel reinforced concrete beam according to SANS 10100-1: 2000

3.5.3.1 Dimensioning of the steel reinforced concrete beam and determination of the maximum load

Steel reinforced concrete beams served as control beams during the experiments, therefore they had to have the same physical specifications such as the length, width, depth and the shear length as indicated in Figures 3.23 and 3.24. The loading configuration was also the same as shown in Figure 3.23.

In the previous sections, the design of the GFRP reinforced concrete beams was conducted in such a way that the beam would be over-reinforced. Thus, 4 rebars were used in the tension zone, creating splices along the whole rebar length. Moreover, no compression reinforcement was needed for structural purposes but rather for construction purposes as the moment redistribution was kept to be limited to 10%, in order to keep the maximum depth of the neutral axis to $^{d}/_{2}$ to eliminate the need of compression reinforcement (SANS 10100-1:2000,2000). Hence, the same configuration was adopted with the concrete beams,

however 10 mm diameter steel rebars were used in the tension zone and the minimum area of reinforcement was used in the compression zone (8 mm diameter steel rebars). First, the concrete resistance was calculated:

$$M_u = 0.156 \times f_c \times b \times d^2 \quad (42)$$

Where $d = h - \frac{d_b}{2} - c$

d_b= 10 mm, h= 220 mm and c = 25 mm (Appendix C), the value of c was taken according to SANS 10100-1:2000 for steel reinforced concrete beams design and was therefore different from c in GFRP reinforced concrete beams.

$d = 220 - \frac{10}{2} - 25 = 190$ mm

$M_u = 0.156 \times 15.765 \times 170 \times 190^2$

$M_u = 15092969$ Nmm or 15.093 kNm

Then the steel resistance was determined by: $M_u = 0.87 \times f_y \times A_s \times Z$ (43)

For 4Y10 mm diameter steel rebars, the area of reinforcement $A_s = 314$ mm^2 (Appendix D), $f_y = 450$ MPa and Z the lever arm from the centroid of the full compression area to the centroid of the tension reinforcement calculated as:

$$\frac{Z}{d} = 1 - \left(\frac{0.974 \times f_y \times A_s}{f_c \times b \times d}\right) \leq 0.950 \quad (44)$$

$$\frac{Z}{d} = 1 - \left(\frac{0.974 \times 450 \times 314}{15.765 \times 170 \times 190}\right) \leq 0.950$$

$\frac{Z}{d} = 0.730 \leq 0.95$

$Z = 138.700$ mm

Hence, the steel resistance was equal to: $M_u = 0.87 \times 450 \times 314 \times 138.700 = 17050529.700$ Nmm or 17.051 kNm

Equation 43 was then equated to Equation 7:

$M_u = (-0.060 + 0.120P)$

$17.051 = (-0.060 + 0.120P)$

$P_{max} = 142.593$ kN

3.5.3.2 Calculation of the shear reinforcement

The first step was to determine the maximum shear force of the beam from Equation 6 and the maximum load equal to 142.593 kN.

$V = R_A = R_B = \frac{142.593}{2} + 0.863$ (in kN)

$V = 72.159$ kN

Then the shear stress was calculated as:

$$\tau_s = \frac{V}{b \times d} \quad (45)$$

τ_s had to be equal or less than either of $\left[0.8\sqrt{f_c}\right.$ and 5 MPa$\left.\right]$ (SANS 10100-1:2000, 2000).

$$\tau_s = \frac{72159}{170 \times 190} \leq \left[0.8\sqrt{15.765}\right. \text{ and 5 MPa}\left.\right]$$

$$\tau_s = 2.234 \text{ MPa} \leq [3.176 \text{ MPa and 5 MPa}]$$

Then, the area of shear reinforcement was calculated from the equation:

$$A_{sv} = \frac{0.4 \times b \times S_v}{0.87 \times f_{fv}} \quad \text{(SANS 10100-1:2000,2000) (46)}$$

Where f_{fv} is the design tensile strength of mild steel equal to 250 MPa and S_v is the spacing between the stirrups that should be taken as:

$$80 \text{ mm} \leq S_v \leq 0.75d \quad (47)$$

$$80 \text{ mm} \leq S_v \leq 0.75 \times 190$$

$$80 \text{ mm} \leq S_v \leq 142.5 \text{ mm}$$

S_v was taken equal to 80 mm to achieve the same arrangement as for GFRP reinforced concrete beams. The minimum shear reinforcement was then equal to:

$A_{sv} = \frac{0.4 \times 170 \times 80}{0.87 \times 250} = 25.011$ mm^2. Therefore, Mild steel rebars of 8 mm diameter was used with a nominal sectional area of 50.300 mm^2, spaced at 80 mm centre to centre.

3.5.3.3 Determination of the beam deflection

The maximum deflection the beam would be subjected to was calculated as followed:

$$\delta_{max} = \frac{P_{max} \times \left(\frac{L}{4}\right) \times \left(3 \times L^2 - 4 \times \left(\frac{L}{4}\right)^2\right)}{48 \times E_c \times I_g} \quad (48)$$

Where

$E_c = 21242.646$ MPa , $P_{max} = 142.593$ kN and $I_g = 1.508 \times 10^8$ mm^4. Therefore,

$$\delta_{max} = \frac{142.593 \times 1000 \text{ x } \left(\frac{960}{4}\right) \times \left(3 \times 960^2 - 4 \times \left(\frac{960}{4}\right)^2\right)}{48 \times 21242.646 \times 150846666.667} = 0.564 \text{ mm} < 3.840 \text{ mm } (\delta_{allowable})$$

3.5.3.4 Determination of the ultimate bending strength

To calculate the ultimate bending strength, Equation 39 was used where M is the maximum bending moment of the beam equals to 17050529.700 Nmm or 17.051 kNm, I_g is the gross moment of inertia equals to 1.508 x 10^8 mm^4, σ is the bending strength and y is the distance from the extreme compression fibre to the Neutral axis N.A and was computed as follows:

$$y = 0.9 \times \frac{d}{2} \tag{49}$$

If $d = 190$ mm , $y = 0.9 \times \frac{190}{2} = 85.500$ mm

Substituting Equation 48 into Equation 38 to calculate σ:

$$\sigma = \frac{17050529.700 \times 85.500}{150846666.667} = 9.664 \text{ MPa}$$

3.5.3.5 Physical properties of the proposed beam

Figures 3.29 and 3.30 show the resulting designed reinforced concrete steel beam used in this study.

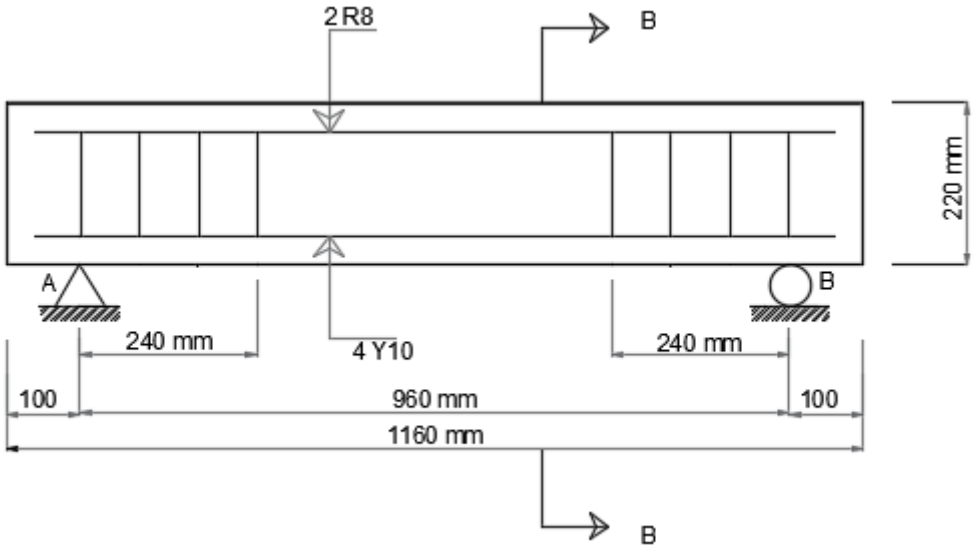

Figure 3.29 Designed steel reinforced concrete beam

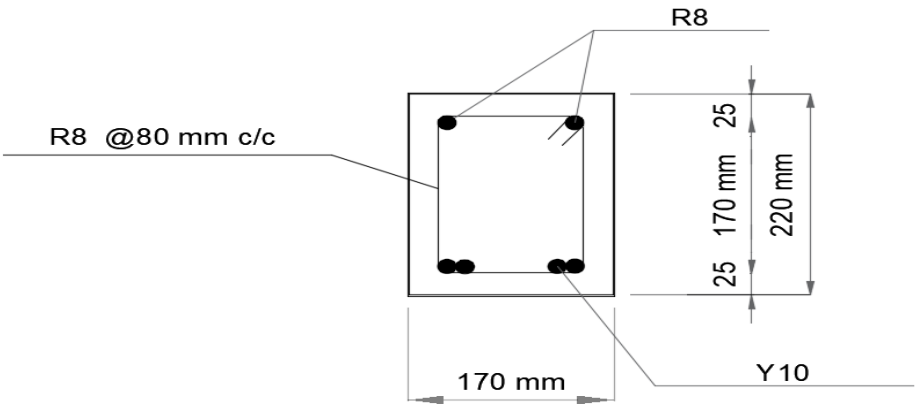

Figure 3.30 Cross section B-B of designed steel reinforced concrete beam

3.5.3.6 Determination of the maximum theoretical bond strength

The predicted bond strength was determined using ACI 440.1R-15 (2015)'s formula (Equation 41):

$$\frac{\mu_{th-steel}}{0.083\times\sqrt{f_c}} = 4 + 0.3\ \frac{C_0}{d_b} + 100 \times \frac{d_b}{l_e}$$

Where $\mu_{th-Steel}$ is the predicted bond strength of steel rebars in concrete beams, f_c is the compressive strength of the concrete cube equal to 20 MPa, d_b is the rebar diameter, l_e is the development length of the bar equal to 1080 mm and C_0 is the lesser of the cover to the centre of the bar or one-half of the centre-on-centre (c/c) spacing of the bar being developed.

$$\text{Thus, } C_0 = \min\left\{\frac{d_b}{2} + 25;\ \frac{^c/_c\ \text{Spacing}}{2}\right\} \leq 3.5d_b$$

$$C_0 = \min\{30;\ 45\} \leq 35$$

$$C_0 = 30\ \text{mm}$$

The predicted bond strength was then equal to:

$$\frac{\mu_{th-Steel}}{0.083\times\sqrt{15.765}} = 4 + 0.3\ \frac{30}{10} + 100 \times \frac{10}{1080}$$

$$\mu_{th-Steel} = 1.920\ \text{MPa}$$

4. PRESENTATION AND ANALYSIS OF RESULTS

4.1 Introduction

In this chapter, the data gathered over the experimental work were collected, analysed and interpreted with reference to the standards stated in section 3.2 and works conducted by other researchers in order to achieve the objectives of the study.

4.2 Tensile Test Results

4.2.1 Introduction

The tensile tests were performed in order to characterize the tensile strength of the ribbed GFRP rebars prior to the subsequent flexural tests. The tests were conducted according to ASTM A370. A representative specimens size of 5 rebars were tested as recommended by the ASTM 3916. Tensile tests were not performed on steel rebars since steel rebars properties have been standardized worldwide. Therefore, their properties are well known.

4.2.2 Presentation of results

The general coding applied for the specimens in tensile test is as follows: The letter A indicates the type of reinforcing bar which is ribbed GFRP and the number 1 indicates the rebar number in the series. Table 4.1 summarises the supplier specifications of the rebars (Table 3.3) and the experimental specifications values of the rebars derived from the cross-section test (section 3.3.2) and the tensile tests (Appendix D).

Table 4.1 Results of the tensile tests of the ribbed GFRP rebars

Specifications	**Unit**	**Supplier values**					**Experimental values**				
		Samples					**Samples**				
		A1	**A2**	**A3**	**A4**	**A5**	**A1**	**A2**	**A3**	**A4**	**A5**
Cross-sectional area	mm^2					113					106.06
Diameter	mm					12					11.62
Maximum Tensile Load	kN					97	53	56	57	56	62
Maximum Tensile strength	MPa					850	466	489	526	521	533
Average Maximum Tensile strength	MPa										507
Standard deviation	MPa										28.45

4.2.3 Load-Extension curves of ribbed GFRP rebars

Figures 4.1, 4.2, 4.3, 4.4 and 4.5 present the load-extension curves of the tensile tests performed on GFRP rebars.

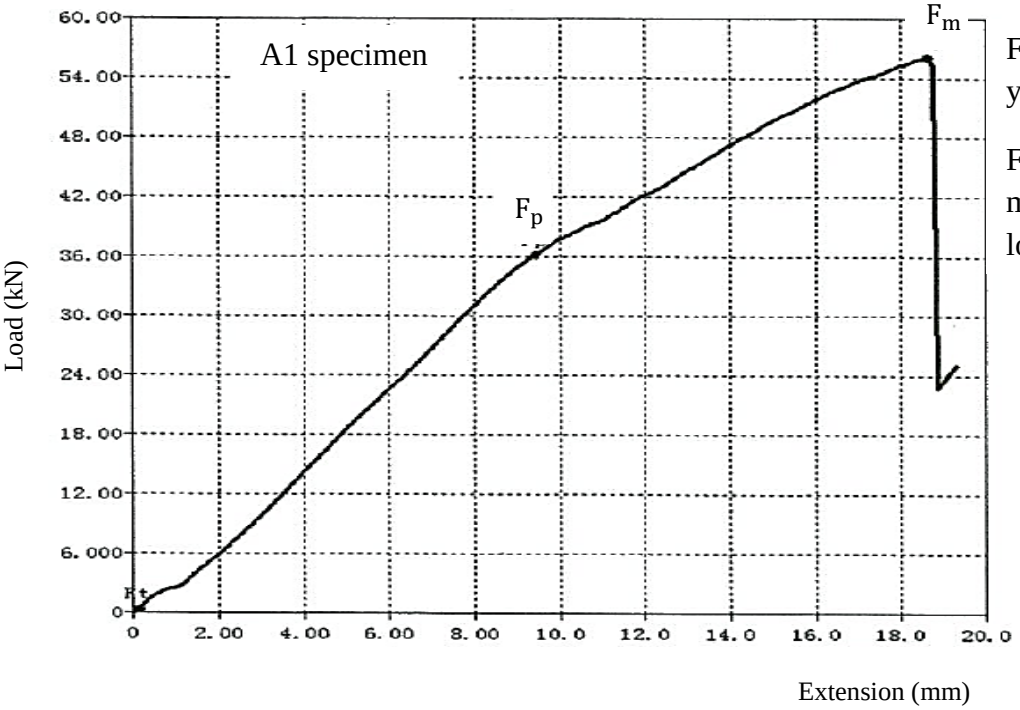

Fp: Apparent yield load

Fm: Apparent maximum yield load

Figure 4.1 A1 load-extension curve

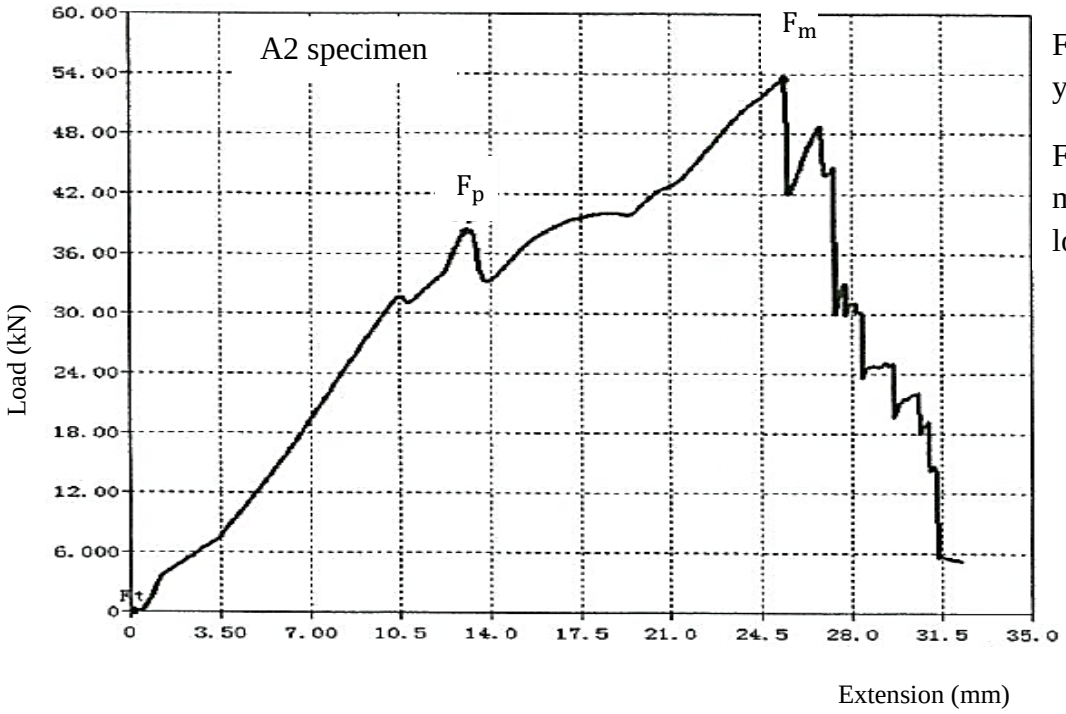

Fp: Apparent yield load

Fm: Apparent maximum yield load

Figure 4.2 A2 load-extension curve

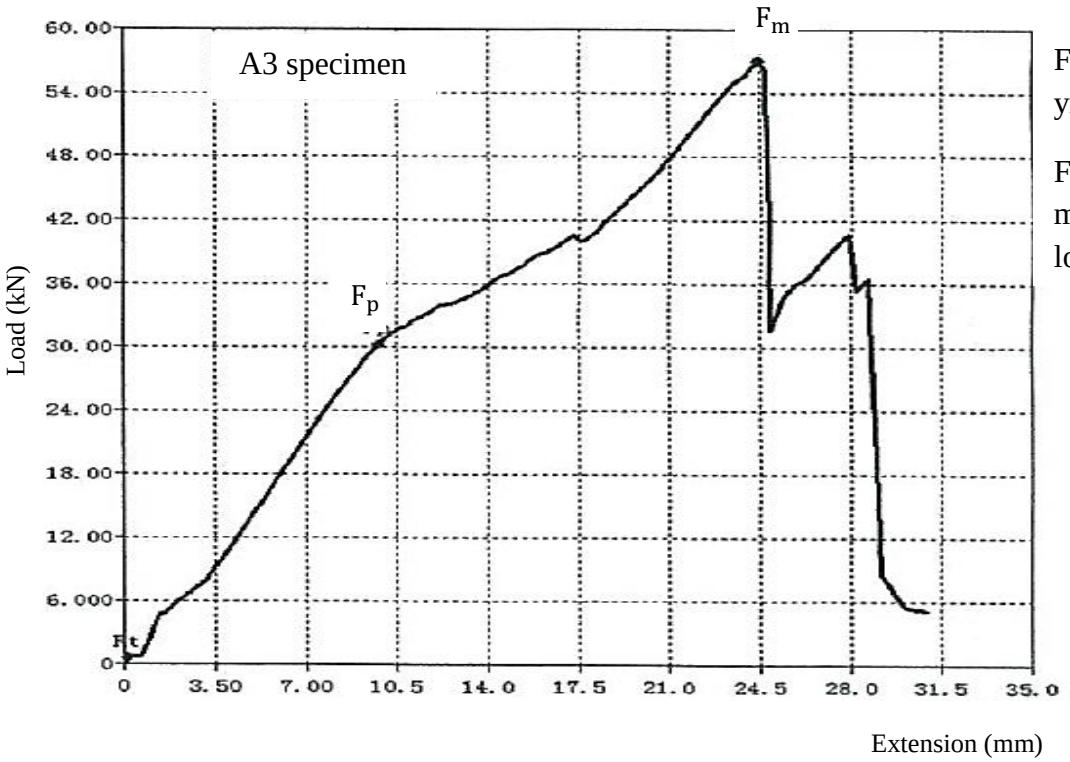

Fp: Apparent yield load

Fm: Apparent maximum yield load

Figure 4.3 A3 load-extension curve

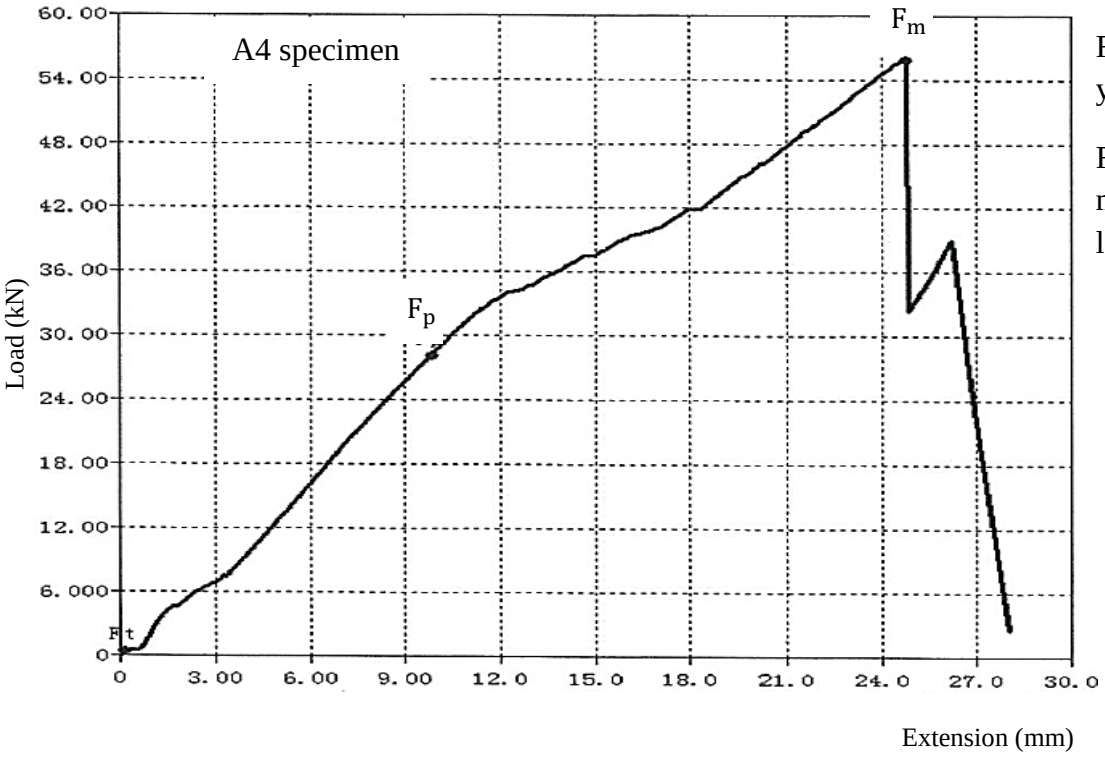

Fp: Apparent yield load

Fm: Apparent maximum yield load

Figure 4.4 A4 load-extension curve

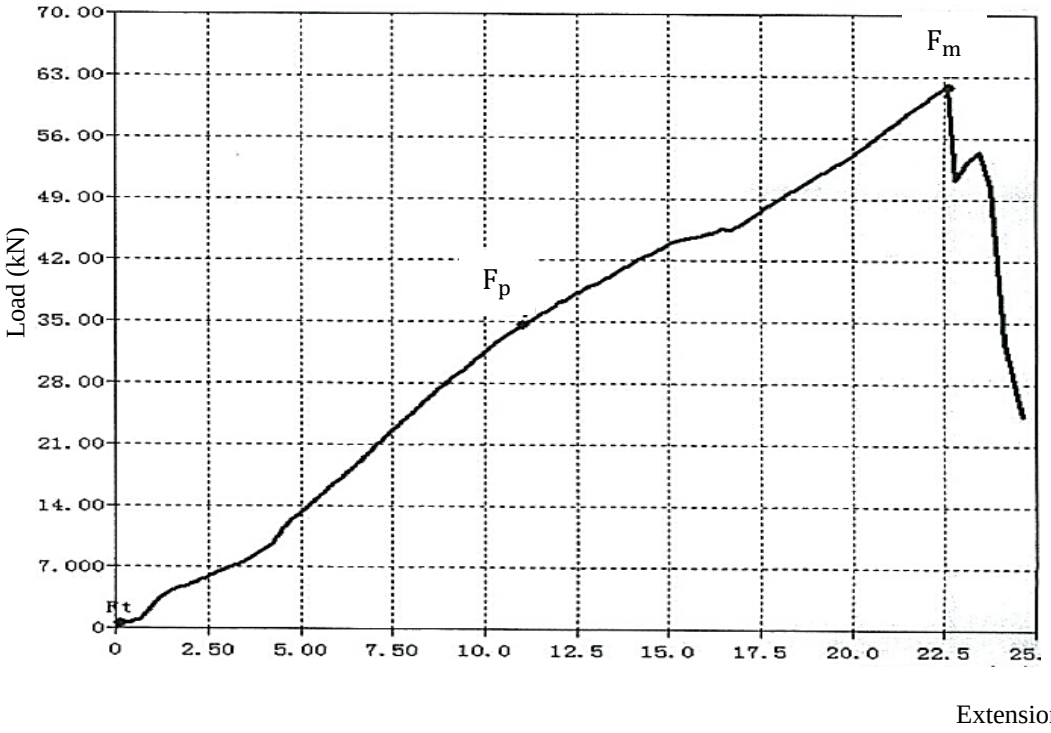

Fp: Apparent yield load

Fm: Apparent maximum yield load

Figure 4.5 A5 load-extension curve

The load–extension curves were characterized by the following behaviours:

a. A1 specimen

It can be seen from Figure 4.1 that the load on the load-extension curve of specimen A1 increased in a non-linear manner up to the apparent yield load F_P of 38 kN. Afterwards, the load dropped during an extension length of about 9 mm. The load then increased in a non-linear manner up to the apparent maximum yield load F_m (53 kN). After reaching the apparent maximum yield load F_m, the curve described a dropping broken line up to the complete failure of the rebar.

b. A2 specimen

Figure 4.2 revealed that the load on the load-extension curve of specimen A2 increased in a non-linear manner up to the apparent yield load F_P of 36 kN. After reaching F_P, the load still increased in a non-linear manner up to the apparent maximum yield load F_m (56 kN). However, it could be seen that the curve slope decreased between F_P and F_m. The rebar failed suddenly after reaching the maximum load F_m of 56 kN.

c. A3 specimen

Figure 4.3 revealed that that the load on the load-extension curve of specimen A3 increased in a non-linear manner up to the apparent yield load F_P of 30 kN. Between F_P and F_m, the load increased however it was characterized by a slight dropped in load value. When F_m (57 kN) was reached, the rebar failed suddenly, and the curve described a broken line.

d. A4 specimen

It can be seen in Figure 4.4 that the load on the load-extension curve of specimen A4 increased in a non-linear manner up to the apparent yield load F_P of 28 kN. After reaching F_P, the load still increased in a non-linear manner up to the apparent maximum yield load F_m (56 kN). However, the curve slope decreased between F_P and F_m as compared to the slope between the point 0 and F_P. The rebar failed suddenly after reaching the maximum load F_m of 56 kN.

e. A5 specimen

Figure 4.5 showed that the load on the load-extension curve of specimen A5 increased in a non-linear manner between the point 0 and the apparent yield load F_P (35 kN) and almost similarly between F_P and the apparent maximum yield load F_m (62 kN). The rebar failed suddenly after reaching the maximum load F_m of 56 kN and described a dropping broken curve.

4.2.4 Failure mode and analysis of results

The analysis of Table 4.1 (Section 4.2.2) showed that:

(a) The experimental specifications values of the rebars were way more modest than the supplier's. The cross-sectional test of the rebar showed that the average cross-sectional area of the rebar was actually 106.06 mm^2, which represented about 94% of the supplier's value; and the average experimental diameter of the rebar was of 11.62 mm which was close to an average of 97% of the supplier value. The tensile strength of the rebar found experimentally ranged between 466 MPa (A1) to 533 MPa (A5) as seen in Table 4.1 (Section 4.2.2). The rebars barely reached 59.65 % (Maximum average tensile strength of 507 MPa, in Table 4.1) of the supplier tensile strength which was about 850 MPa.

(b) All the specimens exhibited no severe damages on the surface, but inside as seen in Figure 4.6 (a and b). GFRP rebars are made by combining fibres and the resin that glue the fibers together. The resin needs to be strong enough to sustain the effect of Poisson ratio when the rebar is pulled. This study revealed that the resin holding the longitudinal fibres was not strong in tension and would fail due to the high Poisson ratio the rebar was subjected to in tension (ACI 440 R1-06, 2006). These phenomena were mostly observed at the midspan of the rebars.

(a) Resin failure in A1 specimen

(b) Resin failure in A3 specimen

Figure 4.6 (a) A1 specimen resin failing, (b) A3 specimen resin failing

(c) To characterize the rebars used in this study, it could be said that they only reached up to 59.65 % of the nominal tensile strength (Table 4.1) on the supplier sheet due to the brittle resin matrix used in the manufacturing process. The tensile strength obtained in the tensile tests, basically represented the tensile strength of the resin matrix and not the tensile strength of the entire composite material.

(d) The behaviour of GFRP rebars in tension was not linear and was characterized by no clear yielding phase (ACI 440 R1-06, 2006). This showed the lack of ductility of the material (Issa, et al., 2011). The rebars failed suddenly after reaching their maximum load (Figures 4.1, 4.3, 4.4 and 4.5). In this case, this can be explained by the severe damage of the resin matrix as it reached its peak load.

Thus, the average maximum tensile strength of ribbed GFRP rebars used in this study was evaluated to be equal 507 MPa or 59.65% of the nominal tensile strength on the supplier data sheet. This answered the first specific objective of this study which was to evaluate the maximum tensile strength of GFRP rebars.

4.3 Concrete Compressive Strength Results

4.3.1 Introduction

The concrete compressive strength was tested according to SANS 5863:2006 in order to characterize the average concrete compressive strength used in this study. The supplier specifications for the concrete indicated a value of 20 MPa, it was important to establish the actual average compressive strength of the concrete for the experiment related to the new laboratory environment (temperature), casting, compaction and curing processes

4.3.2 Presentation of the results

The compressive strength of the concrete was determined using the formula:

$$f_{cu} = \frac{F}{A_c} \qquad \text{(SANS 5863: 2006) (50)}$$

Where f_{cu} represents the cube compressive strength of the concrete in MPa; F represents the maximum normal load at failure (in N) and A_c represents the cross-sectional area of the concrete cube in mm^2. The ready mix concrete was supplied by Wearne Readymix (Pty) Ltd as mentioned in section 3.3.1. Table 4.2 summarizes the average compressive strength of the concrete at 14, 21 and 28 days.

Table 4.2 Average concrete compressive strengths obtained from cube tests.

Concrete age (days)	**Curing period (days)**	**Supplier average concrete Compressive strength (MPa)**	**Actual average concrete compressive strength (MPa)**
14	**14**	-	20.51
21	**21**	-	22.71
28	**28**	20	23.17

The tests results were validated by SANS 5863: 2006 which states that the difference between the highest result and the lowest result should not exceed 15% of the average concrete compressive strength.

In this study, the highest concrete strength was of 23.44 MPa and the lowest concrete strength was 22.98 MPa at 28 days. With regard to the above statement, the difference between highest result and the lowest result was of 0.46 MPa and the 15% of the average

concrete compressive strength was of 3.476 MPa (15x23.17/100). Hence, the results of the concrete compressive strength agreed with SANS 5863:2006.

4.4 Flexural Test Results

4.4.1 Introduction

A four-point loading system utilizing two load points equally spaced from their adjacent support points, with a distance between load points of one-half of the support span was used in the experiments as represented in Figure 3.23 (Section 3.5.1) (ASTM D7264 / D7264M-15, 2015). The purpose of this test was to evaluate and characterize the average bond strength of ribbed GFRP rebars through average maximum tensile strength of GFRP rebars and to compare the GFRP rebars average bond strength to steel rebar average bond strength in static and dynamic. The tests were conducted according to ASTM D7264/D7264M.

4.4.2 Presentation of results

The four-point bending test was used in order to induce a uniform bending moment and maximum flexural stress between the loading points, causing the beam to sag. The longitudinal top fibre became shorter due to the bending and was stressed in compression, while the longitudinal bottom fibre became longer and stressed in tension. The rebars in the bottom part were then more likely to slip; hence the slippage values could be recorded. The deflection of the beam was experimentally recorded during the experiments using the extension meter of the UTM, while the maximum bending strength and the bond strength were respectively calculated using the following formulae for four point bending test:

$$\sigma_{max} = \frac{3\times P\times L}{4\times b\times h^2} \qquad \text{(ASTM D7264/D7264M) (51)}$$

Where P is the maximum load on the beam, L is the span of the beam, b is the width of the beam and h is the height.

$$\mu_{max} = \frac{P}{\pi\times d_b\times l} \qquad \text{(ACI 440.1R-15) (52)}$$

Where μ_{max} is the maximum bond strength of the rebars, P is the maximum load on the beam, l is the development length of the longitudinal reinforcement, d_b is the diameter of the rebar.

To investigate the flexural behaviour, the following was analysed:

- The load-deflection curves; the load was investigated in order to determine the failure point of the bond as the load increased which helped to calculate the maximum bond strength of the rebars in the concrete beam. Whereas determining the deflection helped to understand and characterize the bond behaviour in the concrete;
- The stress-strain curves: Determining the stress was as important as determining the load because it helped to characterize the bond strength, meaning the maximum stress that the bond between the rebar and the concrete could sustain before undergoing damages;
- Mode of failure: It helped understanding the failure of the composite material (the concrete and GFRP rebar); and
- The bond- slip relationship. It was impossible to observe the bond between the rebars and the surrounding concrete but the result of the bond failure which is the slip could be recorded. The bond was then quantified by the level of the GFRP rebar slip recorded.

The results presented in this section were analysed with respect to two main variables, which were:

- The type of reinforcement used (steel or GFRP rebars); and
- The loading scheme (Static or dynamic).

The results of the flexural test are presented in Table 4.3.
The following symbols are used in upcoming sections to identify the different beams:

- For a beam named RCGFRP34: RC meant Reinforced Concrete, GFRP denoted the type of reinforcement which was Glass Fibre-Reinforced-Polymer and the number '34', denoted the specimen's number for that type of reinforcement.
- For a beam named RCS1: RC meant Reinforced Concrete, S denoted the type of reinforcement which was steel and the number '1', denoted the specimen's number for that type of reinforcement.

Table 4.3 Results of the beams flexural tests at serviceability

Sample	Reinforcement type	Concrete age (days)	Concrete compressive strength (MPa) f_{cu}	Load type	Maximum load (kN) P_{max}	Maximum bending strength (MPa) σ_{max}	Maximum bond strength (MPa) μ_{max}
RCGFRP1	GFRP	14	20.51	Dynamic	360.20	31.52	9.14
RCGFRP2	GFRP	14	20.51	Dynamic	359.88	31.49	9.13
RCGFRP3	GFRP	14	20.51	Dynamic	360.73	31.56	9.15
RCGFRP4	GFRP	14	20.51	Dynamic	360.98	31.59	9.16
RCGFRP5	GFRP	14	20.51	Dynamic	264.78	23.17	6.72
RCGFRP6	GFRP	14	20.51	Dynamic	360.35	31.53	9.14
RCGFRP7	GFRP	14	20.51	Static	338.71	29.64	8.60
RCGFRP8	GFRP	14	20.51	Static	340.44	29.79	8.64
RCGFRP9	GFRP	14	20.51	Static	338.71	29.64	8.60
RCGFRP10	GFRP	14	20.51	Static	345.47	30.23	8.77
RCGFRP11	GFRP	14	20.51	Static	103.11	9.02	2.62
RCGFRP12	GFRP	14	20.51	Static	345.76	30.26	8.77
RCGFRP13	GFRP	21	22.71	Dynamic	464.09	40.61	11.77
RCGFRP14	GFRP	21	22.71	Dynamic	445.00	38.94	11.29
RCGFRP15	GFRP	21	22.71	Dynamic	440.06	38.51	11.17
RCGFRP16	GFRP	21	22.71	Dynamic	450.60	39.43	11.43
RCGFRP17	GFRP	21	22.71	Dynamic	438.40	38.36	11.13
RCGFRP18	GFRP	21	22.71	Dynamic	413.49	36.18	10.49
RCGFRP19	GFRP	21	22.71	Static	345.42	30.31	8.77
RCGFRP20	GFRP	21	22.71	Static	332.71	29.11	8.44
RCGFRP21	GFRP	21	22.71	Static	346.36	30.31	8.79
RCGFRP22	GFRP	21	22.71	Static	342.44	29.07	8.69

Sample	Reinforcement type	Concrete age (days)	Concrete compressive strength (MPa) f_{cu}	Load type	Maximum load (kN) P_{max}	Maximum bending strength (MPa) σ_{max}	Maximum bond strength (MPa) μ_{max}
RCGFRP23	GFRP	21	22.71	Static	329.19	28.81	8.35
RCGFRP24	GFRP	21	22.71	Static	348.45	30.49	8.84
RCGFRP25	GFRP	28	23.17	Static	365.41	31.98	9.27
RCGFRP26	GFRP	28	23.17	Static	232.46	20.34	5.90
RCGFRP27	GFRP	28	23.17	Static	351.36	30.75	8.92
RCGFRP28	GFRP	28	23.17	Static	348.04	30.46	8.83
RCGFRP29	GFRP	28	23.17	Static	358.49	31.37	9.10
RCGFRP30	GFRP	28	23.17	Static	338.59	29.63	8.59
RCGFRP31	GFRP	28	23.17	Dynamic	431.36	37.75	10.95
RCGFRP32	GFRP	28	23.17	Dynamic	414.96	36.31	10.53
RCGFRP33	GFRP	28	23.17	Dynamic	410.68	35.94	10.42
RCGFRP34	GFRP	28	23.17	Dynamic	410.81	36.95	10.43
RCGFRP35	GFRP	28	23.17	Dynamic	412.93	36.13	10.48
RCGFRP36	GFRP	28	23.17	Dynamic	410.63	35.93	10.42
RCS1	Steel rebar	14	20.51	Dynamic	424.08	37.11	12.51
RCS2	Steel rebar	14	20.51	Static	325.85	28.51	9.61
RCS3	Steel rebar	14	20.51	Dynamic	421.37	36.87	12.43
RCS4	Steel rebar	14	20.51	Dynamic	423.51	37.05	12.49
RCS5	Steel rebar	21	22.71	Dynamic	428.14	37.46	12.63
RCS6	Steel rebar	21	22.71	Static	350.28	30.65	10.33
RCS7	Steel rebar	21	22.71	Dynamic	423.84	37.09	12.50
RCS8	Steel rebar	21	22.71	Static	355.99	31.15	10.50
RCS9	Steel rebar	28	23.17	Dynamic	417.46	36.53	12.31
RCS10	Steel rebar	28	23.17	Dynamic	424.54	37.15	12.52
RCS11	Steel rebar	28	23.17	Dynamic	424.65	37.16	12.52
RCS12	Steel rebar	28	23.17	Static	347.93	30.45	10.26

4.4.3 Load-deflection curves for GFRP and Steel reinforced concrete beams

Table 4.3 on pages 64 and 65 showed that GFRP reinforced concrete beams could carry bigger maximum loads in dynamic tests than in static tests. It could be seen from Figure 4.7 that the deflection of GFRP reinforced beams was larger at failure, especially in the dynamic tests. Whereas, steel reinforced beams exhibited less deflection compared to GFRP reinforced concrete beams, however larger deflections were recorded in static tests than in dynamic tests at failure.

Table 4.1 on page 55 shows that the average tensile strength for GFRP was 507 MPa and is bigger than steel tensile strength which was 450 MPa (Section 3.3.2 (b) on page 23). However, it seemed that the average tensile strength of the rebars had no direct effect on the bond strength of the beams. This was indicated in Figure 4.7 by the fact that steel reinforced concrete beams developed smaller deflections than GFRP reinforced concrete beams.

It was also observed from Table 4.3 that the GFRP reinforced concrete beams as well as steel reinforced concrete beams developed bigger bond strength in dynamic tests than in static tests. Moreover, Figure 4.7 showed that because of the small bond strengths that were developed in static tests, larger deflections were recorded in static tests than in dynamic tests.

It could also be seen from Table 4.3 on pages 64 and 65 that GFRP reinforced concrete beams only developed up to 86.67 % (10.95 MPa) of steel reinforced concrete beams bond strength (12.63 MPa). This justifies the limited deflections of steel reinforced concrete beams (before failure) while compared to GFRP reinforced concrete beams as seen in Figure 4.7.

Equation 52 shows that the maximum load is a function of the maximum bond strength, which helped characterize the bond strength. Therefore, it can be said that if a GFRP reinforced concrete beam has the capacity of sustaining relative big loads it should also develop relative higher bond strength.

This answered the second objective of this study which was to evaluate and characterize the bond strength of GFRP rebars through the average maximum tensile strength of GFRP and steel rebars.

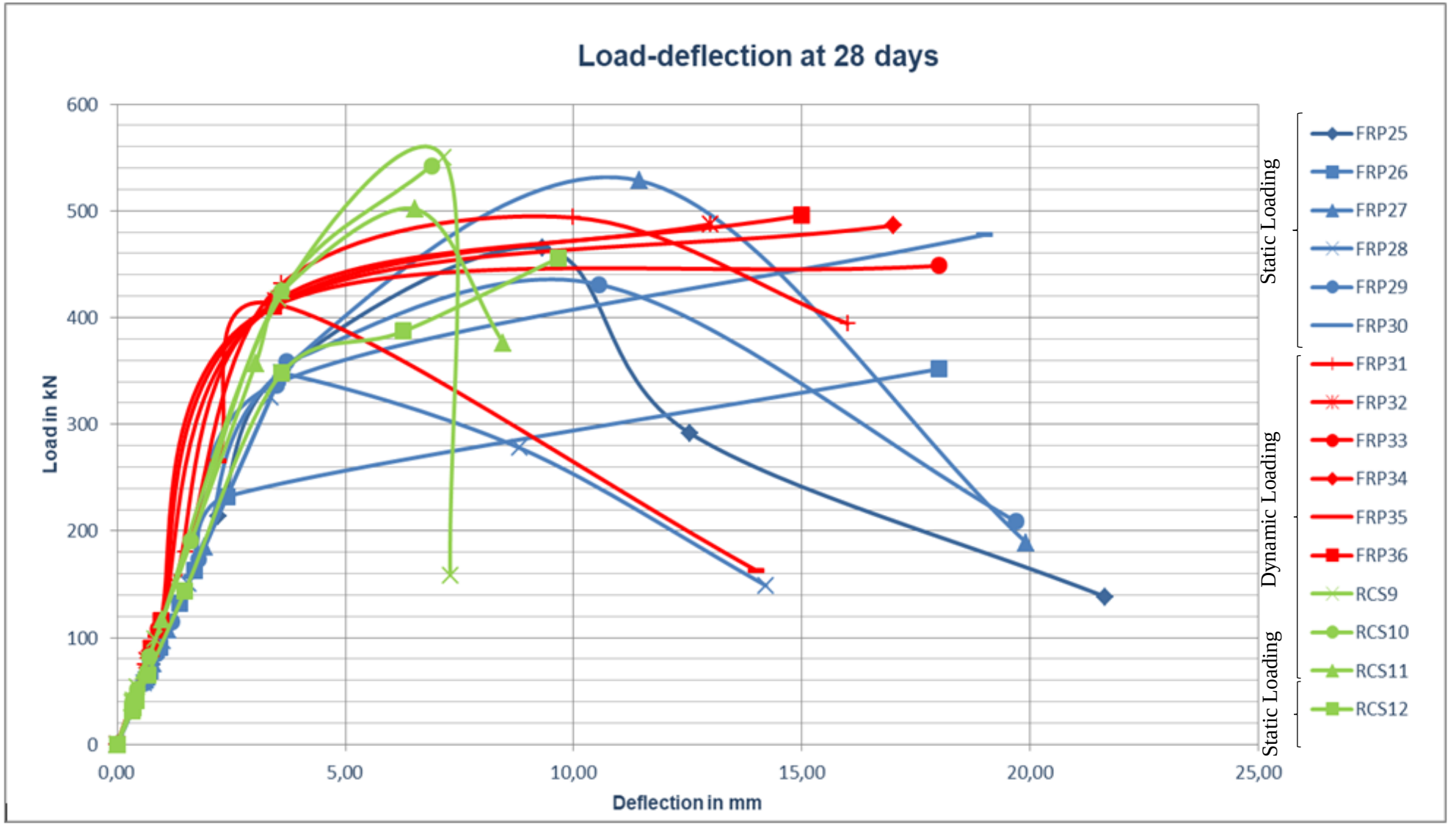

Figure 4.7 Load-deflection curves for GFRP and Steel reinforced concrete beams

4.4.4 Stress-strain curves for GFRP and Steel reinforced concrete beams

Figure 4.8 shows that both GFRP and steel reinforced beams showed a linear phase up to the apparent yield stresses (ranging between 20.34 MPa to 37.75 MPa). They then went through a stiffening phase up to the ultimate yield stresses (ranging between 30.78 MPa to 48.13 MPa). This phase was also characterized by the crushing of the reinforced concrete beams as the apparent yield stresses exceeded the average maximum compressive strength of the reinforced concrete beams. Afterwards, the effects of the loading mode, as well as the effect of the reinforcement set the different curves apart as it could be seen in Figure 4.8.
For GFRP reinforced beams under dynamic loading, the stiffening phase curved out towards the failure and the beams behaviour as well as the stress-strain curves showed that the bond between the rebars and the concrete was not severely destroyed after reaching the maximum stresses. Whereas in static the stiffening phase lasted a bit longer and was then characterized by a sudden failure as seen in Figure 4.8. It also seemed that there was no resulting bond after reaching the maximum stresses and that's why the beams failed suddenly afterwards.

For steel reinforced beams under dynamic loading, the failure was more sudden after the stiffening phase than in static.

Greater tensile strengths were recorded in dynamic tests (ranging from 35.93 MPa for RCGFRP36 to 37.75 MPa for RCGFRP31) rather than in static tests (ranging from 20.34 MPa for RCGFRP26 to 31.98 MPa for RCGFRP25). This also helped address the second objective of this study as it can be said that the bond strength of GFRP and steel reinforced concrete beams were directly proportional to the bending stresses of the beams as well as to the maximum load carried by the beams. This could be observed in both dynamic tests and static tests as seen in Table 4.3.

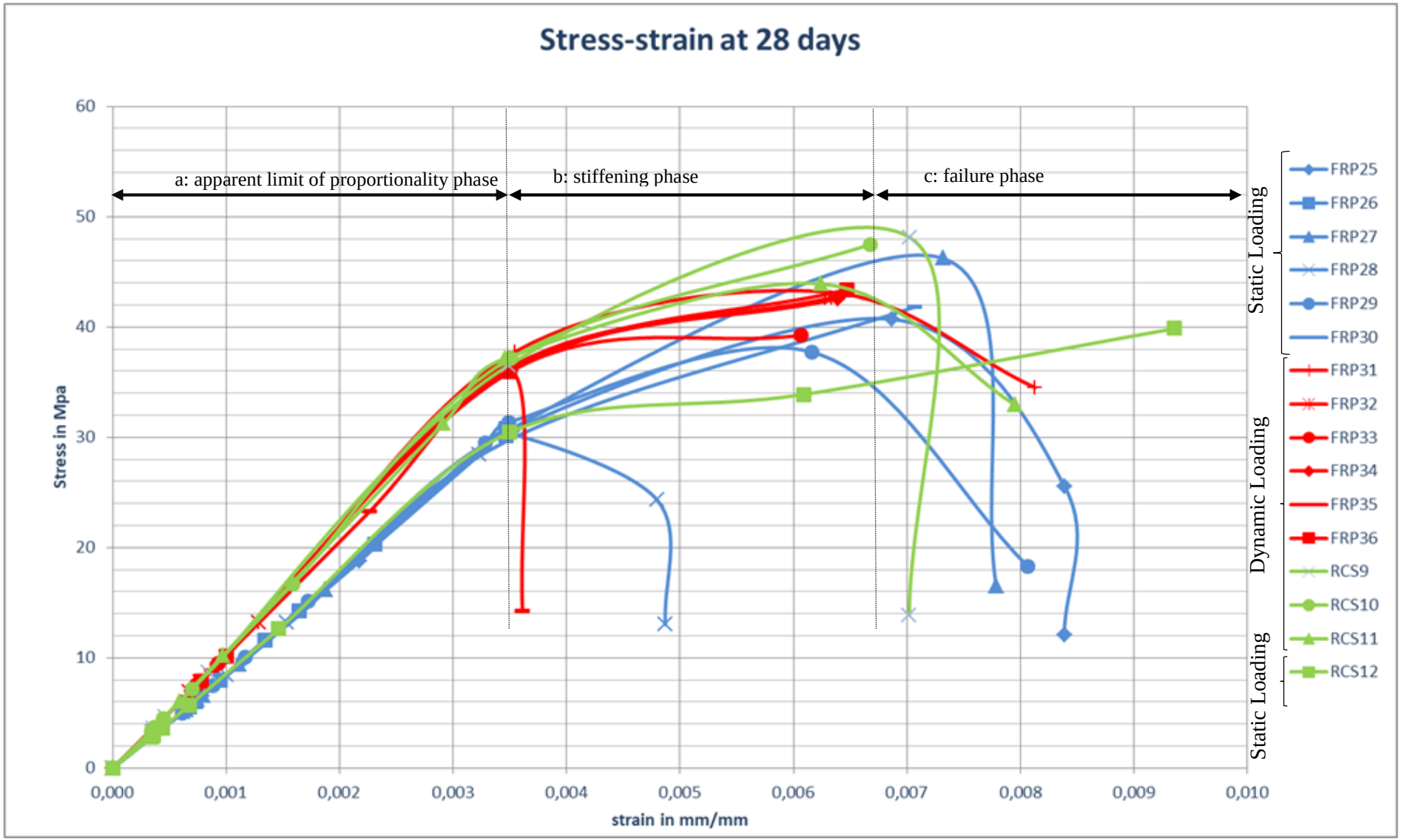

Figure 4.8 Stress-strain curves for GFRP and Steel reinforced concrete beams

4.4.5 Slips measurement results

The bond between the reinforcement and the surrounding concrete could not be observed or quantified during the experiments. However, the results of bond failure which was the slippage could be measured using LVDTs. The LVDTs were connected to a logger to facilitate the reading as shown in Figures 3.11, 3.12 and 3.13. The logger reading for the LVDT gave output voltages which were interpreted as the reading of a voltmeter. Thus, position of the LVDT's stroke corresponded to an output voltage. Thus, a trial test was run onto the LVDT prior to the flexural tests in order to calibrate the displacement of the stroke to specific voltages values. It was then set that a displacement of 10 mm corresponded to a voltage value of 0.004 on the logger.

The slip was then calculated as follows:

$$\Delta s = \Delta \mu V \times \frac{10[mm]}{0.004\ [Volts]} \tag{53}$$

Where Δs was the slippage during the testing period in mm and ΔμV was the change in voltage from the beginning (μV_1) to the end (μV_2) of the test and equal to ($\mu V_2 - \mu V_1$). ΔμV was taken regardless of the sign and was expressed in Volts. The slippage values recorded during the tests are listed in Table 4.4.

The calculations were then performed as followed:

For RCGFRP1, ($\mu V_2 - \mu V_1$) = $[-4.97 - (-4.967)] = -0.003$ volts

$$\Delta s = -0.003 \times \frac{10}{0.004} = 7.5 \text{ mm}$$

The initial output signal was read off from the logger at the beginning of the loading process, and the final output signal was read off and recorded when the loading process stopped.

Table 4.4 Slip values recorded via LVDT

Bar	Load type	Initial output signal (μV_1)	Final signal output (μV_2)	$\Delta\mu V$	Converted slip value Δs (mm)
RCGFRP1	Dynamic	-4.967	-4.970	-0.003	7.500
RCGFRP2	Dynamic	-4.976	-4.972	0.004	10.000
RCGFRP3	Dynamic	-4.971	-4.970	0.001	2.500
RCGFRP4	Dynamic	-4.970	-4.972	-0.002	5.000
RCGFRP5	Dynamic	-4.969	-4.967	0.002	5.000
RCGFRP6	Dynamic	-4.967	-4.966	0.001	2.500
RCGFRP7	Static	-4.060	-4.065	-0.005	13.000
RCGFRP8	Static	-4.102	-4.113	0.007	17.200
RCGFRP9	Static	-4.116	-4.113	0.003	7.000
RCGFRP10	Static	-4.925	-4.922	0.003	7.500
RCGFRP11	Static	-4.931	-4.922	0.009	22.500
RCGFRP12	Static	-4.926	-4.925	0.001	2.500
RCGFRP13	Dynamic	-4.952	-4.954	-0.002	5.000
RCGFRP14	Dynamic	-0.951	-4.953	-0.002	5.000
RCGFRP15	Dynamic	-4.957	-4.958	-0.001	2.500
RCGFRP16	Dynamic	-4.957	-4.958	-0.001	2.500
RCGFRP17	Dynamic	-4.960	-4.961	-0.001	2.500
RCGFRP18	Dynamic	-4.096	-4.100	-0.004	10.000
RCGFRP19	Static	-4.046	-4.045	0.001	2.500
RCGFRP20	Static	-4.919	-4.918	0.001	2.500
RCGFRP21	Static	-4.928	-4.921	0.007	17.500
RCGFRP22	Static	-4.924	-4.917	0.007	17.500
RCGFRP23	Static	-4.922	-4.925	-0.003	7.500
RCGFRP24	Static	-4.919	-4.920	-0.001	2.500
RCGFRP25	Static	-4.952	-4.953	-0.001	2.500
RCGFRP26	Static	-4.961	-4.963	-0.002	5.000
RCGFRP27	Static	-4.961	-4.963	-0.002	5.000
RCGFRP28	Static	-4.964	-4.965	-0.001	2.500
RCGFRP29	Static	-4.962	-4.961	0.001	2.500
RCGFRP30	Static	-4.917	-4.915	0.002	5.000
RCGFRP31	Dynamic	-4.919	-4.915	0.004	10.000
RCGFRP32	Dynamic	-4.920	-4.918	0.002	5.000
RCGFRP33	Dynamic	-4.919	-4.915	0.004	10.000
RCGFRP34	Dynamic	-4.920	-4.916	0.004	10.000
RCGFRP35	Dynamic	-4.922	-4.918	0.004	10.000
RCGFRP36	Dynamic	-4.921	-4.916	0.005	12.500
RCS 1	Dynamic	-4.926	-4.927	-0.001	2.500
RCS 2	Static	-4.923	-4.871	0.052	12.800
RCS 3	Dynamic	-4.927	-4.929	-0.002	5.000
RCS 4	Dynamic	-4.930	-4.926	0.004	10.000
RCS 5	Dynamic	-4.922	-4.920	0.002	5.000

RCS 6	Static	-4.926	-4.923	0.003	7.500
RCS 7	Dynamic	-4.096	-4.098	-0.002	5.000
RCS 8	Static	-4.930	-4.924	0.006	15.000
RCS 9	Dynamic	-4.913	-4.912	0.001	2.500
RCS 10	Dynamic	-4.916	-4.913	0.003	7.500
RCS 11	Dynamic	-4.917	-4.910	0.007	17.500
RCS 12	Static	-4.956	-4.963	-0.007	17.500

It can be seen from Table 4.4 that at 28 days, the slip values of GFRP reinforced concrete beams ranged between 5 mm (RCGFRP32) to 12.5 mm (RCGFRP36) under dynamic loading and between 2.5 mm (RCGFRP25, RCGFRP28 and RCGFRP29) to 5 mm (RCGFRP26, RCGFRP27 and RCGFRP30) under static loading. For steel reinforced concrete beams, the slip values ranged between 2.5 mm to 17.5 mm both under static as well as under dynamic loading. In regard to those results, it could be seen that the beams reached bigger loads, bond strengths in dynamic tests, however they ended up slipping more. Whereas in static tests, smaller loads and bond strengths were recorded while compared to dynamic tests, but less slips were recorded (Tables 4.3 and 4.4).

Looking at Figure 4.8, it could be seen that the failure was sudden in static tests and more gradual in dynamic tests which implied the time factor. This means that the slips were limited in statics tests due to limited or short time of failure (the termination of the tests after reaching the maximum stresses) while larger slips were recorded in dynamic tests due to the continuation of the experiments after reaching the maximum stresses. From this analysis, it could be seen that the slip was a parameter related to the mode of failure of the bond strength rather than the bond strength itself.

4.4.6 Strain measurement results

GFRP rebars are known to dissipate strain energy through the degradation of the rebar itself, the microscopic failure of the bond, the degradation of the toughness and the tensile strength of the rebar (Bank, 2013 and Ray & Rathore, 2015). The strain was measured during the flexural tests in order to characterize the strain values to the bond behaviour (slippage) and the bond strength values during the tests. Strain gages were mostly connected to dynamic tested beams rather than to static beams. Once again, the logger reading provided output voltages (at initial and final position). To determine the actual strain quantity in the rebar, a formula provided by the supplier of the strain gauge was used (Kyowa, 2011).

$$e_0 = [E_s.\frac{Ks}{4}].\varepsilon_0 \quad (54)$$

$$\varepsilon_0 = \frac{e_0}{[E_s.\frac{Ks}{4}]} \quad (55)$$

Where e_0 is the increment output voltage from the beginning (μV_1) of the test to the end (μV_2) and is equal to ($\mu V_2 - \mu V_1$), E_s is the voltage of the Wheatstone bridge interface equal to 12 V, K_s is the gauge factor of the strain gauge provided by the supplier (equal to 2.1 for KFRP strain gauges) (Kyowa, 2011) and finally ε_0 is the strain quantity. The strain values were presented in Table 4.5.

Table 4.5 Strain values recorded via strain gauges

Bar	**Load type**	**Initial output signal (μV_1)**	**Final signal output (μV_2)**	**e_0(μV)**	**Quantity strain $\varepsilon_0 . 10^{-6}$**
GFRP1	Dynamic	1.020	4.065	3.045	0.483
GFRP2	Dynamic	10.022	10.860	0.838	0.133
GFRP3	Dynamic	6.500	8.608	2.108	0.335
GFRP4	Dynamic	0.524	4.001	3.477	0.552
GFRP5	Dynamic	1.604	4.002	2.398	0.381
GFRP6	Dynamic	4.228	4.369	0.141	0.022
GFRP7	Static	-	-	-	-
GFRP8	Static	-	-	-	-
GFRP9	Static	-	-	-	-
GFRP10	Static	-	-	-	-
GFRP11	Static	-	-	-	-
GFRP12	Static	-	-	-	-
GFRP13	Dynamic	0.601	2.300	1.699	0.270
GFRP14	Dynamic	0.086	2.800	2.714	0.431
GFRP15	Dynamic	0.121	1.750	1.629	0.259
GFRP16	Dynamic	0.121	1.750	1.629	0.259
GFRP17	Dynamic	0.016	2.000	1.984	0.315
GFRP18	Dynamic	0.113	0.639	0.526	0.083
GFRP19	Static	0.026	0.026	0.000	0.000
GFRP20	Static	-	-	-	-
GFRP21	Static	-	-	-	-
GFRP22	Static	-	-	-	-
GFRP23	Static	0.005	9.598	9.593	1.523
GFRP24	Static	0.113	0.639	0.526	0.083
GFRP25	Static	0.014	0.054	0.040	0.006
GFRP26	Static	-	-	-	-
GFRP27	Static	-	-	-	-
GFRP28	Static	-	-	-	-

GFRP29	Static	-	-	-	-
GFRP30	Static	0.827	0.707	-0.120	-0.019
GFRP31	Dynamic	0.044	9.992	9.948	1.579
GFRP32	Dynamic	0.107	1.563	1.456	0.231
GFRP33	Dynamic	1.330	6.281	4.951	0.786
GFRP34	Dynamic	1.160	2.690	1.530	0.243
GFRP35	Dynamic	0.428	2.395	1.967	0.312
GFRP36	Dynamic	0.005	0.007	0.002	0.000
Steel 1	Dynamic	-	-	-	-
Steel 2	Static	-	-	-	-
Steel 3	Dynamic	-	-	-	-
Steel 4	Dynamic	-	-	-	-
Steel 5	Dynamic	0.007	9.992	9.985	1.585
Steel 6	Static	-	-	-	-
Steel 7	Dynamic	-	-	-	-
Steel 8	Static	-	-	-	-
Steel 9	Dynamic	-	-	-	-
Steel 10	Dynamic	-	-	-	-
Steel 11	Dynamic	0.006	9.986	9.98	1.584
Steel 12	Static	-	-	-	-

It can be seen that the strain in the rebars were very small both in dynamic and static tests, for all type of reinforcement. This was due to the high longitudinal young modulus of the GFRP (40 000 MPa, from Table 3.4) and steel rebars (200 000 MPa, Section 3.2.2 b). The values of the strains presented in Table 4.5 represented the elastic strain of the GFRP and steel rebars as their respective maximum strains are equal to 0.0015 and 0.002 (ACI 440 R1-03 , 2005; ACI 440 R1-06, 2006 and Nutt, 2007).

4.4.7 Results of the beams failure modes

The mode of failure of reinforced concrete structures is known to be complex due to the heterogeneous property of the concrete microstructure, and varies according to the type of stress and the internal structure of the specimen. It was important to understand the mode of failure of the concrete beams in order to characterize the bond behaviour and failure in the study. The study of the mode of failure brought more clarity on the mechanisms leading to the destruction of the bond strength, whether it was the bending, the shear or the concrete crushing. The mode of failure of the beams could then be proposed with regards to Equation 1($1 < \frac{L_{sh}}{h} < 2.5$) (Section 2.2.5), considering a depth h of 220 mm and a shear length of 480 mm (Figure 3.25), the ratio $\frac{L_{sh}}{h}$ was equal to 2.18. Therefore, the failure mode of the

concrete beams could be interpreted according to Equation 1. The concrete beams modes of failure were proposed in Table 4.6 (Appendix E).

Table 4.6 Mode of failure

Sample	Proposed mode of failure
RCGFRP1	Predominant bending cracks development with deep shear cracks
RCGFRP2	Predominant bending cracks development
RCGFRP3	Predominant bending cracks with small shear cracks
RCGFRP4	Predominant shear cracks with shallow bending cracks
RCGFRP5	Crushing failure at loading points with bending cracks
RCGFRP6	Bending cracks-shear cracks
RCGFRP7	Predominant bending-shear cracks development
RCGFRP8	Bending cracks with shear cracks development
RCGFRP9	Bending cracks with shear cracks development
RCGFRP10	Bending cracks with shear cracks development
RCGFRP11	Bending cracks with shear cracks(shallow) development
RCGFRP12	Bending cracks-shear cracks
RCGFRP13	Deep bending cracks-localized deep shear cracks
RCGFRP14	Predominant deep bending crack
RCGFRP15	Deep bending cracks-deep shear cracks
RCGFRP16	Deep bending cracks developing into shallow shear cracks
RCGFRP17	Bending cracks and development of shear cracks
RCGFRP18	Concrete crushing in the compression zone-bending cracks.
RCGFRP19	Predominant bending cracks- deep shear cracks
RCGFRP20	Predominant bending cracks
RCGFRP21	Insignificant bending cracks- deep localized shear cracks
RCGFRP22	Predominant bending cracks
RCGFRP23	Predominant bending cracks
RCGFRP24	Shallow bending cracks-shear cracks
RCGFRP25	Deep bending cracks developing into shear cracks
RCGFRP26	Predominant deep bending cracks
RCGFRP27	Bending cracks with shallow shear cracks
RCGFRP28	Predominant bending cracks
RCGFRP29	Crushing of concrete in the compression zone-shear cracks development
RCGFRP30	Bending cracks towards localized shear cracks
RCGFRP31	Predominant bending cracks
RCGFRP32	Predominant bending cracks towards shear cracks
RCGFRP33	Predominant bending cracks
RCGFRP34	Bending cracks with shear cracks distribution
RCGFRP35	Bending crack developing towards shear cracks
RCGFRP36	Predominant bending cracks
RCS 1	Concrete crushing in compression zone- bending cracks- development of shear cracks

RCS 2	Deep shear cracks-side section cracking
RCS 3	Deep shear cracks
RCS 4	Deep shear cracks- side section cracking
RCS 5	Shear cracks
RCS 6	Bending cracks-Concrete crushing at loading points
RCS 7	Shear cracks- shallow bending cracks
RCS 8	Deep shear cracks- shallow bending cracks- side section cracking
RCS 9	Concrete crushing at loading points-shallow shear cracks-shallow bending cracks
RCS 10	Shallow shear cracks-shallow bending cracks
RCS 11	Shear cracks
RCS 12	Localized shear cracks

4.4.8 Analysis of Results for flexural tests

The analysis of the different factors investigated in this study showed that the compressive strength, the surface configuration of the GFRP rebars, the mechanical properties of the GFRP rebars and loading mode affected the bond strength of GFRP rebars in concrete, the maximum achievable load and even the mode of failure of the reinforced concrete beams. In the following paragraphs, the influences of each above mentioned parameters on the bond will be discussed:

4.4.8.1 Effects of the concrete compressive strength on the bond strength and the resulting modes of failure

This study aimed to understand the bond strength behaviour of GFRP rebars under dynamic loading by investigating the bond strength behaviour in normal strength concrete. Only one class of concrete was used in this study (Class 20), hence to study the effect of concrete compressive strength on the average bond strength, additional secondary data from Silva and Biscaia research (2008) were used. Silva and Biscaia (2008) investigated the degradation of bond between GFRP rebars in high strength concrete using a beam test similar to the one used in this study. Table 4.7 presents the experimental data of this study (in static and dynamic loadings), the theoretical data and Silva and Biscaia' experimental results.

Table 4.7 Concrete compressive strength data

Data source	**Concrete compressive strength f_{cu} (MPa)**
Experimental data: Static loading	23,17
Experimental data: Dynamic loading	
Theoretical data	20
Silva and Biscaia experimental results (2008)	38,55

The analysis of the peak bond strength of the GFRP rebars versus the concrete compressive strength of concrete showed that the peak bond strength of GFRP rebars is not proportional to the concrete compressive strength. As it could be observed from Figure 4.9, the bond strength of GFRP rebar in concrete in this experiment gave higher bond strength than when high strength concrete is used. This could be attributed to the fact that when concrete has a normal compressive strength (23.17 MPa) it grips to the ribs of the rebars without damaging it. This statement also supported other researchers' findings (Davalos, et al., 2008). The surrounding concrete and the rebar indentations seemed to both fail simultaneously as the load increased. The opposite phenomenon is assumed when high strength concrete is used. This is attributed to the fact that the very stiff concrete exerted very high stresses on the interface so that it destroyed the weakest spots, which are the rebar indentations. This led to the destruction of the bond. The analytic data gave more conservative results for 20 MPa of concrete compressive strength because it actually represents the maximum load that the beam could sustain before any crack could form.

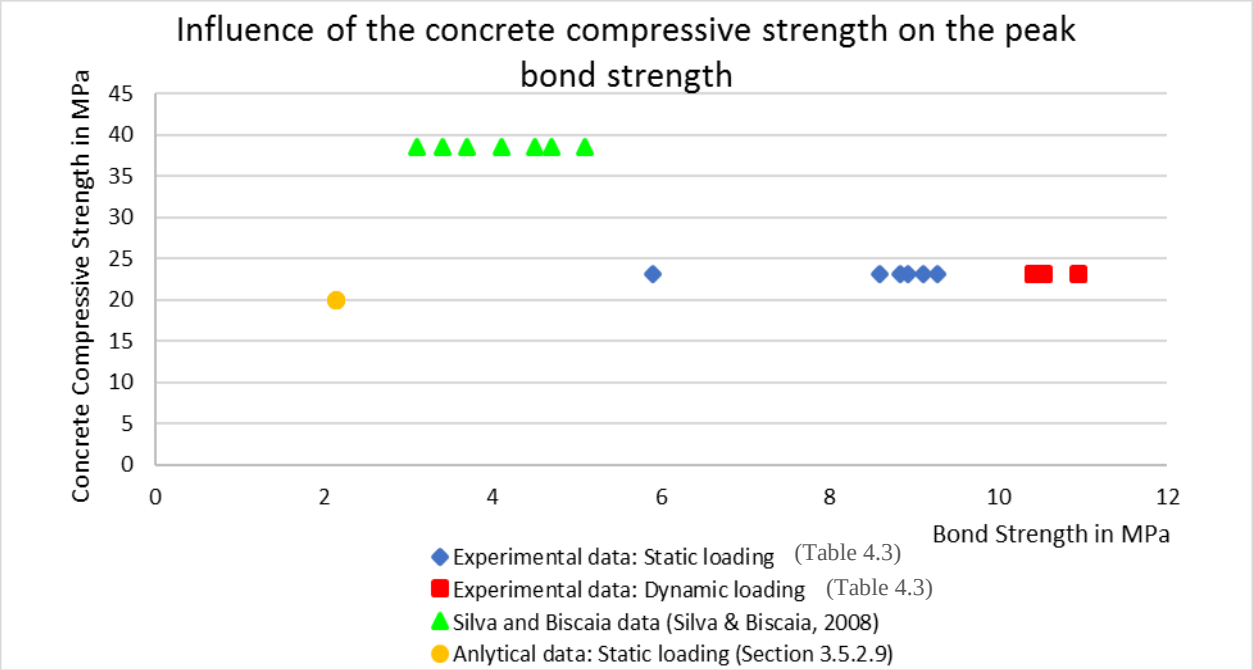

Figure 4.9 Influence of the concrete compressive strength on the peak bond strength

Moreover, in order to characterize the bond behaviour of GFRP rebars in the concrete, the bond strength was investigated with regards to the maximum midspan deflection as shown in Figure 4.10. It could be seen that although high bond strength values were reached in this experiment, the deflection values were also high, which means that the beams encountered larger deformations than in high strength concrete. This showed that the concrete compressive strength did not influence the peak bond strength but rather the bond strength behaviour of GFRP rebars in concrete.

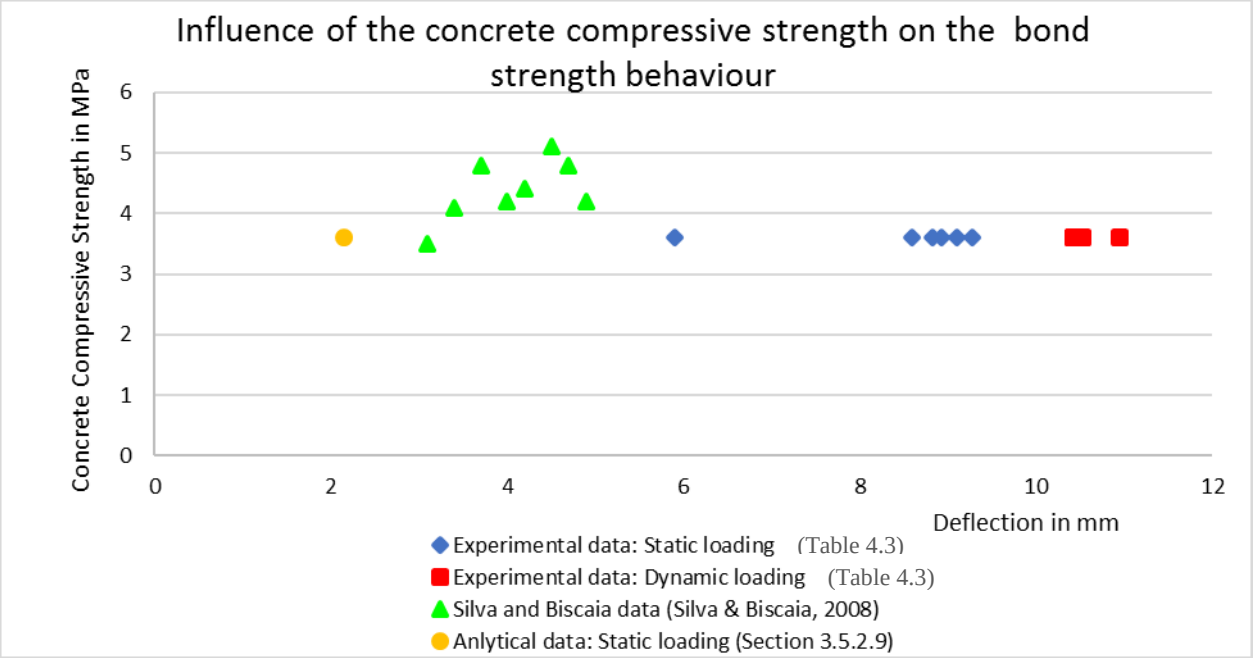

Figure 4.10 Influence of the concrete compressive strength on the bond strength behaviour

4.4.8.2 Effects of the surface configuration on the bond strength and the resulting modes of failure

The bond strength of GFRP rebars in concrete beams under dynamic loading was also investigated through the surface texture of the rebars. Since only one type of GFRP rebars were investigated (ribbed GFRP rebars), the experimental data were then compared to Xue et al. (2016) data who also investigated the bond strength of deformed sand-coated GFRP rebars in normal concrete beam through a beam test. Figure 4.11 shows the bond-slip relationship between each type of GFRP rebars. Figure 4.11 also showed that the surface treatment played a great role in developing high bond strength values but also in limiting the slip of the rebars. Xue, et al. (2016) GFRP reinforced concrete beams showed high bond strength values accompanied with less slip values when compared to the bond and slip values exhibited in this study. This could be attributed to the surface treatment enhancement by sand coating. The experimental reinforced concrete beams in this experiment developed low bond strength accompanied with large slip values. This is attributed to the surface treatment of the ribbed GFRP rebars. Moreover, the large slip values could also be attributed to the fact that the measurement of the slip was conducted on the free ends of the rebars which was not the case in Xue, et al. (2016) investigation. This means that the rebars were confined on one side only and free to move on the other end.

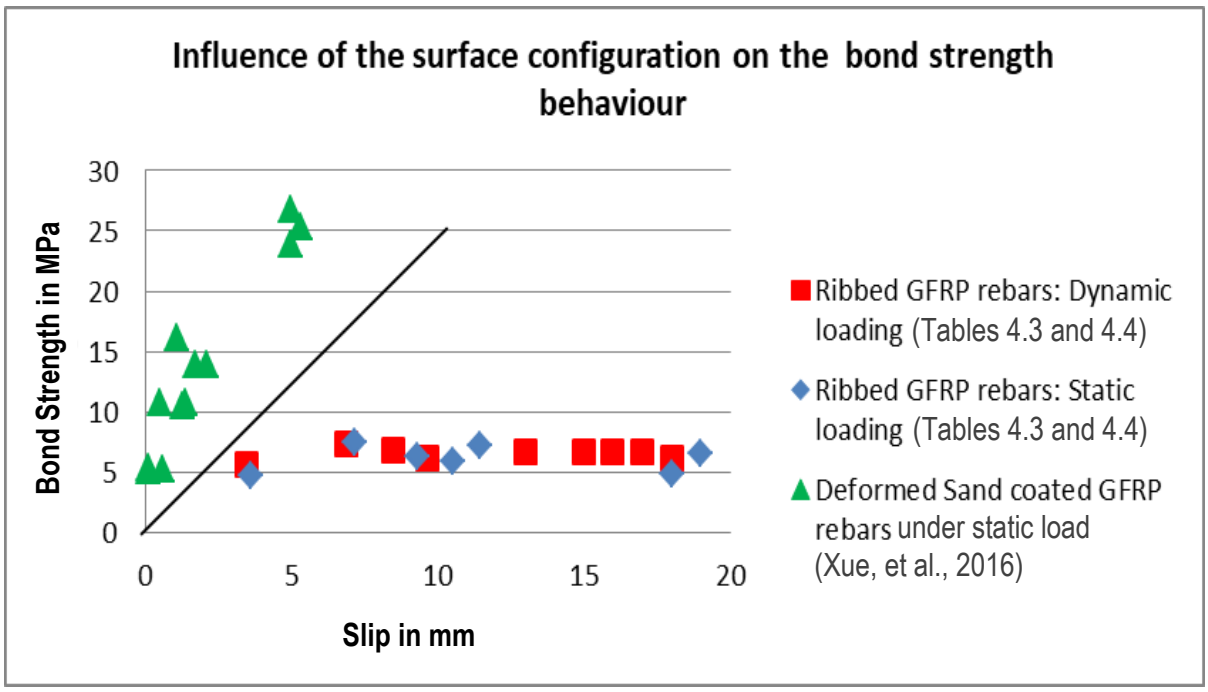

Figure 4.11 Influence of the surface treatment on the bond strength behaviour

The study of the bond-slip relationship of GFRP reinforced concrete beams in this study also revealed that the bond strength behaviour is governed by three mechanisms as stated by other authors (Cosenza, et al., 1997 and Hao, et al., 2008), namely:

i. The adhesion resistance: This mechanism can be explained as the first natural bond formed between the rebar and the concrete after casting. It was observed on all the beams and occurred from the beginning of the flexural tests up until the apparent limit of proportionality of the reinforced concrete beams curves (apparent limit of proportionality phase) as seen in Figures 4.8 on page 69. During this period, the slippage values ranged between 2.5 mm to 10 mm under dynamic loading and between 2.5 mm to 22.5 mm (Table 4.4, on page 71) as the bond strength was still developing (relatively low). It was also observed that's the only mechanism developing in concrete with low compressive strength as the concrete strength was not enough to develop any other mechanism (friction resistance and mechanical interlocking) without crushing completely.

ii. The friction resistance: This mechanism can be explained as the bond created between the rebar and the concrete when the natural first bond is broken. The bond is created by the resulting friction of the slipping rebar against the concrete. This

mechanism occurred after the apparent limit of proportionality phase on Figure 4.8 (stiffening phase). The friction resistance was the second mechanism governing the bond strength behaviour in concrete beams and it was characterized by no increase of slippage values.

iii. The mechanical interlocking: This mechanism was the final bond created between the rebar and the concrete. It was a bond reconstitution mechanism that occurred when the crushed concrete at the interface filled the void between the rebar and the concrete creating a temporary bond that broke as the load increased. During that period, the beam could carry more loads and consequently the bond strength was increasing. This was due to the fact that the mechanical interlocking did not prevent the slippage but rather temporary slowed it down. As the load was increasing, more damage was created at the interface and more crushed concrete was stuck at the interface. More slippage was then recorded until the damage became severe and a bond reconstitution was no longer possible causing the complete bond failure (failure phase in Figure 4.8) as stated by previous authors (Baena, et al., 2009). This mechanism was characterized by the increase of the bond strength values ranging between 5.90 MPa to 10.95 MPa (peak bond strength at 28 days) (Table 4.3, page 64), but also the increase of the slippage values of up to 12.5 mm (Table 4.4, page 71) and large deflection of the beams at failure as observed by other authors (Baena, et al., 2009; Wang & Belarbi, 2009 and Owens, et al., 2009). The bond strength behaviour under this last mechanism also showed an agreement with the Miner's hypothesis stipulated by previous authors (Wang & Belarbi, 2009).

These results can be presented using a diagram as seen in Figure 4.12:

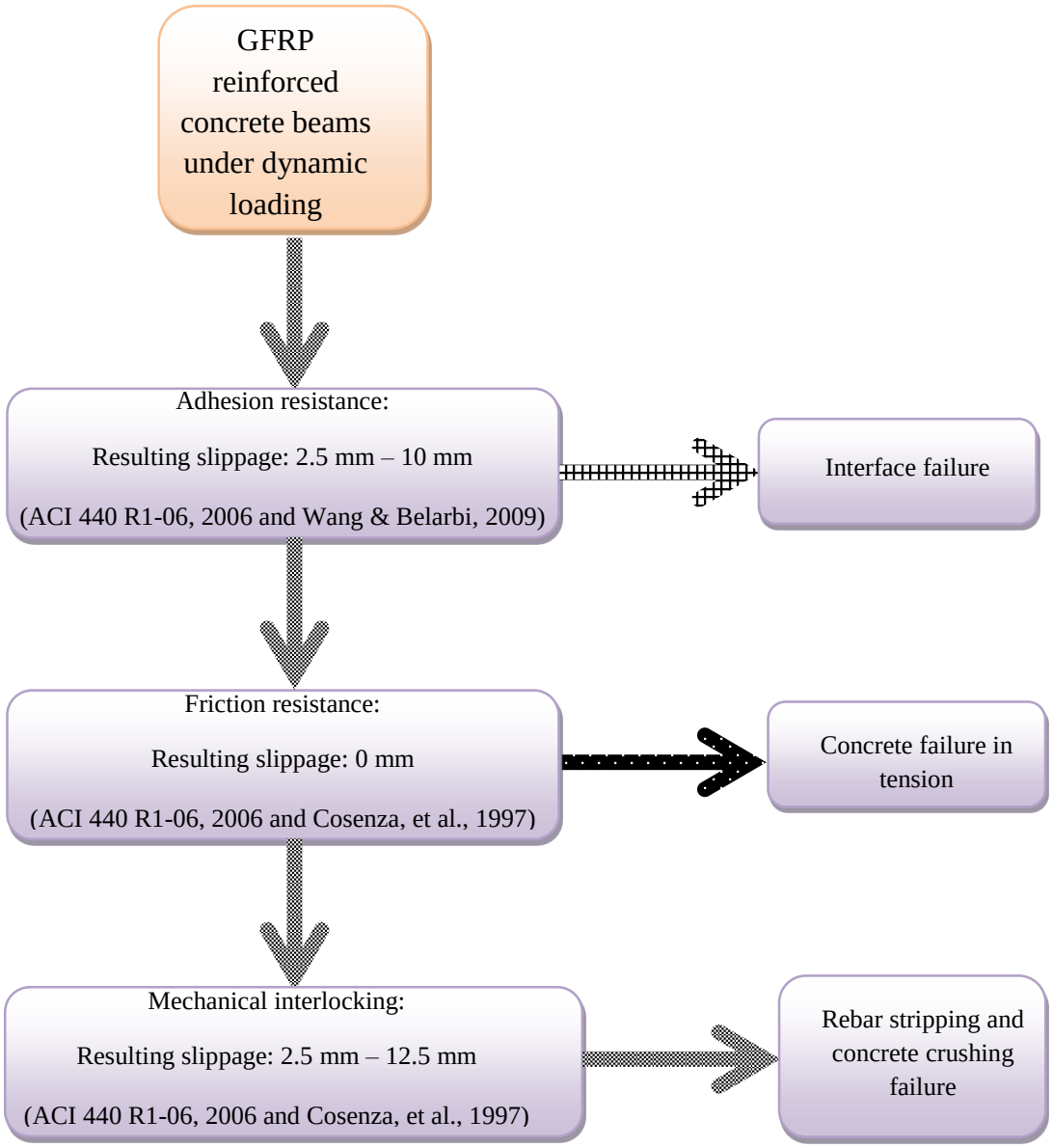

Figure 4.12 Effects of the surface texture mechanisms on the bond behaviour

4.4.8.3 Effects of the rebars mechanical properties on the bond strength and the resulting modes of failure

The effects of the GFRP rebars mechanical properties on the bond strength behaviour were examined by using steel reinforced concrete beams as benchmark.

The large deflections of GFRP reinforced concrete beams were justified by the fact that the young modulus of GFRP rebars was 5 times less than steel rebars' as seen in Table 4.8. This lead to the damage of the bond in the tension zone (large deformations). However, the slippage values in Table 4.4 (page 71) showed that GFRP rebars in general slipped less (2.5 mm -12.5 mm) than steel rebars (2.5 mm – 17.5 mm). This was attributed to the mechanical interlocking mechanism of the bond between GFRP rebars and concrete. It could be understood that GFRP reinforced concrete beams went through a 'bond reconstitution phase' which allowed the beams to sustain loads of up to 232.46 kN to 431.36 kN. The large slippage values of steel rebars were an indication that steel did not rely upon the mechanical interlocking to sustain loads of 347.93 kN up to 424.65 kN (Table 4.3), but rather sustained the load until the failure of the bond without any 'bond reconstitution phase'.

Table 4.5 (page 73) indicated that the maximum strain in the rebars (GFRP and steel rebars) were still very small (1.579×10^{-6} and 1.584×10^{-6} respectively). Therefore, the strain dissipation in the rebars could not damage the interface but rather the high strain in the tension zone of the concrete zone. This assumption was supported by the results in Table 4.6 (page 75) which showed that GFRP reinforced concrete beams at 28 days were mostly characterized by bending cracks (flexural) in the tension zone and steel reinforced concrete beams were mostly characterized by shear cracks in the tension zone. This last statement also helped to understand that shear cracks are more severe than bending cracks and they did not allow 'bond reconstitution' mechanisms to take place (RCGFRP 25, RCGFRP 29, RCGFRP 30 and RCGFRP 35). In order to characterize the bond behaviour with regards to the mechanical properties of ribbed GFRP rebars and steel rebars, the following factors were considered:

1. The maximum experimental mid span deflections of GFRP reinforced concrete beams (19 mm) and steel reinforced concrete beams (9.66 mm) in static and the maximum experimental mid span deflections of GFRP reinforced concrete beams (18 mm) and steel reinforced concrete beams (8.46 mm) in dynamic. It could be noticed that in static loading mode the mid span deflection of GFRP reinforced concrete beams is twice that of steel's. However, in dynamic there was no apparent relationship between the two categories of reinforced concrete beams. This could be due to the considerably long stiffening phase that occurred in GFRP reinforced concrete beams specimens which also increased the load carrying capacity for GFRP reinforced concrete beams specimens.

Table 4.8 Comparison of GFRP and steel rebars mechanical properties

Type of Beam	Modulus of Elasticity (MPa)	$\frac{E_f}{E_s}$	Supplier Rebar Tensile strength (MPa)	Theoretical Rebar Tensile strength (MPa)	Experimental Rebar Tensile strength (MPa)	Maximum mid-span deflection (mm)
GFRP beams	$E_f = 40000$ (Table 3.3)	$\frac{1}{5}$	$f_{fu-s} = 850$ (Table 3.3)	$f_{fu-th} = 680$ (Equation 18)	$f_{fu-Ex} = 507$ (Table 4.1)	δ_{GFRP_Static}=19
Steel beams	$E_s = 200000$		$f_y = 450$	$f_y = 450$		δ_{Steel_Static} =9.66

2. The mechanical properties of the ribbed GFRP rebars and steel rebars. Figure 4.7 was analysed and it showed that large deflections values were recorded at failure for GFRP reinforced concrete beams while compared to steel reinforced concrete beams. This was due to the fact that E_s is five times bigger than E_f as seen in Table 4.8. However, factors such as the tensile strengths of the rebars (GFRP and steel) showed no apparent effect on the bond strength of the reinforced concrete beams. On the other hand, the surface texture of the different rebars seemed to have played a considerable role in developing the bond strength. This is justified by the fact that the relatively hard steel surface texture developed relatively high bond strength (10.95 MPa) while compared to GFRP rebars texture and the maximum bond strength developed (10.42 MPa).

4.4.8.4 Effects of the loading type on the bond strength and the resulting modes of failure

From the analysis in the previous sections, number of observations were made:
All GFRP reinforced concrete beams behaved similarly up to their apparent limit of proportionality as seen in Figure 4.8. Moreover, the dynamic loading mode affected the bond behaviour and also the maximum loads of the beams as it can be seen in Table 4.3 (page 64), Figures 4.7 (page 67) and 4.8 (page 69). While in static loading, GFRP reinforced concrete beams were characterized by a stiffening phase and gradual failure as seen in Figure 4.8. In dynamic loading, GFRP reinforced concrete were characterized by a stiffening phase and sudden failure.

In static tests, it could be seen from Table 4.6 (page 75) that RCGFRP25, RCGFRP29 and CRGFRP30 specimens were affected by shear cracks which severely destroyed the bond at the interface. The bond strength values (9.27 MPa, 9.10 MPa and 8.59 MPa respectively) and the mode of failure from Table 4.6 were indications of that. However, the slip values of RCGFRP25 and RCGFRP29 (2.5 mm, from Table 4.4) indicated that the bonds were either partially destroyed or the shear cracks developed in the tension zone were not severe to the point to interrupt the mechanical interlocking mechanism (bond reconstitution mechanism) to develop. For RCGFRP30, the slip value (5 mm) indicated that shear cracks prevented any bond reconstitution. RCGFRP27 and RCGFRP28 were mostly subjected to bending cracks. The bond strength (8.92 MPa), the slip value (5 mm) indicated that RCGFRP27 developed shallow shear cracks that did not prevent the bond reconstitution mechanism. RCGFRP26 developed deep bending cracks that severely destroyed the bond (Appendix E).

Under dynamic loading, all RCGFRP concrete beams' modes of failure were dictated by bending cracks, sometimes with even shear cracks development (RCGFRP34 and RCGFRP35) or without shear cracks development (RCGFRP31, RCGFRP32, RCGFRP33 and RCGFRP36) (Table 4.6 and Appendix E). However, there was more slippage in the dynamic tests when compared with the static tested specimens (Table 4.4 on page 71), therefore there were more micro cracks formations and more crushed concrete that filled the interface between GFRP rebars and the concrete matrix as stated by other authors (Owens, et al., 2009 and Wang & Belarbi, 2009). That phenomenon contributed to the development of the mechanical interlocking mechanism (bond reconstitution mechanism) that allowed the increase of bond strength during the stiffening phase of the beams. This phenomenon was also confirmed by the analysis of the load-deflection curve (Figure 4.7 on page 67). The beams however deflected a lot during that 'bond reconstitution' period.

In Steel reinforced concrete beams, it was seen that the beams rather developed shear cracks and as stated in section 4.4.8.3, which prevented the mechanical interlocking to take place. The slip (Table 4.4 on page 71), deflection at failure (Figure 4.7 on page 67) and bond strength values (Table 4.3 on page 64) were indications of that assumption. Contrary to GFRP reinforced concrete beams, steel reinforced concrete beams loads increased as long as the bond was still sound. The beams failed when the bond was destroyed and no mechanical interlocking took place as indicated by the slip values in Table 4.4. This could be explained by the fact that steel ribs rather destroyed the interface as the rebars were slipping.

The stress-strain curve (Figure 4.8 on page 69) also indicated that the dynamic loading affected the failure of the specimens as the failures were more sudden than in static (Figure 4.8).

5. CONCLUSIONS AND RECOMMENDATIONS

5.1 General Conclusions

The main objective of this research was to experimentally determine the bond behaviour of ribbed GFRP rebars in concrete beams under dynamic loading, in order to understand the limit of use of ribbed GFRP rebars in concrete (class 20) in general and in dynamic loading in particular as applied in the Construction Industry. The bond strength behaviour was investigated using a four-point bending test and a dynamic test set-up was constituted using a UTM machine, a universal dynamic shaker and a function generator that allowed building up the desired frequency of 41 kHz with a number of cycles of 500. The bond strength behaviour was investigated through the study of several parameters which are the concrete compressive strength, the GFRP rebars texture, the mechanical properties of the GFRP rebars, the loading mode, the slip, the stress-strain relationship, the concrete beams mode of failure and the deflection of the beams. Thus, in regard to the specific objectives of this study the following conclusions were drawn:

a) The tensile strengths of ribbed GFRP rebars used in this study were evaluated and found to be 59.65% of the nominal tensile strength provided on the supplier data sheet.

b) The average maximum bond strength of GFRP and steel reinforced concrete beams were found to be greater in dynamic loading (10.42 MPa -10.95 MPa) rather than in static loading (5.90 MPa -9.27 MPa). On the other hand, GFRP reinforced concrete beams only developed 86.67 % of steel reinforced concrete bond strength and this justified the larger deflections of GFRP reinforced concrete beams while compared to steel reinforced concrete beams. The results of the tests also showed no apparent relationship between the average bond strength of the rebars (GFRP and steel) and the bond strength of the reinforced beams.

   The slip was limited in static loading as the tests duration for static specimens was also short when compared to dynamic loading tests. Hence, relatively low bond strengths (5.90 MPa – 9.27 MPa) were developed when compared to the relatively high bond strengths developed in dynamic (10.42 MPa – 10.95 MPa). This was explained by the prominent stiffening phase in dynamic loading which increased the load carrying capacity of the reinforced concrete beams in dynamic. As a consequence, higher slip values were recorded in dynamic over time than in static

loading. Moreover, it was also noticed that the slip then governed the destruction of the bond strength in the reinforced concrete beams.

The average maximum bond strength was also characterized by the fact that it was directly proportional to the maximum load carried by the beam and the bending stresses which happened to be correlated factors.

c) The study showed that in general, the average bond strength of GFRP and steel reinforced concrete beams were greater in dynamic loading than in static loading.

The study also showed that in static loading, GFRP rebars developed 88.29% of steel rebars bond strength in concrete beams, while in dynamic loading, GFRP rebars only developed 86.67% of steel rebars bond strength in concrete beams. Moreover, the bond strength values recorded showed that the steel reinforcement developed greater bond strength while compared to GFRP rebars. This was attributed to steel rebars mechanical and physical properties such as a Young modulus that is five times bigger than GFRP rebar's and the hard surface texture of steel rebars that developed great friction resistance.

Besides the above-mentioned findings, the experimental study of the bond strength of GFRP reinforced concrete beams in dynamic loading also revealed that the failure of the GFRP rebars in tensile tests was mostly due to the failure of the resin matrix which happened to be brittle. This was observed through the tensile tests that showed that the fibres of the rebars were intact while the damages were localized in the matrix resin. This showed that the average maximum tensile strength of the rebar basically represented the average bond strength of the matrix resin and was only of 59.65% of the rebar nominal tensile strength.

The study also helped characterizing the slippage of GFRP rebars in concrete with regard to the bond strength mechanism such as the adhesion resistance, the friction resistance and the mechanical interlocking. The study revealed that only the friction resistance mechanism does not induce additional slippage (0 mm slippage). While within the adhesion resistance phase there was an increment of slippage which varies from 2.5 mm to 10 mm. The mechanical interlocking phase also showed an increment of slippage values varying from 2.5 mm to 12.5 mm.

Finally, the experimental study revealed that the concrete compressive strength did not have any direct effect on the bond strength but rather on the bond strength behaviour throughout the experiments.

5.2 Recommendations

With regard to this study and the results obtained, the following recommendations are made:

1) This study revealed that GFRP rebars used in the experiments failed in tension due to the brittle nature of the matrix rather than the fibres. And as the tensile strength is a determinant factor that dictates the behaviour of the GFRP reinforced concrete beams, this study will recommend that the manufacturers of GFRP rebars should standardize the manufacturing of the rebars as to ensure that the actual tensile strength of the rebars would be more or less equal to the specifications provided by the manufacturers. This will would be the first step to the full acceptance of FRP rebars material by the Construction Industry, but also will allow to set more specific design guidelines.
2) The same study could be done with GFRP rebars of higher average tensile strength which could be equal to or higher than the supplier nominal specification to study the influence of the tensile strength on the bond strength.
3) It is also recommended that more studies could be done on the structural bond behaviour of GFRP rebars in concrete beams under dynamic with a concrete of higher grade to study the behaviour of the bond strength in this case.
4) It was observed through the experiments that GFRP reinforced concrete beams could not develop large bond strength as compared to steel reinforced concrete beams, due to their relative soft surface texture as compared to steel rebars. From these results, it can be recommended that another type GFRP rebars with another type of surface texture should be investigated to study the behaviour of the structural bond strength of GFRP rebars in concrete under dynamic loading.
5) This study relied and used most of the supplier specifications for the GFRP rebars used. Only the tensile strengths of the GFRP rebars were tested experimentally. Due to that reason, the influence of some mechanical parameters on the bond strength might have been overlooked. Hence, the study also recommends that most if not all mechanical parameters of the GFRP rebars should be experimentally tested or evaluated in order to determine their variations first, and influence on the bond strength.
6) The results of this study could be used to rebuilt damaged wharfs and quays in the Port of Cape Town which are notorious for violent winters that causes excessive moisture and reduces the alkalinity of these reinforced concrete structures.

REFERENCES

ACI 318-05, 2005. *Building code requirements for structural concrete.* Skokie IL: The Portland Cement Association.

ACI 440 R1-03 , 2005. *Guide test methods for Fiber-Reinforced Polymers for Reinforcing or strengthening concrete structures.* Michigan: American Concrete Institute.

ACI 440 R1-06, 2006. *Guide for the design and construction of structural concrete reinforced with FRP bars.* Michigan: American Concrete Institute.

ACI 440 R1-15, 2015. *Guide for the Design and Construction of Structural Concrete Reinforced with Fiber-Reinforced Polymer (FRP) Bars.* Michigan: American Concrete Institute.

Adhikary S.D., Li B. & Fujikake K., 2012. Dynamic behavior of reinforced concrete beams under varying rates of concentrated loading. *International Journal of Impact Engineering,* Volume 47, pp. 24-38.

Akbarzadeh , H. & Maghsoudi , A., 2009. Experimental and analytical investigation of reinforced high strength concrete continuous beams strengthened with fiber reinforced polymer. *Materials And Design,* Volume 31, pp. 1130–1147.

Alexander, M. & Beushausen, H., 2010. Concrete technology for Structural Engineers: Lecture 2 and 3, University of Cape Town.

Ametrone, D., 2001. *Bond characteristics of Glass fiber reinforced polymer bars embedded in high performance and ultra-high performance concrete.* Theses and dissertation paper. ed. s.l.:s.n.

ASTM A370-15, 2015. *Standard Test Methods and Definitions for Mechanical Testing of Steel Products*. West Conshohocken: ASTM International Volume 15.03.

ASTM A944-10, 2010. *Standard Test Method for Comparing Bond Strength of Steel Reinforcing Bars to Concrete Using Beam-End Specimens.* West Conshohocken: ASTM International Volume 15.03.

ASTM D3916-08, 2016. *Standard Test Method for Tensile Properties of Pultruded Glass-Fiber_Reinforced Plastic rod.*. West Conshohocken: ASTM International Volume 15.03.

ASTM D5379/D5379M-05, 2005. *Standard Test Method for Shear Properties of Composite Materials by the V-Notched Beam Method.* West Conshohocken: ASTM International Volume 15.03.

ASTM D618-13, 2013. *Standard Practice for Conditioning Plastics for Testing.* West Conshohocken: ASTM International Volume 08.01

ASTM D7264/D7264M-15, 2015. *Standard Test Method for Flexural Properties of Polymer Matrix Composite Materials.* West Conshohocken: ASTM International Volume 15.03.

ASTM D7616/D7616M-11, 2011. *Standard Test Method for Determining Apparent Overlap Splice Shear Strength Properties of Wet Lay-Up Fiber-Reinforced Polymer Matrix Composites Used for Strengthening Civil Structures.* West Conshohocken: ASTM International Volume 15.03.

Baena, M., Torres, L., Turon, A. & Barris, C., 2009. Experimental study of bond behaviour between concrete and FRP bars using a pull-out test. *Composites: Part B,* Volume 40, pp. 784–797.

Bank, L., 2013. Progress failure and ductility of FRP composites for construction. *Journal of Composites for Construction,* Volume 17, pp. 406-419.

Billah, A. & Alam, M., 2012. Seismic performanceof concrete columns reinforced with hybrid shape memory alloy (SMA) and fibre reinforced polymer (FRP) bars. *Construction and Building Materials,* Volume 28, pp. 730-742.

Bru, T., Hellstrom, P., Gutkin, R. & Ramantani, D., 2016. Characterization of the mechanical and fracture properties of a uni-weave carbon fibre/epoxy non-crimp fabric composite. *Data Brief,* Volume 6, pp. 680-695.

Ceroni, F., Cosenza, E., Gaetano, M. & Pecce, M., 2006. Durability issues of FRP rebars in reinforced concrete members. *Cement And Concrete Composites,* Volume 28, pp. 857-868.

Cheng, G., Yang, J., Alkhrdafi, J. & Nanni, A., 1999. Condition assessment of concrete structures by dynamic signature tests. *Baltimore, 13th Engineering mechanics specialty conference. John Hopkins University, Baltimore, MD,* June 13-16, 1999.

Chin, J., 1996. Materials aspects of Fibre Reinforced Polymer composites in infrastructure. NISTIR 5888, National Institute of standards and Technology. Building and Fire Research Laboratory [accessed 13.0.2015].

Choi, D., Chun, S. & Ha, S., 2011. Bond strength of glass fibre-reinforced polymer bars in unconfined concrete. *Engineering Structures,* Volume 34, pp. 303-313.

CNR-DT 203/2006, 2007. *Guide for the design and construction of concrete structures reinforced with Fibre-Reinforced Polymer bars.* Rome: National Research Council.

Cosenza, E., Manfredi, G. & Realfonzo, R., 1997. Behaviour and modelling of bond of FRP rebars to concrete. *Journal of Composites for Construction,* Volume 1, pp. 40-51.

Davalos, J., Chen, Y. & Ray, I., 2008. Effect of FRP bar degradation on interface bond with high strength concrete. *Cement & Concrete Composites,* Volume 30, pp. 722–730.

Ding, Y., Ning, X., Zhang, Y., Pacheco-Torgal, F. & Aguiar, J.B., 2014. Fibres for enhancing of the bond capacity between GFRP rebar and concrete. *Construction and Building Materials,* Volume 51, pp. 303–312.

Egyptian Standing Committee, 2005. *Egyptian code of practice for the use of Fibre Reinforced Polymer (FRP) in the construction fields.* Cairo: Ministry of Housing, Utilities and Urban Utilities.

Ehsani, M.R., Saadatmanesh, H. and Tao, S., 1996. Design recommendations for bond of GFRP rebars to concrete. *Journal of Structural Engineering,* Volume 122, pp. 247-254.

Farshadfar, O., Ajaam, A., Hano, M., O'Reilly, M. & Darwin, D., 2014. Bond strength of reinforcing bars with deformation spacings that exceed maximum specified in ASTM A615. *University of Kansas Center for Research, Lawrence, Kansas.*

Fico, R., 2007. Limits states design of concrete structures reinforced with FRP bars. *PHD thesis, University of Naples Federico II.*

Foccaci, F., Nanni, A. & Bakis, C., 2000. Local bond slip relationship for FRP reinforcement in concrete. *Journal of Composites for Construction,* Volume 4, pp. 24-31.

Groblacher, S., 2010. Quantum opto-mechanics with micromirrors:combiningnano-mechanics with quantum optics. *Thesis, University of Vienna, Austria.*

Hao, Q., Wang, Y., He, Z. & Ou, J., 2008. Bond strength of glass fiber reinforced polymer ribbed rebars in normal strength concrete. *Construction and Building Materials,* Volume 23, pp. 865-871.

INC, C. a., December 2011. *Cantat associates INC.* [Online] Available at: http:/www.cantat-associates.com/gfrpbrigde
[Accessed 4th February 2013].

Issa , M., Metwally, I. & Elzeiny , S., 2011. Structural performance of eccentrically loaded GFRP reinforced concrete columns. *International Journal of Civil Struct. Engineering,* Volume 2(1), pp. 395-404.

Jalili, M., Moradian, S. & Hosseinpour, D., 2009. The use of inorganic conversion coatings to enhance the corrosion resistance of reinforcement and the bond strength at the rebar/concrete. *Construction and Building Materials,* Volume 23, pp. 233–238.

Katz, A., 1999. Bond mechanism of FRP rebars to concrete. *Materials and Structures,* Volume 32, pp. 761-768.

Kocaoz, V., Samaranayake, A. & Nanni, A., 2005. Tensile characterization of Glass FRP bars. *Composites: Part B,* Volume 36, pp. 127-134.

Kyowa Electronic Instruments Co.2005, What's a strain gauge?: Introduction to Strain Gauges. Tokyo, [online]. Available at <http;//www.kyowa-ei.com> [Accessed: 17th June 2016].

Lee, J., Yi , C., Kim, B. & Cheong, Y., 2013. Bond degradation of glass fiber reinforced plastic bars in concrete subjected to tensile cycle loads. *Journal Of Reinforced Plastics And Composites*, pp. 1-13.

Lin, X. & Zhang, Y., 2013. Bond–slip behaviour of FRP-reinforced concrete beams. *Construction and Building Materials,* Volume 44, pp. 110–117.

Lin, X. & Zhang, Y., 2014. Evaluation of bond stress-slip models for FRP reinforcing bars in concrete. *Composite Structures* , Volume 107, pp. 131-141.

Makitani, E., Irisawa, I. & Nishiura, N., 1993. Investigation of bond in concrete member with Fiber-Reinforced plastic bars. *ACI SP 138-20, International Symposium on Fiber Reinforce Plastic Reinforcement for Concrete Structures, eds., Vancouver, BC, Canada,* March, pp. 315-331

Marfia, S., Rinaldi, Z. & Sacco, E., 2004. Softening behaviour of reinforced concrete beams under cyclic loading. *International Journal of Solids and Stuctures,* Volume 41, pp. 3293-3316.

Meier, U., 2000. The development of composites and its utilizations in Switzerland. *Advanced Polymer Composites For Structural Applications In Construction,* pp. 23-31.

Nanni, A., 2003. North American design guidelines for concrete reinforcement and strengthening using FRP: Principles, applications and unresolved issues. *Construction and Building Materials,* Volume 17, pp. 439-446.

Newhook, J., Ghali, A. & Tadros, G., 2002. Concrete flexural members reinforced with fibre reinforced polymer: design for cracking and deformability. *Canadian Journal of Civil Engineering,* Volume 19, pp. 125-134.

Nutt, A., 2007. The history of steel Reinforced concrete. s.l.: http:/Ezine-Articles.com/[Accessed: 12th May 2014].

Obrien, E., Dixon, A. & Sheils, E., 2012. Reinforced and prestressed concrete Design to EC2. *Second edition: The complete process.* Abingdon, Oxon , New York : Spon Press.

Ochola, R., 2004. Investigation of strain rate sensitivity of polymer matrix composite. *PHD Thesis, University of Cape Town.*

Orozco, A. & Maji, A., 2003. Failure modes of FRP reinforced concrete beams. *Proc. of SEM International Conference, Charlotte, NC,* June 2003.

Oshan, X. & Zhang, Y., 2013. Bond-slip behaviour of FRP reinforced concrete beams. *Construction and Building Materials,* Volume 44, pp. 110-117.

Owens, G., Fulton, F.S. & Cement and Concrete Institute., 2009. *Fulton's Concrete Technology.* Ninth edition ed., Cement and Concrete Institute. Midrand, South Africa

Pleinmann, L., 1991. Strength modulus of elasticity and bond of deformed FRP rods. *Advanced Composites Materials in Civil Engineering Structures. ASCE, Las Vegas: American Society of Civil Engineers,* pp. 99-110.

Quayyum, S., 2010. Bond behaviour of fibre reinforced polymer rebars in concrete. *Masters thesis, The University of British Columbia.*

Ray, B. & Rathore, D., 2015. Review on mechanical behaviour of FRP composites at different loading speeds. *Critical Reviews in Solid State and Materials Sciences,* Volume 40, pp. 119-135.

SANS (South African National Standard) 10100-1:2000, 2000. *The Structural Use of Concrete Part 1: Design*. Pretoria.

SANS (South African National Standard) 5863: 2006, 2006. *Concrete Tests: Compressive Strength of Hardened Concrete*. Pretoria.

Seffo, M. & Hamcho, M., 2016. Strength of concrete cylinder by composite materials (CFRP). *Energy Pocedia,* Volume 19, pp. 276-285.

Silva, M.A.G. & Biscaia, H., 2008. Degaradation of bond between FRP and RC beams. *Composites Structures,* Volume 85, pp. 164-174.

Shi, Y., Zhang, z. & Li, z., 2011. Experimental Study of the Shear Capacity of Glass FiberReinforced Polymer Reinforced Concrete Beam withCircular Cross Section. *Shanghai Jiaotong University,* Volume 17, pp. 408-414.

Shillings, C., 2015. Dynamic Behavior of Materials Subjected to Extreme Environments. *Master's Thesis, University of Rhode Island.*

Taher, K. & Burgoyne, CJ., 2011. Differences between FRP bond behavior in cracked and uncracked regions. *American Concrete Institute, ACI Special Publication,* 1 (ISSN 0193-2527), pp. 335-351.

Taher, K. & Burgoyne, CJ, 2011. Differences between FRP bond behavior in cracked and uncracked regions. *American Concrete Institute, ACI Special Publication,* 1 (ISSN 0193-2527), pp. 335-351.

Tamuzs, V., Apinis R., Modniks J. & Tepfers R., 2001. The performance of bond of FRP reinforcement in concrete. *SAMPE (Society for the Advancement of Material and Process Engineering) Symposium,* Issue California, pp. 1738-1748.

Tighiouart, B., Benmokrane, B. & Mukhopadhyaya, P., 1999. Bond strength of glass FRP rebar splices in beams under static loading. *Construction and Building Materials,* Volume 13, pp. 383-392.

Tuakta, C., 2005. Use of FRP composites in bridge structures. *Masters thesis, Massachusettes Institute of Technology, USA.*

Ullah, H., Tsigkourakos, G., Vartzopoulos, F., Ashcroft, I.A. & Silberschmidt, V.V., 2014. Damage in Fibre-Reinforced laminates under dynamic loading. *10th World Congress on Computational Mechanics,* Volume 1, May 2014.

Vogel, H. & Svecova, D., 2009. Effective moment of inertia expression for concrete beams reinforced with Fiber-Reinforced polymer (FRP). *Special Publication* Volume 264, pp. 77-94.

Wan, B., Petou, M.F., Harries, K.A., Sutton, M.A. & Yang B., 2002. Experimental investigation of bond between FRP and concrete. *ASCE Journal of Engineering Mechanics,* Volume 130 (12), pp. 1467–1475.

Wang, H. & Belarbi, A., 2009. Static and Fatigue bond characteristics of FRP rebars embedded in Fiber-Reinforced concrete. *Journal of Composite Materials,* Volume 44, pp. 1605-1622.

Xue, W., Yang, Y., Zheng, Q., & Fang Z., 2016. Modeling of bond of sand-coated deformed Glass Fibre-Reinforced Polymer Rebars in concrete. *Journal of Reinforced Plastics and Composites 2014,* Volume 33(10), pp 895–910.

Yan, Jenkins & Pendleton, 2000. Polyolefin Fiber-Reinforced concrete composites. *Damping And Frequency Characteristic: Part I: Cement And Concrete Research,* Volume 30, pp. 391-401.

Yoon-lee, J., Yi, C., Kim, B. & Cheong, Y., 2013. Bond degradation of glass fiber reinforced plastic bars in concrete subjected to tensile cycle loads. *Journal of Reinforced Plastics and Composites,* pp. 1-13.

Young-Jun, Y., Ki-Tae, P., Dong-Woo, S. & Ji-JHyun, H, 2015. Tensile strength of GFRP bars with hollow section. *Advances in Materials Science and Engineering,* 2015, pp. 8.

Zhai, T., Xu, Y., Martin, J. & Wilkinson , A., 1999. A self-aligning four-point bend testing rig and sample geometry effect in four-point bend fatigue. *International Journal of Fatigue,* Volume 21, pp. 889–894.

APPENDICES

Appendix A: Environmental reduction factor for various fibres and exposure conditions (ACI 440.1R-06,2006)

Exposure condition	Fiber type	Environmental reduction factor C_E
Concrete not exposed to earth and weather	Carbon	1.0
	Glass	0.8
	Aramid	0.9
Concrete exposed to earth and weather	Carbon	0.9
	Glass	0.7
	Aramid	0.8

ε_{fu} = design rupture strain of FRP reinforcement; and

ε^*_{fu} = guaranteed rupture strain of FRP reinforcement defined as the mean tensile strain at failure of a sample of test specimens minus three times the standard deviation ($\varepsilon^*_{fu} = \varepsilon_{u,ave} - 3\sigma$).

The design modulus of elasticity will be the same as the value reported by the manufacturer as the mean elastic modulus (guaranteed value) of a sample of test specimens ($E_f = E_{f,ave}$).

Appendix B

Appendix B1: 12 mm GFRP rebars properties_Supplier data

Shanghai Xuyao Fibreglass Reinforcement Products Co.,Ltd

Product Specification
(产品规格)

Part No.(型号)	XY61—12	Name(名称)	Standard FRP Rebar

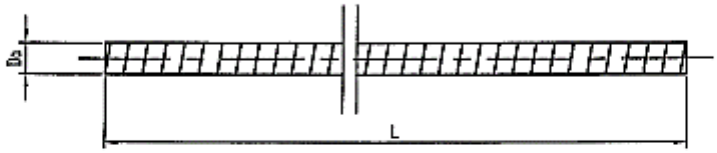

Item(项目)	Unit (单位)	Standard Specification (标准参数)
Breaking Load(抗拉)	kN	97
Effective cross section(截面积)	mm^2	113
Tensile strength in core(抗拉强度)	N/mm^2	850
Tensile E-modulus(弹性模量)	N/mm^2	40,000
Shear strength(剪切强度)	N/mm^2	150
Weight(重量)	g/m	240—270
Pitch(P)(螺距)	mm	2.0 ±0.3
Dia,Top(Da)(外径)	mm	12.0 ±0.3
Head part(端面切角)	60°/90°	90°
Length(长度)	mm	L标+20/+0

Appendix B2: 6 mm GFRP rebars properties_Supplier data

Shanghai Xuyao Fibreglass Reinforcement Products Co.,Ltd

Product Specification
(产品规格)

Part No.(型号)	XY61－6	Name(名称)	FRP Rebar

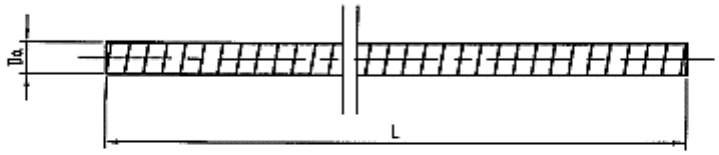

Item(项目)	Unit (单位)	Standard Specification (标准参数)
Breaking Load(抗拉)	kN	25.5
Effective cross section(截面积)	mm^2	28.3
Tensile strength in core(抗拉强度)	N/mm^2	900
Tensile E-modulus(弹性模量)	N/mm^2	40,000
Weight(重量)	g/m	55－65
Dia,Top(Da)(外径)	mm	6.0 ±0.5
Head part(端面切角)	60°/90°	90°
Length(长度)	mm	L(订)+20/+0

Appendix C: Minimum concrete cover for steel reinforced concrete structures

(SANS 10100:1, 2000)

This is covered by part two of SABS 0100, but generally the following table may be used to choose suitable nominal cover according to the conditions of exposure.

Exposure conditions	Concrete grade				
	20	25	30	40	50
Mild	25	25	25	25	25
Moderate	--	40	30	25	20
Severe	--	50	40	40	35
Very severe	--	--	--	60	50

Appendix D: Tensile tests result sheets

D1: Tensile tests results form

	WITNESS BY:	TECHNICAL SIGNATORY	REMARKS	ACCREDITATION
MTL Metallurgical Testing Laboratory	JOELLA MUKALAY	J. Junior Lumbu.		tsanas Testing Laboratory T0580

Certificate Number: 2017-76978 (2017-76978-A) Date Received: 31 Aug 2017 Date Tested: 31 Aug 2017

TENSILE PROPERTIES	Test Temperature:		21°C									ASTM A370	
Test direction:	Thickness (mm)	Width (mm)	OD (mm)	Area (mm^2)	Gauge (mm)	Yield load (kN)	Max Load (kN)	Extension (mm)	Final Ø (mm)	Yield Point Rp0.2/eH (MPa)	UTS (MPa)	Elongation (%)	R/A (%)	Fracture Location
Spec Min										-	-	-	-	
Spec Max										-	-	-		
Sample A1	-	-	12.09	114.80	-	38.27	53.49	-	-	333	466	-	-	Head of Tensile
Sample A2	-	-	12.09	114.80	-	36.17	56.11	-	-	315	489	-	-	Head of Tensile
Sample A3	-	-	11.75	108.62	-	30.24	57.08	-	-	278	526	-	-	Head of Tensile
Sample A4	-	-	11.69	107.33	-	28.14	55.92	-	-	262	521	-	-	Head of Tensile
Sample A5	-	-	12.15	115.94	-	34.74	61.82	-	-	300	533	-	-	Head of Tensile

D2: Tensile tests results form

T0580

13 Betschana Road
Sebenza
Edenvale, 1610
Tel: 082 779 6777
Fax: 086 293 6154
Email: Technical@mtlabs.co.za
Web: www.mtlabs.co.za

MTL
Metallurgical Testing Labs Pty Ltd
Reg. No: 2012/027591/07

Certificate Number:	
2017-76978 (2017-76978-A)	
Pass	Fail
Customer info	

Customer Job Number:	2017-76978 (2017-76978-A)
Client:	Vaal University of Technology

Terms and conditions

All equipment used in attaining these results are traceable to National and International Standards
Test results contain herein relate only to the sample supplied
Off-cuts of material as supplied by the client will be retained for a period not less than 2 months unless agreed otherwise in writing and confirmed by MTL.
Hand written changes made to the certificate are not valid
Any changes to the certificate will be made under the heading of the original certificate number followed by the prefix "Revised" i.e. XXXXXXX-A Revised
Electronic copies of the certificates will be kept on file for a period no less than 3 years
This certificate may not be partially replicated without the written consent of MTL
This certificate is issued according to the requirements set out by BS EN 10204 3.1, as indicated below:

Customer:	Vaal University of Technology	Test Results, in accordance with spec. provided		Material:	Unknown
Order No.	COD	Test Results, not in accordance with spec. provided			
Address:	Andries Potgieter	No requirements provided	X	Description:	±12mm round bar
	Vanderbijlpark	TESTING WAS CARRIED OUT IN ACCORDANCE WITH THE FOLLOWING MTL PROCEDURES (Supporting international procedures): MECH001, 001.1, & 004 (ASTM A370; E8, E21; ISO 6892; EN10002-5) MECH002 (ASTM A370; E23; BS EN 10045-1) HARD001 (ASTM E92; E384) HARD002 (ASTM E10; A370) HARD003 (ASTM E18; A370) CORR001 (ASTM B117) MET001 (ASTM A255; E18) MET002 (ASTM E1077) MET003 (ASTM E340; E381) CORR002 (ASTM E9; A262) MET004 (ASTM E3; E45) MET005 (ASTM E3; E45) MET006 (ASTM E3; E45; E112; E407) MET008 (ASTM B499) MET009 (ASTM B487) Hard004 (ASTM E110). CHEM001 & 004 (ASTM E415) CHEM0016 (ASTM E1019) & **ASTM A370**			
	1900				
Telephone:	079 664 0457				
Telefax:	N/A				
Email:	joellamukalay@yahoo.fr				
Attention:	Joella Mukalay			Material ID Number:	Glass reinforced polymer bars
TEST REPORT IN ACCORDANCE WITH EN 10204 3.1 OF SAMPLE AS SUPPLIED					

D3: Tensile tests results form

	WITNESS BY:	TECHNICAL SIGNATORY	REMARKS	ACCREDITATION
MTL Metallurgical Testing Labs	JOELLA MUKALAY	J. Junior Lumsden		sanas Testing Laboratory T0580

Certificate Number: 2017-76978 (2017-76978-A) Date Received: 31 Aug 2017 Date Tested: 31 Aug 2017

Metallurgical Testing Labs

17-76978 A1

Customer	VUT	TestDate	2017/8/31
Coil No/Packet No		Size(mm)	12.09
So(mm²)	114.80	Lo(mm)	48.36
Fp(kN)	38.27	Rp(MPa)	333
Fm(kN)	53.49	Rm(MPa)	466

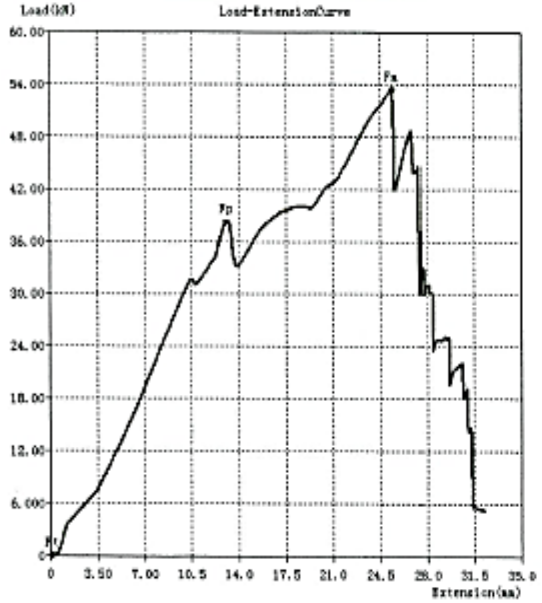

Metallurgical Testing Labs

17-76978 A2

Customer	VUT	TestDate	2017/8/31
Coil No/Packet No		Size(mm)	12.09
So(mm²)	114.80	Lo(mm)	48.36
Fp(kN)	36.17	Rp(MPa)	315
Fm(kN)	56.11	Rm(MPa)	489

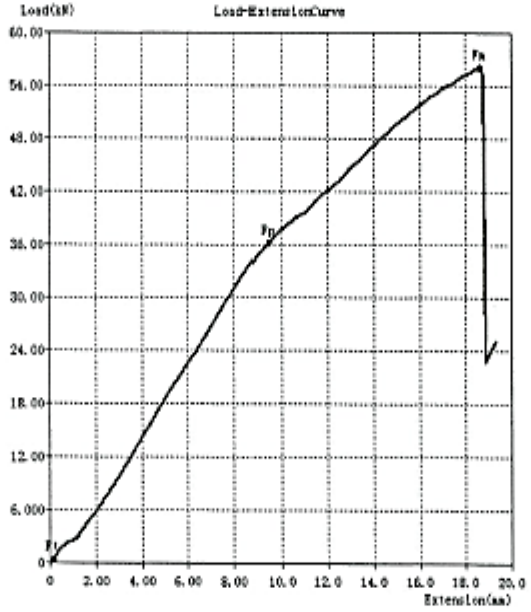

Metallurgical Testing Labs

17-76978 A3

Customer	VUT	TestDate	2017/8/31
Coil No/Packet No		Size(mm)	11.79
So(mm²)	108.62	Lo(mm)	
Fp(kN)	30.24	Rp(MPa)	278
Fm(kN)	57.08	Rm(MPa)	526

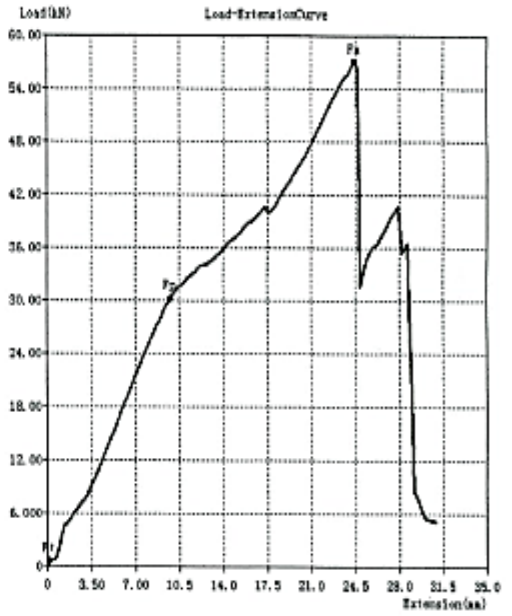

D4: Tensile tests results form

	WITNESS BY:	TECHNICAL SIGNATORY	REMARKS	ACCREDITATION
MTL Metallurgical Testing Labs Ltd	JOELLA MUKALAY	J. Junior Lumsa.		sanas Testing Laboratory T0580

Certificate Number: 2017-76978 (2017-76978-A) Date Received: 31 Aug 2017 Date Tested: 31 Aug 2017

Metallurgical Testing Labs

17-76978 A4

Customer	VUT	TestDate	2017/8/31
Coil No/Packet No	4	Size(mm)	1.69
So(mm²)	107.33	Lo(mm)	
Fp(kN)	28.14	Rp(MPa)	262
Fm(kN)	55.92	Rm(MPa)	521

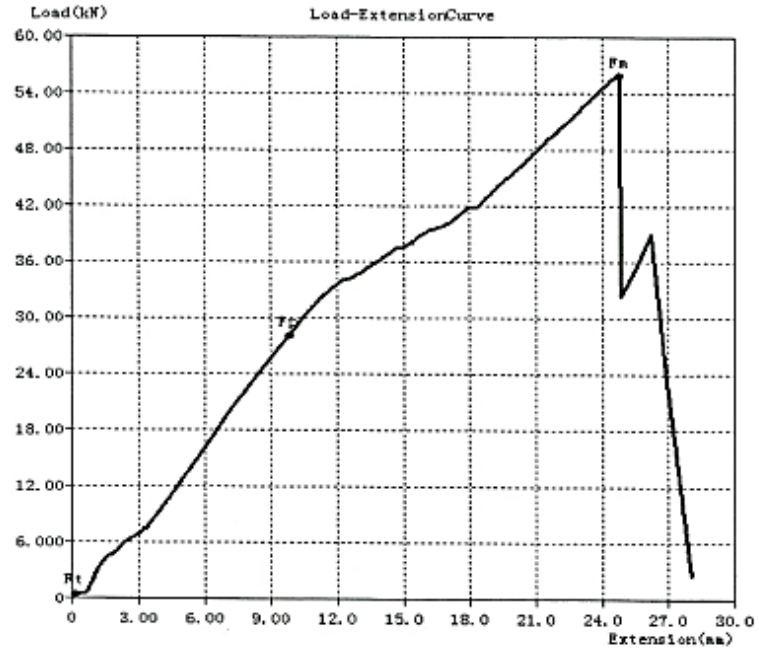

Metallurgical Testing Labs

17-76978 A5

Customer	VUT	TestDate	2017/8/31
Coil No/Packet No		Size(mm)	12.15
So(mm²)	115.94	Lo(mm)	
Fp(kN)	34.74	Rp(MPa)	300
Fm(kN)	61.82	Rm(MPa)	533

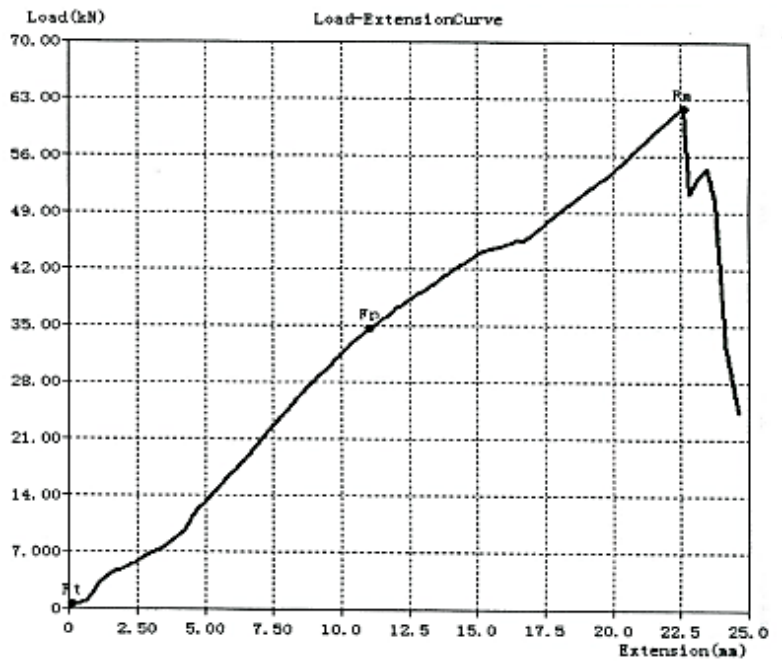

Appendix E: Concrete beams failure

RCGFRP1

RCGFRP2

RCGFRP3

RCGFRP4

RCGFRP5

RCGFRP6

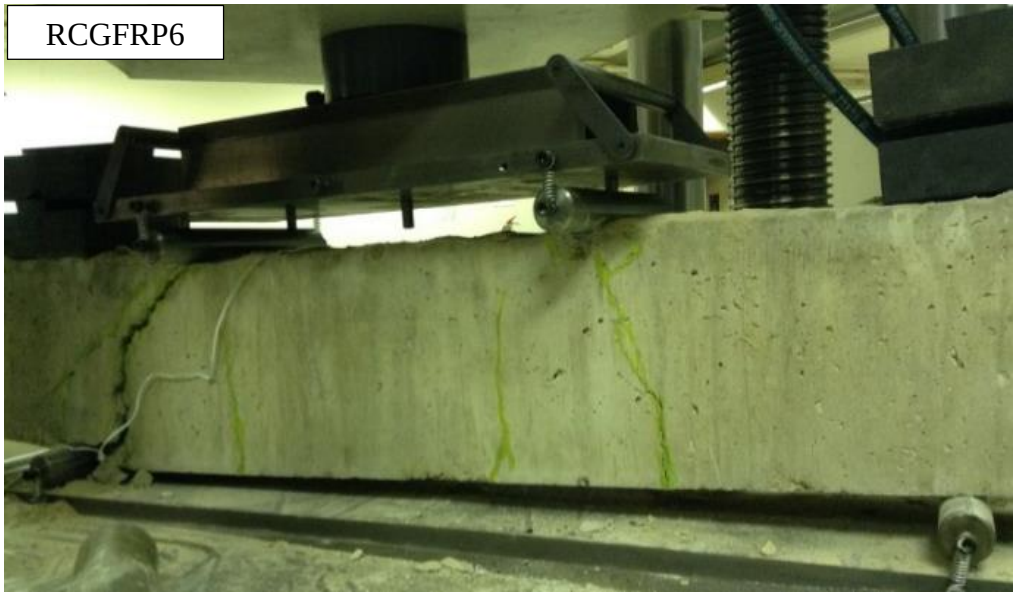

RCGFRP7

RCGFRP8

RCGFRP9

RCGFRP10

RCGFRP11

RCGFRP12

RCGFRP13

RCGFRP14

RCGFRP15

RCGFRP16

RCGFRP17

RCGFRP18

RCGFRP19

RCGFRP20

RCGFRP21

RCGFRP22

RCGFRP23

RCGFRP24

RCGFRP25

RCGFRP26

RCGFRP27

RCGFRP28

RCGFRP29

RCGFRP30

RCGFRP31

RCGFRP32

RCGFRP33

RCGFRP34

RCGFRP35

RCGFRP36

RCS1

RCS2

RCS2-Cross-section

RCS3

RCS4

RCS4-Cross-section

RCS5

RCS6

RCS7

RCS8

RCS8_ Cross-section

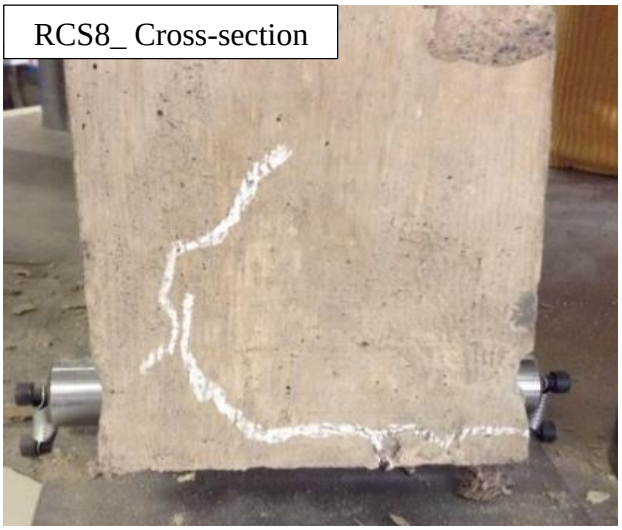

RCS9

RCS10

RCS11

RCS12